



MONASH University

Structure-Based Studies in the Development of Anti-Cancer Enzyme Inhibitors

Krithika Sundaram

BSc (Microbiology), MS Biotech

A thesis submitted for the degree of *Doctor of Philosophy* at

Monash University in 2015

Faculty of Pharmacy and Pharmaceutical Sciences

Copyright notice

© Krithika Sundaram (2015). Except as provided in the Copyright Act 1968, this thesis may not be reproduced in any form without the written permission of the author.

I certify that I have made all reasonable efforts to secure copyright permissions for third-party content included in this thesis and have not knowingly added copyright content to my work without the owner's permission.

Abstract

Cancer is one of the most prevalent causes of death worldwide. This thesis focuses on structural studies of two targets from the Aldo-Keto Reductase family (Section A) and Phosphoinositide 3-kinase family (Section B).

The Aldo-Keto reductases are associated in the pathogenesis of various diseases including cancer. Section A of the thesis includes structural and functional studies of two aldo-keto reductases: AKR1B14 and AKR1C3. AKR1B14 is a recently identified member of AKR1B subfamily and previous crystallographic studies have revealed the importance of a non-conserved residue in coenzyme binding. The mutagenesis studies of this residue have confirmed the decrease in binding affinity of the coenzyme. The findings presented in this section examine the different AKR1B14 mutants to structurally understand and explain the loss of affinity of coenzyme associated with mutation of this residue using crystallography and molecular modelling. AKR1C3 is believed to be involved in the catalytic metabolism of various steroids. AKR1C3 has gained immense attention as a potential therapeutic target due to its upregulation in breast and prostate cancer. Molecular modelling was used to investigate the structure-activity relationships governing AKR1C3 with various inhibitors and have enabled us in the identification of the structural determinants of inhibition. This information may aid in future development of selective inhibitors for both the targets.

The second section of this thesis focuses on Phosphoinositide 3-kinases which are critical regulators of intracellular signalling pathways and are involved

in various cellular processes. The class II PI3Ks have gained attention recently as they are believed to be upregulated in certain types of cancers and hence present as a potential therapeutic target. Section B of this thesis investigates the structural features of class II PI3KC2 β to identify key residues that could be targeted for inhibitor selectivity. Computational and inhibition studies of various inhibitors of PI3KC2 β has presented information that may be useful in future development of class II selective inhibitors.

Declaration

This thesis contains no material which has been accepted for the award of any other degree or diploma at any university or equivalent institution and that, to the best of my knowledge and belief, this thesis contains no material previously published or written by another person, except where due reference is made in the text of the thesis.

KRITHIKA SUNDARAM

Publications during enrolment

Mountford, S. J., Z. Zheng, **K. Sundaram**, I. G. Jennings, J. R. Hamilton and P. E. Thompson (2015). "Class II but Not Second Class—Prospects for the Development of Class II PI3K Inhibitors." ACS Medicinal Chemistry Letters **6**(1): 3-6.

Endo, S., T. Matsunaga, A. Kanamori, Y. Otsuji, H. Nagai, **K. Sundaram**, O. El-Kabbani, N. Toyooka, S. Ohta and A. Hara (2012). "Selective inhibition of human type-5 17 β -hydroxysteroid dehydrogenase (AKR1C3) by baccharin, a component of Brazilian propolis." J Nat Prod **75**(4): 716-721.

Sundaram, K., S. Endo, T. Matsunaga, N. Tanaka, A. Hara and O. El-Kabbani (2012). "Structure of the His269Arg mutant of the rat aldose reductase-like protein AKR1B14 complexed with NADPH." Acta Crystallogr Sect F Struct Biol Cryst Commun **68**(Pt 4): 400-403.

Acknowledgements

First and foremost, I am sincerely grateful to my supervisor Associate Prof. Phil Thompson for believing in me and giving me an opportunity to undertake such an interesting project under his supervision. His continuous support, patience and wonderful guidance has been the driving force during the entire course of my Ph.D.

My heartfelt gratitude to my associate supervisor Dr. Ian Jennings, for his support and mentorship. Thanks for essentially teaching me everything. You are the coolest supervisor!

I wish to thank Dr. Ossama El-Kabbani for his guidance and support with the AKR project during initial stages of my Ph.D. project.

My sincere thanks to Dr. David Chalmers and Dr. Elizabeth Yuriev for their valuable advice and insightful comments with my computational work.

Special thanks to my Ph.D. progress committee members Dr. David Manallack and Associate Prof. Helen Irving for their constant support and guidance throughout my Ph.D.

I am also thankful to Dr. Roland Chung for his support, encouragement and for giving up his valuable time to guide me with the operation of the in house X-ray machine.

I would like to thank our collaborators Prof. Akira Hara (Gifu University, Japan) and Dr. Alexandre Arcaro (University of Bern, Switzerland) for providing me with

constructs, protein samples and their expertise and input which has contributed greatly towards the development of this Ph.D. project.

I also wish to acknowledge the support of Department of Medicinal Chemistry and Department of Drug Discovery biology for providing me access to equipment needed to produce and complete my thesis. In addition, I appreciate the financial support provided by MIGR during the course of this Ph.D.

I owe a great deal of thanks to my colleagues and friends Trayder, Matt, Anthony, Tamir, Tony, Amin, Andrew , Carmen, Anita, Murray, Shayna, Luke, Stephan, Estelle, Sam, Steven, Jo- Anne, Oscar, Yasmin, Krishna and Balu for all the fun times in the uni and for keeping me sane and brightening up my spirits through difficult times.

I am gifted to have a wonderful and understanding family whose unconditional love has been my backbone and motivational force throughout my Ph.D. project. Thank you Amma, Appa, Mummy, Daddy and Pratyu for your all rounded support and blessings. I would also like to express my sincere thanks to extended family in Melbourne: Uma aunty, Jay uncle, Ragu uncle, Renuka aunty, Rev and Sindhu for being there during difficult times. .

Last but not the least, I owe my deepest appreciation to my husband without whose moral support and encouragement this Ph.D. journey would have been impossible.

Table of Contents

COPYRIGHT NOTICE	II
ABSTRACT.....	III
DECLARATION.....	V
PUBLICATIONS DURING ENROLMENT.....	VI
ACKNOWLEDGEMENTS	VII
LIST OF FIGURES	XIII
LIST OF TABLES.....	XVI
LIST OF ABBREVIATIONS	XVIII
AMINO ACID CODE.....	XXIII
PREFACE.....	1
<u>SECTION A: STRUCTURAL AND FUNCTIONAL STUDIES OF ALDO-KETO REDUCTASES INVOLVED IN CANCER</u>	
1 CHAPTER 1: INTRODUCTION TO THE AKR SUPERFAMILY	10
1.1 OVERVIEW OF THE AKR FAMILY.....	10
1.2 CLASSIFICATION OF ALDO-KETO REDUCTASES	10
1.3 GENERAL STRUCTURAL FEATURES	11
1.4 MEMBERS OF THE AKR SUPERFAMILY	13
1.5 HUMAN AKRS	15
1.5.1 <i>Members of the AKR1B subfamily</i>	16
1.5.2 <i>AKR1C subfamily</i>	19

1.6	AIMS AND RATIONALE	28
2	METHODOLOGY	30
2.1.1	<i>Biochemical analysis</i>	<i>30</i>
2.1.2	<i>Computational studies.....</i>	<i>32</i>
3	RESULTS AND DISCUSSION	35
3.1	STRUCTURAL STUDIES OF AKR1B14 HIS269ARG MUTANT	35
3.2	WHY IS TOLFENAMIC ACID A POTENT AND SELECTIVE INHIBITOR OF AKR1C3?	
	42	
3.2.2	<i>Molecular modelling studies of baccharin, an AKR1C3 inhibitor.....</i>	<i>49</i>
3.2.3	<i>Molecular docking studies of structural analogues of baccharin.....</i>	<i>56</i>
3.2.4	<i>Influence of protein structure as a starting point for virtual screening for AKR1C3 inhibitors.....</i>	<i>63</i>
4	CONCLUSIONS, LIMITATIONS AND FUTURE OUTCOMES.....	68
<u>SECTION B: CLASS II PI3KC2β AS A NOVEL CANCER TARGET</u>		
1	CHAPTER 1: INTRODUCTION TO PI3KS	72
1.1	OVERVIEW OF PI3K FAMILY	72
1.2	CLASSIFICATION OF PI3K FAMILY	72
1.2.1	<i>Class I PI3K.....</i>	<i>72</i>
1.2.2	<i>Class II PI3K</i>	<i>76</i>
1.2.3	<i>Class III PI3K.....</i>	<i>78</i>
1.2.4	<i>Class IV PI3Ks.....</i>	<i>78</i>
1.3	PI3KS IN SIGNALLING PATHWAYS.....	79
1.4	PI3K AND CANCER.....	81
1.5	INHIBITORS OF PI3K IN CANCER RESEARCH AND THERAPY.....	81
1.5.1	<i>First-generation PI3K inhibitors</i>	<i>82</i>

1.5.2	<i>New-generation PI3K inhibitors.....</i>	83
1.5.3	<i>Inhibitors of class II PI3KC2β.....</i>	85
1.6	<i>RATIONALE AND AIMS</i>	88
2	CHAPTER 2: MATERIALS AND METHODS.....	89
2.1	COMPUTATIONAL STUDIES.....	89
2.1.1	<i>Sequence alignment and selection of template</i>	89
2.1.2	<i>Generation of PI3KC2β homology models</i>	89
2.1.3	<i>Molecular modelling studies.....</i>	89
2.2	BIOCHEMICAL ANALYSIS.....	90
2.2.1	<i>Generation of the recombinant vector.....</i>	90
2.2.2	<i>Generation of recombinant bacmid</i>	95
2.2.3	<i>Production of the recombinant baculovirus.....</i>	98
2.2.4	<i>Expression and Purification of PI3KC2β</i>	101
2.2.5	<i>Protein separation by SDS-PAGE</i>	102
2.2.6	<i>Western blot</i>	102
2.2.7	<i>Enzyme assays</i>	103
2.2.8	<i>Inhibition assays.....</i>	103
3	CHAPTER 3: RESULTS AND DISCUSSION	105
3.1	DEVELOPMENT OF HOMOLGY MODELS OF PI3KC2B: INSIGHTS FOR THE DEVELOPMENT OF ISOFORM-SELECTIVE INHIBITORS OF PI3KC2B	105
3.1.1	<i>Introduction</i>	105
3.1.2	<i>Protein sequence comparison of human PI3Ks to identify a suitable template protein for development of homology model of PI3KC2β.....</i>	105
3.1.3	<i>Docking of known PI3KC2β inhibitors into homology models.....</i>	111
3.1.4	<i>Molecular docking of PI-701 and PI-702: insights into development of isoform-selective inhibitors of PI3KC2β.....</i>	125

3.2	INHIBITION STUDIES OF CLASS I PI3K INHIBITOR ZSTK474 AND ITS	
	STRUCTURAL ANALOGUES AGAINST CLASS II PI3KC2B	129
3.2.1	<i>Introduction</i>	129
3.2.2	<i>Cloning, expression, purification and Characterization of PI3KC2β ..</i>	130
3.2.3	<i>Inhibitory activity of ZSTK474 against the class II PI3KC2β</i>	139
3.2.4	<i>Inhibitory activities of ZSTK-474 analogues:.....</i>	140
4	CHAPTER 4: CONCLUSIONS AND FUTURE OUTCOMES.....	147
	APPENDICES.....	149
	REFERENCES.....	150

List of Figures

SECTION A

FIGURE 1-1: SCHEMATIC REPRESENTATION OF THE REACTION CATALYSED BY AKRS.	10
FIGURE 1-2: NOMENCLATURE SYSTEM OF THE AKR SUPERFAMILY.....	11
FIGURE 1-3: TERTIARY STRUCTURE OF ALDO-KETO REDUCTASES.	12
FIGURE 1-4: REDUCTION OF ESTRONE TO 17 β -ESTRADIOL AND 4-ANDROSTENE-3,17-DIONE TO TESTOSTERONE BY AKR1C3.....	21
FIGURE 1-5: REPRESENTATIVE AKR1C3 INHIBITORS.....	27
FIGURE 3-1: INTERACTIONS OF THE AKR1B14 WILD TYPE AND AKR1B14 His269ARG MUTANT.....	37
FIGURE 3-2: SUPERIMPOSITION OF THE CRYSTAL STRUCTURES	39
FIGURE 3-3: SUPERIMPOSITION OF THE MODELS	40
FIGURE 3-4: DOCKED POSE OF TOLFENAMIC ACID (YELLOW) SUPERIMPOSED ON THE CRYSTAL STRUCTURE OF AKR1C3 IN COMPLEX WITH FLUFENAMIC ACID (ORANGE).....	44
FIGURE 3-5: INTERACTIONS BETWEEN THE AKR1C3 AND TOLFENAMIC ACID.....	45
FIGURE 3-6: SCHEMATIC DIAGRAM OF THE RESIDUES MAKING VAN DER WAAL'S CONTACT WITH TOLFENAMIC ACID.	46
FIGURE 3-7: SUPERIMPOSITION OF DOCKED POSES OF TOLFENAMIC ACID IN THE OTHER HUMAN ISOFORMS.....	47
FIGURE 3-8: STRUCTURE OF BACCHARIN AND ITS INHIBITORY POTENCIES IN THE HUMAN AKR1C ISOFORMS.....	49
FIGURE 3-9: INTERACTIONS OF BACCHARIN IN AKR1C3.....	51
FIGURE 3-10: DIFFERENCES IN THE KEY RESIDUES INVOLVED IN INHIBITOR BINDING IN AKR1C3 AND THE OTHER THREE HUMAN ISOFORMS.....	52
FIGURE 3-11: SUPERIMPOSITION OF DOCKING RESULTS OF BACCHARIN IN MUTANTS ON DOCKING RESULTS OF BACCHARIN IN WILD TYPE.	55
FIGURE 3-12: STRUCTURES OF BACCHARIN, BA-25 AND BA-28.....	57
FIGURE 3-13: SUPERIMPOSITION OF DOCKED POSES OF BA-25 (GREEN) AND BA-28 (MAGENTA) ON THE DOCKED POSE OF BACCHARIN (YELLOW).	58

FIGURE 3-14: BA-25 AND BA-28 MAKE SIMILAR BONDS AS BACCHARIN.	59
FIGURE 3-15: INTERACTIONS OF BA-25 WITH AKR1C3.....	60
FIGURE 3-16: INTERACTIONS OF BA-28 WITH AKR1C3.....	61
FIGURE 3-17: ASSESSMENT OF DOCKING PERFORMANCE OF THE MODEL PROTEIN (PDB:1S2C) USED IN PREVIOUS DOCKING PROTOCOLS.	64
FIGURE 3-18: IDENTIFICATION OF IDEAL MODEL FOR USE IN MOLECULAR MODELLING STUDIES USING ROC CURVES.	66

SECTION B

FIGURE 1-1: CLASSIFICATION OF PI3KS.....	74
FIGURE 1-2: PI3K SIGNALLING PATHWAY BY DIFFERENT CLASSES OF PI3KS.....	80
FIGURE 1-3: STRUCTURE OF THE FIRST GENERATION PI3K INHIBITORS.....	83
FIGURE 1-4: ATP BINDING SITE IN PI3KS.....	85
FIGURE 1-5: CHEMICAL STRUCTURES OF THE REPORTED CLASS II PI3K INHIBITORS.....	87
FIGURE 3-1: THE FIVE GENERATED HOMOLOGY MODELS	109
FIGURE 3-2: CLOSE-UP OF PI3KC2B BINDING POCKET.....	111
FIGURE 3-3: DOCKED POSES OF PI-103 IN THE FIVE GENERATED MODELS	115
FIGURE 3-4: DOCKED POSES OF PIK-90 IN THE FIVE GENERATED MODELS	116
FIGURE 3-5: DOCKED POSES OF PIK-93 IN THE FIVE GENERATED MODELS	118
FIGURE 3-6: DOCKED POSES OF ZSTK-474 IN THE FIVE GENERATED MODELS	120
FIGURE 3-7: DOCKED POSES OF LY294002 IN THE FIVE GENERATED MODELS	121
FIGURE 3-8: DOCKED POSES OF PIK-108 IN THE FIVE GENERATED MODELS	122
FIGURE 3-9: PIK-108 (MAGENTA) INDUCES A CONFORMATIONAL CHANGE IN THE ONE OF THE RESIDUES MET772 IN THE BINDING POCKET OF CLASS I PI3KS (PDB: 4A55) BY FORMING A SELECTIVITY POCKET.	123
FIGURE 3-10: CHEMICAL STRUCTURES OF PI-701, PI-702 AND PI-103	126
FIGURE 3-11: THE DOCKED POSES OF PI-701 (ORANGE) AND PI-702 (GREEN) SUPERIMPOSED ON PI- 103 IN MAGENTA.....	127

FIGURE 3-12: AGAROSE GEL CONFIRMING THE MW OF THE PI3KC2B INSERT AND THE PFASTBAC HTC.....	132
FIGURE 3-13: AGAROSE GEL CONFIRMING THE PRESENCE OF THE RECOMBINANT BACMID CONTAINING PI3KC2B IN THE SAMPLES.	133
FIGURE 3-14: COOMASSIE STAINED SDS-PAGE GEL AND WESTERN BLOT OF PURIFIED PI3KC2B. ..	136
FIGURE 3-15: ENZYMATIC ACTIVITY OF PI3KC2B AND PI3K P110A MEASURED USING LUMINESCENCE (RLU- RELATIVE LUMINESCENCE UNITS) VS. ATP CONSUMPTION ASSAY.....	138
FIGURE 3-16: DETERMINATION OF ZSTK-474 INHIBITION OF PI3K ACTIVITY AS MEASURED USING A LUMINESCENT ATP CONSUMPTION ASSAY WITH PI AS THE SUBSTRATE.....	139
FIGURE 3-17: CHEMICAL STRUCTURES OF THE STRUCTURAL ANALOGUES OF ZSTK-474	142
FIGURE 3-18: PERCENTAGES OF INHIBITION AT 10 μ M OF THE ELEVEN COMPOUNDS FOR PI3KC2B ..	143
FIGURE 3-19: DETERMINATION OF INHIBITORY POTENCY OF THE ZSTK-474 AND THREE SELECTED COMPOUNDS JP7-126, JP 7-118 AND JP 7-108 MEASURED USING A LUMINESCENCE VS. ATP CONSUMPTION ASSAY WITH PI AS A SUBSTRATE.	145

List of Tables

SECTION A

TABLE 1-1: MEMBERS OF THE AKR FAMILY (ADAPTED FROM [60])	14
TABLE 3-1: SITE MUTAGENESIS OF HIS269 REVEALED THE INCREASE IN BINDING AFFINITY OF NADPH.	35
TABLE 3-2: DATA COLLECTION AND REFINEMENT STATISTICS. VALUES IN PARENTHESES ARE FOR THE HIGHEST RESOLUTION SHELL.	38
TABLE 3-3: N-PHENYLANTHRANILIC ACID INHIBITORS OF AKR1C3. WHERE THE IC ₅₀ VALUES WERE NOT AVAILABLE IT IS REPRESENTED BY N.D.	43
TABLE 3-4: SITE-DIRECTED MUTAGENESIS OF THE RESIDUES	53
TABLE 3-5: PERFORMANCE OF THE SIX MODELS ANALYSED IN THE STUDY.	66

SECTION B

TABLE 1-1: PHOSPHORYLATION OF PHOSPHOINOSITIDES CATALYSED BY PI3KS	73
TABLE 1-2: IC ₅₀ VALUES (μM) FOR REPORTED PI3K INHIBITORS	86
TABLE 2-1: RESTRICTION DIGESTION CONDITIONS FOR CLEAVING P13KC2B INSERT FROM PCDNA... ..	92
TABLE 2-2: CONDITIONS FOR LIGATION OF PFASTBAC HTC WITH PI3C2B INSERT	93
TABLE 2-3: DOUBLE DIGESTION OF PFASTBAC HTC CONTAINING PI3KC2B TO CONFIRM FRAGMENT SIZES	94
TABLE 2-4: PCR REACTION MIXTURE AND CYCLE CONDITIONS	98
TABLE 3-1: SEQUENCE IDENTITY OF THE CATALYTIC SUB-UNIT OF PI3KC2B WITH THE CATALYTIC SUBUNITS OF THE EIGHT HUMAN PI3K ISOFORMS.....	106
TABLE 3-2: FIVE HOMOLOGY MODELS DEVELOPED USING THE CO-ORDINATES OF AVAILABLE CRYSTAL STRUCTURES OF CLASS I AND CLASS III PI3KS.....	108
TABLE 3-3: THE NON-CONSERVED RESIDUES IN BINDING SITE OF THE EIGHT MAMMALIAN PI3K ISOFORMS.....	110
TABLE 3-4: LIST OF THE SELECTED INHIBITORS CHOSEN FOR VALIDATION.....	113

TABLE 3-5: DOCKING SUMMARY OF THE VALIDATION STUDIES OF THE SIX INHIBITORS (RMSD CUTOFF

3 Å).....	124
-----------	-----

List of Abbreviations

AKR	Aldo-Keto Reductase
AML	Acute Myeloid Leukaemia
AR	Aldose Reductase
ARI	Aldose Reductase Inhibitors
ARLP	Aldose Reductase-Like Protein
ATM	Ataxia Telangiectasia Mutated
ATP	Adenosine Triphosphate
ATP	Adenosine Triphosphate
ATR	Ataxia Telangiectasia And Rad3 Related
AUC	Area Under Curve
BCL2	B-Cell Lymphoma 2
BCR	Breakpoint Cluster Region
BH	BCR Homology Domain
CADD	Computer-Aided Drug Discovery
CBM	N-(4-Chlorobenzoyl)-Melatonin

CRPC	Castrate Resistant Prostrate Cancer
DMSO	Dimethyl Sulfoxide
DNA-PK	DNA-Dependent Protein Kinase
DTT	Dithiothreitol
EDTA	Ethylenediaminetetraacetic Acid
ER	Estrogen Receptor
HSD	Hydroxysteroid Dehydrogenase
HTVS	Highthroughput Virtual Screening
IPTG	Isopropyl B-D-1-Thiogalactopyranoside
kDa	Kilodalton
LPA	Lysophosphatidic Acid
MCF-7	Michigan Cancer Foundation-7 (Human Breast Adenocarcinoma Cell Line)
MOI	Multiplicity Of Infection
MPA	Medroxyprogesterone Acetate
MTM	Myotubularins
mTOR	Mammalian Target Of Rapamycin

MW	Molecular Weight
NADP+	Nicotinamide Adenine Dinucleotide Phosphate
NADPH	Reduced Form Of NADP+
Ni-NTA	Nickel- Nitrilotriacetic Acid
NMR	Nuclear Magnetic Resonance
NSAID	Nonsteroidal Anti-Inflammatory Drugs
PAGE	Polyacrylamide Gel Electrophoresis
PBST	Phosphate Buffered Saline With Tween
PCR	Polymerase Chain Reaction
PDB	Protein Data Bank
PFU	Plaque Forming Units
PGD2	Prostaglandin D2
PGF2	Prostaglandin F2 Alpha
PGFS	Prostaglandin-F Receptor
PGH2	Prostaglandin H2
PI	Phosphatidylinositol
PI3K	Phosphoinositide 3-Kinase

PI3P	Phosphatidylinositol 3-Phosphate
PI4P	Phosphatidylinositol 4-Phosphate
PIP2	Phosphatidylinositol 4,5-Bisphosphate
PIP3	Phosphatidylinositol 3,4,5 Trisphosphate
PKB	Protein Kinase B
PtdIns	Phosphatidylinositol
PTEN	Phosphatase And Tensin Homolog
PX	Phox Domain
QSAR	Quantitative Structure–Activity Relationship
RBD	Ras-Binding Domain
RMSD	Root Mean Square Deviation
ROC	Receiver Operating Characteristic
ROS	Reactive Oxygen Species
RPM	Rotations Per Minute
SAR	Structure Activity Relationship
SBDD	Structure Based Drug Discovery
SDS	Sodium Dodecyl Sulfate

SH2	Src Homology 2
SP mode	Standard Precision Mode
TIM	Triosephosphate Isomerase
Vps34	Vacuolar Protein Sorting Protein 34
WT	Wild Type
XP mode	Extra Precision Mode

Amino Acid Code

Amino acid	Three letter code	One letter code
Alanine	ALA	A
Arginine	ARG	R
Asparagine	ASN	N
Aspartic acid	ASP	D
Cysteine	CYS	C
Glutamic acid	GLU	E
Glutamine	GLN	Q
Glycine	GLY	G
Histidine	HIS	H
Isoleucine	ILE	I
Leucine	LEU	L
Lysine	LYS	K
Methionine	MET	M
Phenylalanine	PHE	F
Proline	PRO	P
Serine	SER	S
Threonine	THR	T
Tryptophan	TRP	W
Tyrosine	TYR	Y
Valine	VAL	V

Preface

Computational Molecular Docking in Structure Based Drug Design

The task to discover and develop safe and effective drugs takes at least 12-15 years and is usually a capital intensive process [1, 2]. As such, modern pharmaceuticals are expensive and represent a large economic burden on individuals and governments, and one that is increasing.

Computer-aided drug discovery (CADD) has gained a prominent role in drug discovery due to the potential for reduction in cost as well as time requirements involved in drug design [3-5]. In essence, predictive computational methods can provide a filter on the whole process that reduces the amount of non-productive “wet lab” research that is done.

CADD comprises a wide variety of *in silico* tools spanning almost all stages of the drug discovery process - identification of the biomolecular target, designing novel lead compounds and optimizing them to obtain better affinities and predicting toxicity or metabolism [6]. Several compounds discovered or optimized using CADD methods have been approved for clinical trials and have been recently reviewed by Sliwoski *et al.* [7].

In the design of lead compounds (i.e., chemical structures that bind and modulate the activity of the target) [8], computational approaches are well established and can be classified into two general categories: ligand-based drug design and structure (target)-based design [7]. Ligand-based design, also referred to as indirect drug design, relies on adaptation of known compounds to improve its activity without utilizing structural information regarding the target of interest [9]. Computational techniques include molecular similarity approaches, quantitative structure-activity relationships (QSAR) and the development of pharmacophore models [10, 11]. These techniques identify the attributes of the compounds that contribute to the activity based upon physiochemical properties of ligand [12]. In structure-based drug design (SBDD), the structure of the target macromolecule, usually a protein is the critical piece of information that leads the design, [13] and the huge advances in macromolecular structure determination have made SBDD a prominent feature of drug discovery programs. Techniques such as X-ray crystallography and nuclear magnetic resonance (NMR) have not only enabled experimental determination of three-dimensional protein structures alone but also in complex with small molecule ligands [14, 15] and thus have been crucial in the development of successful approaches to SBDD.

In the absence of experimentally determined structures, homology modelling is used to predict the structure of a protein of interest using a homologous protein as a template [12, 16, 17]. The template-based prediction can be achieved by various programs and servers such as MODELLER [18], SwissModel [19], Prime [20], Prism [21], and COMPOSER [22].

One of the fundamental assumptions of homology modelling is that proteins with high amino acid sequence similarity will fold into similar structures [23]; hence the quality of the homology models is reliant on the sequence identity or similarity between template protein and the target of interest. High sequence identity denotes that the two proteins may be evolutionarily related and possibly share a common three-dimensional structure. A sequence identity greater than 30% is generally considered a good starting point for homology modelling [23] and the models built on templates with sequence identity less than 15% may not be very accurate.

In addition to sequence identity, the resolution and R-factor of the template crystallographic structure and flexibility of protein (especially in the loop regions) impact on the quality of homology model. High-resolution templates generate better models than those created from lower resolution templates, even if the latter share a higher percentage sequence identity [24]. Similarly, the protein flexibility in regions like exposed loops can also affect the quality of the homology model [25]. Hence choosing the right template is critical to obtain a high-quality homology model.

The structural information of the target protein, either experimentally determined or developed *in silico* using homology modelling, provides a starting point to guide drug discovery by determining the possible binding sites and identifying novel small molecule ligands (leads) that can bind and modulate the target activity [15, 26, 27]. One of the commonly used technique to predict the interaction between small molecules in the binding site of target proteins is

molecular docking. Molecular docking can also characterize the likely binding modes of the molecule in the target site computationally [27]. In doing so, docking provides an assessment of the binding affinity of the ligand for the protein that can be used to rank the relative affinity of different conformers and different binding poses of a ligand, as well as a comparison of the affinity of different ligands. The general process of docking involves sampling of various conformations of the compound (ligand) in the active site of the target and then ranking them via a scoring function [8, 28, 29]. The score is a measure of how well the ligand binds in the target binding site and can be measured using simple energy calculations (electrostatic or van der Waals) and the binding free energy (entropy and solvation) [28, 30]. The binding free energy calculations are used to predict binding affinities of the ligands [30]. Various comparative studies have revealed that the scoring functions are often capable of identifying the correct binding pose of a ligand, however predicting the binding affinity with high accuracy still presents a challenge [29, 31]. One useful method of validation for molecular docking has been the ability for a particular docking experiment to reproduce the crystallographically determined pose of a ligand bound to its target. Over the years, many docking programs have been developed and use different scoring functions to predict the binding modes and have used various validation techniques to understand the binding affinities [32-34].

Some of the commonly used software for molecular docking include Glide [35], AutoDock [36], DOCK [37], FlexX [38], GOLD [39], LigandFit [40], FRED [41] eHiTS [42] and Surflex [43]. The docking programs differ from each other in the search algorithms employed for ligand sampling. Programs such as DOCK and

Surflex employ a simple shape-matching ligand-sampling algorithm which places the ligands complementary to the surface of the binding pocket enabling it to adopt various conformations thereby improving the computational efficiency. On the other hand, programs such as Glide, FlexX, eHiTs and FRED use a systemic search algorithm that generates various possible ligand binding conformations by exploring all degrees of freedom of the ligand. The systemic approach is generally used in conjunction with the shape matching algorithm. Aside from the shape-matching and systemic searches, the Stochastic algorithms used in GOLD and AutoDock sample various orientations and conformations of the binding ligand by making random changes to the ligand at each step and accepting the best solution based on probability.

Over the years, many new programs such as Posit [44], AMMOS [45], Dockomatic [46], AutoMap [47], RosettaLigand [48], and GalaxyDock [49] have emerged, and their applications and scoring functions have been discussed in great detail by Yuriev *et al.* [50]

Virtual screening has been a commonly used approach in the identification of new lead compounds. Docking of large virtual libraries of chemical compounds seeks to identify compounds that can bind to the target protein structure [30, 51]. This technique is used as an alternative to the physical screening of large libraries of chemicals against a biological target (high throughput screening) [52], and typically plays the role of a filter to reduce the amount of wet laboratory work to be done. Virtual screening is gaining immense popularity as a productive and cost-effective technology in the search for novel lead compounds [52]. The success and

utility of virtual screening campaigns have been subject to a range of evaluations as to the actual efficiency and predictive power. Testing a virtual screen through the use of decoy libraries spiked with known ligands provides the opportunity to test a protein model and/or docking program for their ability to identify a good proportion of the “actives” [53].

The ultimate value of SBDD techniques then comes in the ability to develop a hypothesis against which laboratory experiments are justified and may then lead to an advancement of the research problem. In rational drug design, we can expect either to have success whereby a compound of interest for further development is identified, or where improved compounds are not identified and mindful of the limitations of computer-based techniques we have further data against which to refine our models [7].

Computational Strategies in Cancer Drug Discovery

This thesis explores two distinct enzyme families that are involved in cancer and the application of computational methods to enable a deeper understanding of these molecular targets for the development of novel anti-cancer therapies. Cancer is one of the leading causes of death worldwide and Australia accounting for about 3 in 10 deaths according to Australian Institute of Health and Welfare (AIHW) (2012) [54]. Over the years, it has attracted considerable interest focusing on prevention, detection, treatment and research. Advances in technology have enabled identification of a wide range of protein targets involved in cancer. One of the first reported a census of cancer associated genes listed 291 entities that demonstrated a causal relation to the development of cancer[55]. The most recent cancer gene census lists around 572 genes that are implicated via mutation in cancer (<http://cancer.sanger.ac.uk/census>). The use of computational tools in cancer drug discovery has grown tremendously. Drugs or small molecule compounds that block the growth and spread of cancer by interfering with specific protein targets are vital for treatment of tumor progression.

Section one describes the structural studies of two distinct members of the AKR family. Aldo-keto reductases are implicated in cancer, as well as other diseases such as diabetes, depression, and asthma. The first member of AKR family described in this section is AKR1B14, a recent addition to the AKR family. The crystal structure of AKR1B14 was recently solved and suggested the importance of a non-conserved residue in coenzyme binding. The main objective of the chapter was to examine AKR1B14 mutants to structurally understand and

explain the loss of affinity of coenzyme associated with mutation of this residue. The second part of this section focusses on AKR1C3, an enzyme involved in the catalytic metabolism various steroids. While playing a key role in controlling cell growth and differentiation, it is also believed to be associated with the pathogenesis of allergic diseases such as asthma and inflammation. AKR1C3 is currently being investigated as a potential therapeutic target for the treatment of breast and prostate cancer. Computational techniques to investigate the structure-activity relationships governing AKR1C3 inhibitor affinity and selectivity have been studied as well as examining the use of virtual screening for the identification of novel ligands

Section two of this thesis involves studies that aim to identify the first potent and selective inhibitors of class II PI3Ks, with a view to examining the role of that enzyme in cancer and other diseases. Phosphatidylinositol 3-kinases (PI3Ks) are vital regulators of intracellular signaling pathways and are involved in various cellular processes. The class II PI3Ks (especially PI3KC2 β) have emerged to be signaling enzymes with potential therapeutic applications. The key objective of this study was to identify the key residues that might facilitate the development of isoform-selective inhibitors of Class II PI3Ks.

SECTION A

*Structural and Functional
Studies of Aldo-Keto
Reductases Involved in
Cancer*

Chapter 1: Introduction to the AKR Superfamily

1.1 Overview of the AKR family

The aldo-keto reductases (AKRs) represent a growing superfamily of enzymes present in bacteria, fungi, protozoans, plants and animals. AKRs are soluble, monomeric, NADPH-dependent oxidoreductases that catalyse the reversible reduction of carbonyl groups to hydroxyl groups (Figure 1-1) [56]. AKRs are involved in numerous biological processes due to their role in the metabolism of steroids, prostaglandins, carbohydrates and various endogenous substrates [56-60]. In humans, these AKRs play a critical role in bioactivation or detoxification of pharmaceutical drugs and known carcinogens [61] implicating them in various diseases such as cancer, diabetes, asthma and endometriosis.

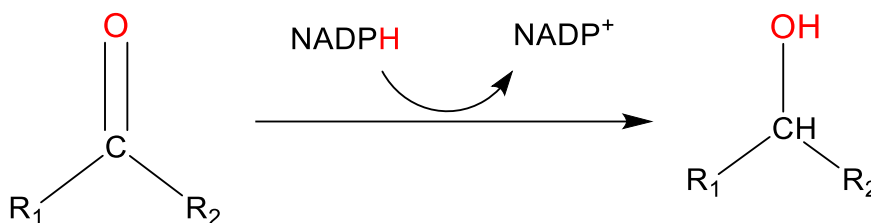


Figure 1-1: Schematic representation of the reaction catalysed by AKRs.

1.2 Classification of Aldo-Keto Reductases

Originally most of the AKR enzymes were titled after their enzymatic activity. However, as a result of their broad substrate preference Jez et al. in 1997 [56] ruled out this nomenclature system and developed a unified and systematic nomenclature system based on amino-acid sequence identity. Currently, over 150 proteins attributed to the AKR superfamily have been identified and grouped into

families based on the amino acid sequence identity. All enzymes with a predicted (α/β)₈-fold have the root name “AKR”, for aldo-keto reductase, followed by an Arabic numeral (1, 2, 3...) designating the family, a letter (A, B, C...) designating the subfamily and an Arabic numeral designating a unique sequence (Figure 1-2). Currently, there are 15 families, designated AKR1 to AKR15.

AKR	Root name
AKR1	Family name :Arabic number (enzymes exhibiting < 40% amino acid identity grouped together in the same family)
AKR1A	Sub-family name :Letter (enzymes exhibiting < 60% amino acid identity grouped together in the same sub-family)
AKR1A1	Unique Protein Sequences: Arabic number (any 2 AKRs exhibiting < 97% amino acid identity are considered alleles of the same gene unless encoded by different genes)

Figure 1-2: Nomenclature system of the AKR superfamily

1.3 General structural features

Since the determination of the first crystal structure of AKR family member AKR1B1 [62, 63], numerous crystal structure of the members of the AKR family, have been solved to help elucidate the structural features of the members of this family. All the members of AKR possess a common (α/β)₈ barrel structural motif (sometimes referred to as TIM barrel) made up of eight parallel β -strands in the core alternating with eight α -helices running anti-parallel on the surface (Figure 1-3) along with loops of varying lengths [64-67].

All members of the AKR family consist of a conserved cofactor-binding site and depend on NADPH as a cofactor for redox chemistry. The cofactor NADPH is

generally bound in an extended conformation towards the central barrel near the active site and held in place via various hydrogen bonds, salt bridges, as well as aromatic stacking interactions [62]. Binding of the cofactor induces conformational changes in one of the loops [68].

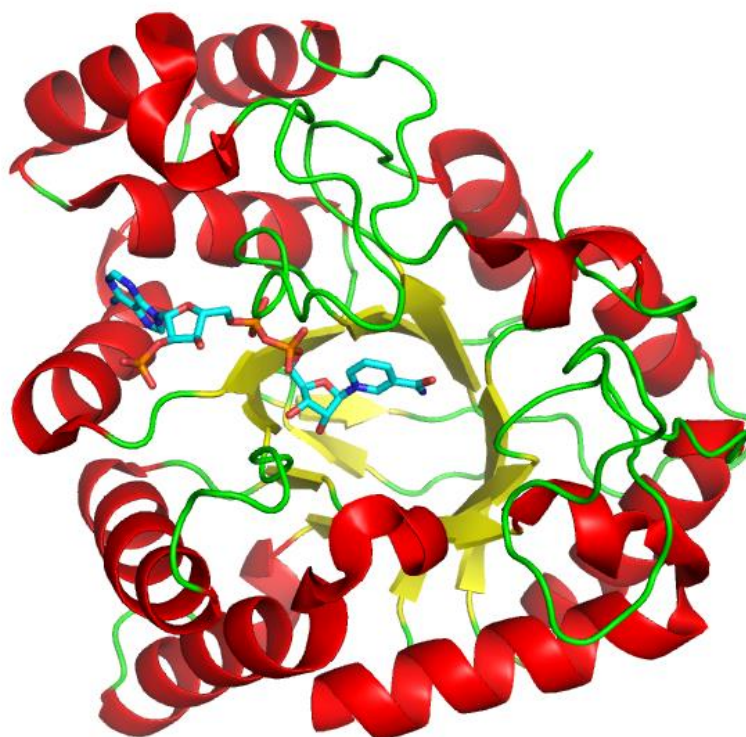


Figure 1-3: Tertiary structure of aldoketo reductases.

AKRs catalyse the oxidation and reduction of various endogenous substrates such as steroid hormones, prostaglandins, bile acids and lipid-derived aldehydes [56-60]. The substrate-binding site of AKRs is wide and consists of a deep elliptical cavity and is lined with various conserved residues. Three flexible loops surround the substrate binding pocket and accommodate various ligands and variations in the residues of the loop regions may dictate the binding modes of various substrates thus acting as selectivity determinants [64].

1.4 Members of the AKR superfamily

Many of the 150 AKR superfamily proteins are either potential therapeutic targets or of other commercial interest (Table 1-1). AKR1 family enzymes are implicated in diabetes, cancer, asthma and depression; members of the AKR2 and AKR5 families are used in the industrial production of bio-ethanol and vitamin C [69]. AKR6 family members also known as shaker channel β -subunit proteins are involved in various functions such as regulating neurotransmitter release, heart rate, insulin secretion, neuronal excitability, epithelial electrolyte transport, smooth muscle contraction, and cell volume [70]. Members of the AKR7 family are involved in detoxification of aflatoxin B1, a known potent carcinogen and also associated with hepato-carcinogenesis [71].

Table 1-1: Members of the AKR family (adapted from [60])

Family	Subfamily	Name	Function
AKR1	A	Aldehyde reductases	Metabolism of neurotransmitters; detoxification; osmoregulation
	B	Aldose reductases	Conversion of glucose to sorbitol; detoxification; retinoic acid synthesis; PGF synthase in the adrenal gland
	C	Hydroxysteroid dehydrogenases	Androgens, estrogens, glucocorticoids and progestins; PGF synthase; detoxification
	D	Δ^4 -3-ketosteroid-5 β -reductases	Bile acid synthesis and steroid hormone catabolism
	E	Mouse keto reductases	Reduction of 1,5-anhydro-D-fructose, a glycogen breakdown product, to 1,5-anhydro-D-glucitol
	G		Unknown function
AKR2	A-E	Xylose reductase	Sugar metabolism
AKR3	A-F		Metabolism of arabinose, fucose, galactose and xylose
AKR4	A-C	Chalcone polyketide reductase	Oxidation and reduction of a wide variety of substrates; stress-responsive enzymes
AKR5	A-G	2,5-diketo-D-gluconic acid reductases	Ascorbic acid synthesis; pgf synthase (pgh2 \rightarrow pgf2 α)
AKR6	A-C	Shaker channel b-subunit	B-subunits of voltage-gated potassium (kv) channels; regulate the opening of the channel
AKR7	A	Aflatoxin aldehyde reductase	Detoxification of the fungal carcinogen aflatoxin
AKR8	A	Pyridoxal reductase	Reduction of carbonyl groups in toxic compounds generated by oxidants and heavy metals; biosynthesis of secondary metabolites
AKR9	A-C	Aryl-alcohol dehydrogenase	
AKR10	A		
AKR11	A-C	Methylglyoxal reductase	
AKR12	A-C		
AKR13	A-C		
AKR14	A	<i>E. coli</i> aldehyde reductase	
AKR15	A	Pyridoxal dehydrogenase	

New members of this family are being discovered from different organisms, and it is important to characterize these proteins to gain a deeper understanding of their structural and functional role compared to other members of the AKR family. A comprehensive database of known AKR proteins is maintained at the AKR superfamily homepage (<http://www.med.upenn.edu/akr/>) [60].

1.5 Human AKRs

Mammalian AKRs are restricted to three families: AKR1, AKR6 and AKR7. AKR1 family is the largest, consisting of about 50 enzymes and encompassing 10 human AKRs.

The AKR1 family is further divided into five sub-families:

- Aldehyde reductases (ALRs) - AKR1A (AKR1A1-AKR1A4)
- Aldose reductases (ARs) - AKR1B (AKR1B1 – AKR1B15)
- Hydroxysteroid dehydrogenases (HSDs) - AKR1C (AKR1C1 – AKR1C25)
- Steroid 5 β -reductases - AKR1D (AKR1D1 – AKR1D3)
- Mouse-keto reductases – AKR1E (AKR1E1 and AKR1E2)

Aldehyde reductases (AKR1A1 and AKR1A2) and aldose reductases (AKR1B1 and AKR1B10) are associated with diabetic complications and retinopathy. The hydroxysteroid dehydrogenases (AKR1C1-4) are involved in steroid metabolism and associated with hormone-dependent and independent cancers. AKR1D1 catalyses bile acid synthesis and any discrepancies in the pathway are associated with bile acid deficiency.

1.5.1 *Members of the AKR1B subfamily*

The AKR1B subfamily is made up of 15 enzymes (AKR1B1-B15). Human aldose reductase (EC 1.1.1.21) commonly referred to as AKR1B1 or AR, was the first member of the AKR family to be crystallized and has been extensively studied due to its role in the development of secondary complications of diabetes [72-74]. AKR1B1 catalyses the reduction of a wide range of substrates [75] which is a common feature of all AKRs. AKR1B1 also functions as prostaglandin F (PGF) synthase involved in PGF₂ α production in the human endometrium [76]. AKR1B1 activity is impaired by various aldose reductase inhibitors (ARIs), and several structures have been solved in complex with these inhibitors.

Recent studies have identified aldose reductase-like proteins (ARLPs) in humans and rodent tissues exhibiting high sequence identity to AKR1B1. AKR1B10 (sometimes referred to as ARL-1), was identified by Cao *et al.* [77] and displayed 71% sequence identity to AKR1B1. AKR1B10 is associated with diverse types of human cancers by influencing cancer cell growth and survival [78].

Two AR-like proteins have also been identified in mice, namely the androgen-regulated *vas deferens* protein AKR1B7 [79, 80] and the growth factor-inducible protein AKR1B8 [80, 81] sharing 67-69% sequence similarity with AKR1B1. Both the ARLPs differ from each in substrate specificity and inhibition by ARIs. AKR1B7 exhibits prostaglandin F₂ α (PGF₂ α) synthase activity and plays an important role in steroidogenesis and lipid peroxidation; however it is insensitive to ARIs [82, 83]. While AKR1B8 is moderately inhibited by ARIs, it does not exhibit PGF₂ α synthase activity.

Recently two AR-like proteins, AKR1B13 [84] and AKR1B14 [85] were identified in rats and share high sequence identity to mouse AKR1B8 (95%) and AKR1B7 (87%), respectively. AKR1B13 and AKR1B14 are thought to be orthologues of AKR1B8 and AKR1B7. AKR1B13 exhibits similar substrate specificity and inhibitor sensitivity to the mouse AKR1B8 [86], and the enzymatic properties of AKR1B14 are equivalent to those of mouse AKR1B7.

1.5.1.1 **AKR1B14**

AKR1B14, the mouse ARLP AKR1B7 orthologue identified from the genomic and proteomic analysis of rats by Val *et al.* [85] is highly expressed in adrenal glands and female rat liver and is believed to be up-regulated by oxidative stress [87, 88]. AKR1B14 exhibits about 68% sequence identity with aldose reductase AKR1B1.

AKR1B14, however, differs from AKR1B7, in its sensitivity towards ARIs [89]. Like all AKRs, AKR1B14 is a monomer (36 kDa) which catalyses the reduction of a variety of substrates, however, it reduces 4-oxononanal, 3-deoxyglucosone and lipid peroxidation products more efficiently than other ARLPs [89]. Additionally, AKR1B14 exhibits low K_m values (0.14 μ M) for the coenzymes, particularly, NADP⁺ [89, 90]. AKR1B14 exhibits PGF2 α synthase activity just like its orthologue AKR1B7 and is considered to play a role in the detoxification of the reactive carbonyl compounds generated from lipid peroxidation and glycation via PGF2 α synthase activity [82, 89, 91].

AKR1B14 is specifically and significantly activated by bile acids (10-fold higher) compared to other mammalian aldose reductases and ARLPs [90].

AKR1B14 is also inhibited by various ARIs such as minalrestat, epalrestat, tolrestat and zopolrestat, with IC₅₀ values in micromolar ranges respectively [92]; however, the structural basis for its inhibition remains unknown.

The recently solved crystal structure of AKR1B14 in complex with NADPH revealed the importance of a critical His269 that is involved in coenzyme binding [93]. The histidine residue H269 π -stacks with the adenosine moiety of NADPH and also hydrogen bonds with the 2'-phosphate group of NADPH locking it tightly in place. Sequence comparison of the members of the AKR1B subfamily (1B1, 1B7, 1B8, 1B10, 1B13 and 1B14) revealed that of the 17 residues that are involved in the cofactor NADPH-binding, 16 residues are conserved; however His269 of AKR1B14 is replaced by Arg in the other enzymes. Site-directed mutagenesis of His269 to Arg (the corresponding residue of AKR1B1 and other AR-like proteins), Phe (without a positively charged side-chain) and Met (without both aromatic and positively charged side-chain) decreased the affinity for the coenzyme suggesting a crucial role of His269 in the coenzyme binding [93].

1.5.2 *AKR1C subfamily*

The members of the AKR1C are generally referred to as hydroxysteroid dehydrogenases (HSDs) due to their role in steroid metabolism by converting active steroid hormones to their less active counterparts and vice versa [94].

Among all the members of the AKR1C subfamily, four isoforms are found in humans and regulate the activity of sex steroid hormones (such as androgens, estrogens and progestins), and any imbalance in the regulation of these steroid hormones has been implicated in the development of hormone-dependent cancers [95, 96]. The four isoforms, namely AKR1C1 (also known as 20 α -HSD), AKR1C2 (or type 3 3 α -HSD), AKR1C3 (or type 2 3 α -HSD, type 5 17 β -HSD) and AKR1C4 (or type 1 3 α -HSD) share around 80% sequence identity [97].

The four isoforms are predominantly expressed in the liver, prostate, breast, endometrium except AKR1C4 that is restricted to the liver. All of the four isoforms catalyse the oxidation/reduction of various steroid substrates at the C3, C17 and C20 positions. Comparison of catalytic efficiencies of these isoforms revealed that AKR1C1 mostly exhibits a 20-ketosteroid reductase activity, AKR1C2 and AKR1C4 both exhibit 3-ketosteroid reductase activity and AKR1C3 exhibits not only 3-ketosteroid reductase activity but also significant 17-ketosteroid reductase activity [98].

1.5.2.1 *AKR1C3 and its role in hormone-related cancers*

AKR1C3 (EC 1.1.1.213) is a 37kDa protein involved in the catalytic metabolism of androgen, estrogen, progesterone and prostaglandins [99-101]. AKR1C3 is currently being investigated as a potential therapeutic target for the treatment of cancer.

Many cancers such as breast, endometrium, ovary, prostate cancer are hormone - driven. Currently, prostate and breast cancers are the second leading cause of cancer-related deaths in males and females, respectively [102-104]. Most common treatments for metastatic prostate cancer include androgen-deprivation therapy, administration of drugs that prevent angiogenesis or in most cases orchiectomy (removal of testicles) and anti-estrogen therapy or mastectomy for breast carcinoma [103, 105]. Although the treatments provide initial benefit and reduce tumours; in some cases cancer relapses in an aggressive form. The aggressive form of tumours, especially in males with prostate cancer, develop resistance to the therapies and hence referred to as castration-resistant prostate cancers (CRPCs) [103, 105-107]. There is a great need to develop new approaches to treating or preventing the hormone-dependent or -independent cancers and their progression.

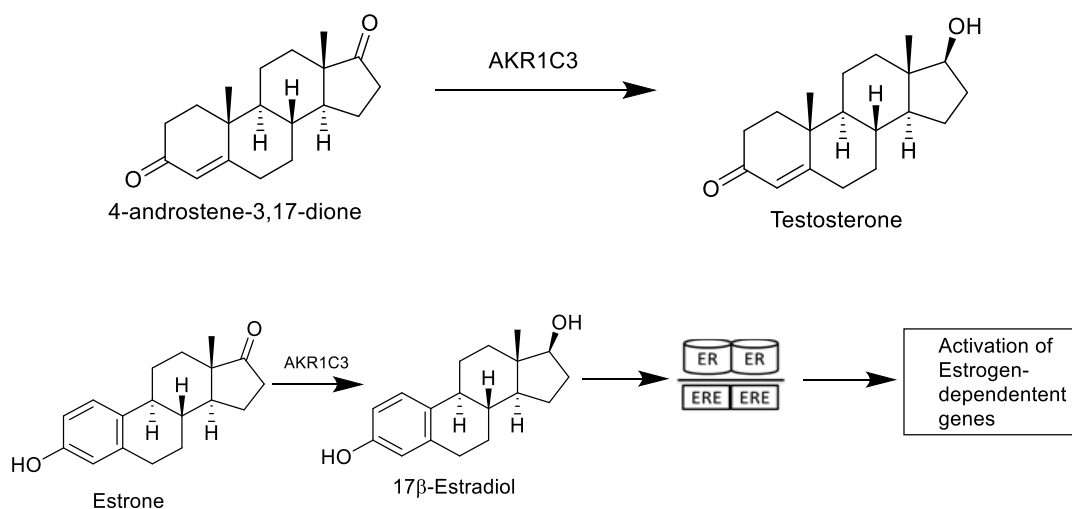


Figure 1-4: Reduction of Estrone to 17β-Estradiol and 4-androstene-3,17-dione to testosterone by AKR1C3 (ER- estrogen receptor, ERE- estrogen response element).

AKR1C3 via its 17β-hydroxysteroid dehydrogenase activity can produce testosterone and 17β-estradiol (Figure 1-4) by reducing the androgen precursor (4-androstene-3,17-dione) and estrone, respectively [108]. The conversion of weak to more potent hormones leads to specific receptor activation resulting in tumour progression.

In vitro studies have shown that overexpression of AKR1C3 leads to increased intra-prostate testosterone that consecutively enhances androgen receptor activation thus promoting cellular proliferation and angiogenesis [109-114]. Reduction of estrone, to 17β-estradiol and progesterone to 20α-hydroxyprogesterone by AKR1C3 enhances estrogen receptor trans-activation and reduces the progesterone receptor trans-activation thereby stimulating the proliferation of mammary cells, leading to ER-positive breast cancer [115-117]. Studies have also revealed that AKR1C3 is highly up-regulated in breast cancer cells. Although the exphysioact logical role of AKR1C3 in breast cancer has not

been determined, it is hypothesized that the reduction of estrone to 17 β -estradiol confers a proliferative advantage to breast cancer cells [118-120]. Thus, AKR1C3 is regarded as a potential anti-cancer drug target in both CRPC and ER-positive breast cancer it is imperative to study in detail the structure-function relationship of this enzyme.

Unlike other members of the AKR1C subfamily, AKR1C3 also consists of Prostaglandin F synthase activity and reduces prostaglandins that are generally associated with luteolysis and parturition [121, 122]. AKR1C3 reduces PGH₂ and PGD₂ to PGF₂ α and 9 α ,11 β -PGF₂, respectively [100, 101, 112, 121, 123]. The by-product 9 α ,11 β -PGF₂ exhibits potent broncho-constrictive activity and the levels of 9 α ,11 β -PGF₂ was found to be enhanced in the plasma and urine of the patients suffering from mastocytosis and bronchial asthma [124-128]. Although there is some evidence pointing towards the involvement of AKR1C3 in asthma and mastocytosis, its exact role in the pathogenesis of the disease is yet to be determined.

1.5.2.1.1 *Structural insights into the mode of binding of substrates and inhibitors of AKR1C3*

Like most members of the AKR superfamily, AKR1C3 is made up of $\alpha_8\beta_8$ TIM barrel consisting of eight parallel β -strands in the core alternating with eight α -helices running anti-parallel on the surface. Four large loops are involved in the formation of the substrate and cofactor binding site at the C-terminal end of the $\alpha_8\beta_8$ superbarrel namely, loop-A (residue 24–33), loop-B (residue 117–143), loop-C (residue 217–238), and loop-D (residue 301–323) which connect each β -strand to a

α -helices; thereby allowing the amino acid side-chains to extend into the active site [67, 121, 129].

The C-terminal end of the barrel forms an elliptical cavity for the cofactor nicotinamide ring of NADP⁺ to bind in an extended conformation across the $\alpha_8\beta_8$ barrel. The NADP⁺ is held tightly in place via safety belt formed by 17 residues [129]. The substrate binding site is situated adjacent to the nicotinamide ring of the NADP⁺ and is mainly made up of hydrophobic and aromatic amino acid side-chains that extend into the pocket. The hydrophobicity and flexibility of this pocket allow the binding of different substrates including the steroids [67, 129].

To date, there are more than twenty crystal structures available in the Protein Data Bank (<http://www.rcsb.org>) and the majority of them are complexed with the cofactor NADP⁺ and various inhibitors. The inhibitor binding pocket is comparatively large and is further divided into several sub-sites comprising of an oxyanion site, a steroid channel, and three sub-pockets (SP1, SP2 and SP3) [121, 129]. The oxyanion site is made up of four conserved amino acids Asp50, Tyr55, Lys84, and His117, which form the catalytic tetrad and the cofactor NADP⁺. The general catalysis involving the oxidation of alcohols and the reduction of ketones functional groups is the result of the push-pull mechanism of a catalytic tetrad and the nicotinamide ring of coenzyme NADP⁺. The functional group (carbonyl group or carboxylic acid or hydroxyl group) of the ligands are involved in strong hydrogen bonds with either His117 or Tyr55, which is vital for effective inhibitor binding. Although the steroid channel particularly does not play a major role in

inhibitor binding, it is believed to accommodate various steroids that occupy the binding pocket [130].

The residues that line the three sub-pockets are believed to play a central role in defining the inhibitory potency and selectivity of the inhibitors. Sub-pocket 1 (SP1) is made up of the residues Ser118, Asn167, Phe306, Phe311, and Tyr319. Many of the inhibitors extend into the inhibitor pocket. The SP2 sub-pocket constitutes of residues Trp86, Ser129, Trp227 and Phe311. The SP2 pocket is specific to only a few inhibitors, however, steroids and prostaglandins prefer binding in this pocket. The SP3 sub-pocket is large and is occupied by few ligands as it surrounds the oxyanion site and is lined by the residues Tyr24, Glu192, Ser217, Ser221, Gln222, Tyr305, and Phe306. A few key residues W227, F306, and F311 exhibit high flexibility due to their ability to undergo various conformations and allow ligands to bind via “induced fit” models [129, 130].

1.5.2.1.2 ***Rationale for development of AKR1C3 inhibitors***

AKR1C3 has attracted interest as a potential therapeutic target for the treatment of both hormone-dependent and hormone-independent cancers. Many small molecule inhibitors have been identified and tested against AKR1C3. A study by Byrns *et al.* [130] has revealed that AKR1C3 is inhibited by numerous compounds including the non-steroidal anti-inflammatory drugs (NSAIDs), steroids, cinnamic acids, flavonoids, cyclopentanes and benzodiazepines. Structures of some of the representative compounds from each known class of inhibitors (Figure 1-5) and their potency towards AKR1C isoforms are discussed below.

Non-steroidal anti-inflammatory drugs (NSAIDs) are widely recognised for their anti-inflammatory and analgesic action and have recently been investigated for their AKR1C3 inhibition [115].

Among the known NSAIDs, N-phenylanthranilic acids are the most potent inhibitors of AKR1C3 and do not exhibit inhibitory potencies towards cyclooxygenase (COX) enzymes which are generally targeted by most NSAIDs [131, 132]. Flufenamic acid ($IC_{50} = 51\text{nM}$), an N-phenylanthranilic acid NSAID inhibitor of AKR1C3 was first described by Lovering *et al.* [67], however, it lacked selectivity towards AKR1C3. A study by Byrns *et al.* [117] also identified mefenamic acid as an AKR1C3 inhibitor with an IC_{50} of $0.7\text{ }\mu\text{M}$, however it also inhibited the other two AKR1C human isoforms (AKR1C1 and AKR1C2). Tolfenamic acid was first described by Endo *et al.* [133] and remains to be the most potent AKR1C3 inhibitor and exhibits 11-fold selectivity compared to flufenamic acid.

Another inhibitor indomethacin ($IC_{50} = 2.3\text{ }\mu\text{M}$) was found to be selective towards AKR1C3 over AKR1C1 and AKR1C2; however was not as potent as mefenamic acid. N-(4-chlorobenzoyl)-melatonin (CBM), an analogue of Indomethacin, was developed by Byrns *et al.* [111] was found to be both potent with a K_i of $3.4\text{ }\mu\text{M}$ and selective for AKR1C3.

Medroxyprogesterone acetate (MPA) and estrogen lactones such as EM 1404 are steroidal analogues of substrates of AKR1C3 and were also found to inhibit AKR1C3 with high inhibitory potencies. However, the selectivity of these steroidal analogues is still unknown [134, 135].

Another promising class of AKR1C3 inhibitors are flavonoids and cinnamic acids. 3-Hydroxyflavone potently inhibits AKR1C3 ($IC_{50} = 300$ nM) and was found to be highly selective towards AKR1C3. However, due to off-target inhibition of other enzymes in vivo, they may not be ideal drug candidates [130, 136, 137]. Propolis, a resinous product present in various plant sources is used as a sealant by the honeybees for their hives and is also believed to have anti-inflammatory properties. The ethanolic extract of Brazilian propolis contains three prenylated cinnamic acid derivatives, namely artepillin C, baccharin and drupanin. Artepillin C has been studied extensively for its role in anti-cancer therapy [138]. Drupanin and baccharin have gained attention recently for their anti-tumour properties [139]. A recent study by Endo *et al.* [140] has identified baccharin to be the selective and potent inhibitor of AKR1C3, with an IC_{50} value of 0.11 μ M.

Cyclopentane based inhibitors have also been explored as AKR1C3 inhibitors since cyclopentane ring is a key structural feature in prostaglandins. Bimatoprost and Jasmonic acid, structural analogues of prostaglandin $F_{2\alpha}$ and plant prostaglandins inhibited AKR1C3 in the low micromolar ranges; however the selectivity of both these compounds are yet to be tested [141].

Benzodiazepines such as diazepam (Valium), cloxazolam were also explored for AKR1C3 inhibition. Cloxazolam was found to be relatively potent with a $K_i = 1.5$ μ M and also selective towards AKR1C3; however, due to major side-effects these drugs are not preferred [142].

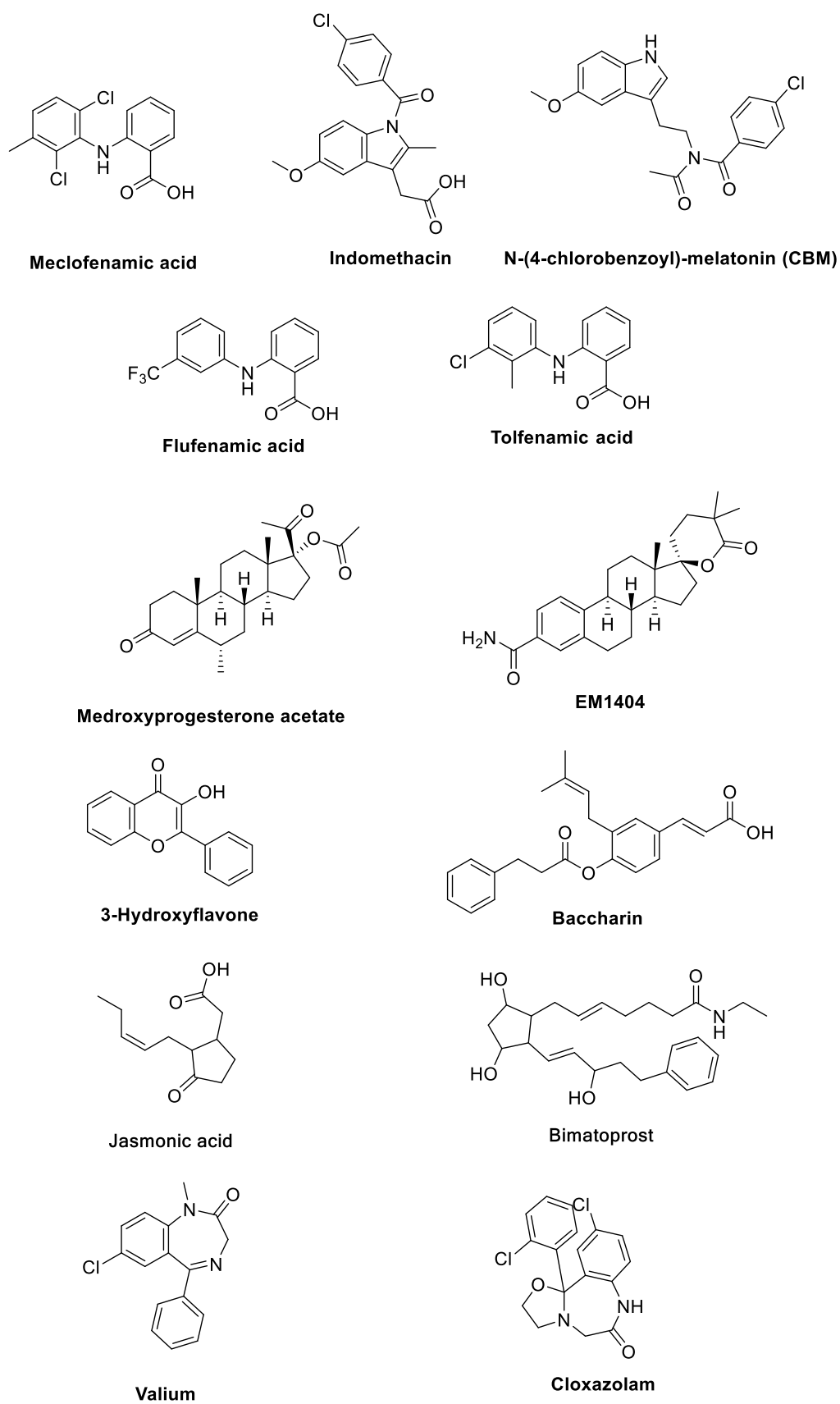


Figure 1-5: Representative AKR1C3 inhibitors

1.6 Aims and Rationale

Understanding the structural features of the members of the AKR family and characterising the binding mode of various substrates and inhibitors within the active site may facilitate the development of novel therapeutics. This section focusses on two particular members of the aldo-keto reductase family: AKR1B14 and AKR1C3.

As described earlier, an aldose reductase-like protein, AKR1B14 was recently identified using proteomic and genomic analyses in rats and is an orthologue of human AKR1B1. The recently solved crystal structure of AKR1B14 in complex with NADPH revealed the importance of a critical His269 that is involved in coenzyme binding [93]. Sequence comparison of other members of the AKR1B subfamily (1B1, 1B7, 1B8, 1B10, 1B13 and 1B14) revealed that His269 of AKR1B14 is a non-conserved residue replaced by Arg in the other enzymes. Site-directed mutagenesis of His269 decreased the affinity for the coenzyme suggesting a crucial role of His269 in the coenzyme binding. The main objective of this study was to validate the importance of this non-conserved residue H269 in coenzyme binding using X-ray crystallography and molecular docking.

Inhibition of AKR1C3 presents an approach to treating hormone-dependent cancers. To date various potent inhibitors have been tested against AKR1C3 [143]; however, only a handful are specific to AKR1C3 (such as baccharin and tolfenamic acid). The high structural similarity of AKR1C3 to the other human AKR1C isoforms (AKR1C1, AKR1C2 and AKR1C4) presents a major challenge in the design of selective inhibitors targeting the types of cancers linked to AKR1C3 that

need to be addressed. Thus, the rationale behind this study was to examine the use of molecular docking as a tool to identify the key determinants that dictate the isoform selectivity and for developing novel, potent and selective inhibitors of AKR1C3.

Methodology

2.1.1 Biochemical analysis

2.1.1.1 Crystallization studies

The AKR1B14 His269Arg mutant enzyme was obtained from Prof. Hara's Lab (Gifu University, Japan) and the purity was confirmed by SDS-PAGE for further crystallographic studies. Crystals of the AKR1B14 His269Arg binary complex were grown using the hanging-drop vapour diffusion method in a crystallization buffer consisting of 0.1 M HEPES pH 7.5, 20% polyethylene glycol 4000 and 5% 2-propanol (optimization of Hampton Research Crystal Screen condition No. 41) at 295 K as described previously [93]. Briefly, the protein and NADPH were mixed in a 1:3 molar ratio and the final concentration of the protein in the binary complex was 22.6 mg/mL. Droplets consisting of 2 μ L of the binary complex solution mixed with an equal volume of crystallization buffer were placed on siliconized coverslips and equilibrated at 295 K against 1 mL crystallization buffer in the well. Within one week, crystals were observed with a maximum dimension of approximately 0.2 mm. The crystals were found to be isomorphous to the crystals of wild-type AKR1B14. Crystals selected for X-ray diffraction analysis were soaked in a cryoprotectant solution consisting of 20% glycerol in the crystallization buffer and then flash cooled at 100 K.

2.1.1.2 *X-ray data collection and structural determination*

X-ray diffraction data were collected in-house at 100 K on an MAR 345 image plate mounted on a Rigaku RU-300 rotating anode generator (operating at

50 kV and 90 mA). The exposure time (10 min), oscillation range (1°) and crystal-to-detector distance (150 mm) were adjusted to optimize data collection and obtain well-resolved spots. X-ray diffraction data were collected from a single crystal which diffracted to 1.87 Å resolution, and the data were processed using HKL-2000 and SCALEPACK [144]. Auto-indexing of the data confirmed that the mutant enzyme crystallized in the monoclinic space group P21, with unit-cell parameters $a = 50.85$, $b = 69.30$, $c = 87.95$ Å, $[\beta] = 96.0^\circ$. The Matthews coefficient (VM) was calculated to be $2.13 \text{ Å}^3 \text{ Da}^{-1}$, with an estimated solvent content of 42% [145].

The crystal structure of the AKR1B14 His269Arg mutant in complex with NADPH was determined by molecular replacement using MOLREP from the CCP4 suite of crystallographic programs [146]. The atomic coordinates of wild-type AKR1B14 (PDB code:3O3R; [93]) were used as the search model, excluding the coenzyme and solvent molecules. The rotation and translation functions of MOLREP identified two molecules per asymmetric unit. The initial model was subjected to rigid-body refinement, which produced a well-defined $F_o - F_c$ difference electron-density map for the coenzyme. The two NADPH molecules were fitted into the electron density using Coot, and the structure was refined using REFMAC5 [147]. This was followed by iterative cycles of manual fitting of amino-acid side chains and solvent molecules into $2F_o - F_c$ and $F_o - F_c$ difference electron-density maps and the structure after refinement was validated using PROCHECK [148].

2.1.2 *Computational studies*

2.1.2.1 *Sequence comparison*

Protein sequences of the four human AKR1C isoforms were retrieved from the UniProtKB database (www.uniprot.org/). Clustal Omega [149] was used to align the sequences to determine percentage identity as well as study the alignment.

2.1.2.2 *Molecular docking studies*

Molecular docking simulations were carried out using Glide (version 5.0) in the Maestro interface version 8.5. (Schrödinger, LLC, NY) Unless otherwise identified, the default settings for all programs were employed. The atomic coordinates of structures were obtained from the RCSB Protein Data Bank (<http://www.rcsb.org>) (AKR1C1 – PDB: 3NTY [150]; AKR1C2 – PDB: 4JTR [to be published, DOI:10.2210/pdb4jtr/pdb], AKR1C3- PDB code 1S2C; [67] and AKR1C4 – PDB: 2FVL [to be published, DOI:10.2210/pdb2fvl/pdb]). Apart from the cofactor NADPH, any other ligands present were deleted and the binary structure prepared using the Protein Preparation module in Maestro which optimizes the geometry of the amino acid residues. In order to eliminate any potential bond length and bond angle biases in the structures, all of the ligands used in the studies were subjected to full minimization prior to the docking using LigPrep. The ligands were docked using the “Extra Precision” (XP) mode of Glide using flexible ligand sampling which allows the ligand to be flexible and rearrange its conformation in response to the receptor [65]. The docked compounds were then examined visually in greater detail using the Pose Viewer module of Maestro. The

top scoring pose was selected in all of the docking experiments. The figures showing the docked model were generated using PyMOL (DeLano Scientific).

2.1.2.3 *In silico mutagenesis*

Residues were mutated using Coot [151] and then processed and energy-minimized using the Protein Preparation module in Maestro (Schrodinger, LLC, Portland, OR) software package Version 8.5 using the “Refinement Only” option which optimizes the hydroxyl and thiol torsions and performs an all-atom constrained minimization to relieve any existing clashes. The structure was further refined by optimizing the hydrogen bonding network and the orientation of protonated residues and then subject to a restrained minimization using IMPREF with the default force field option (OPLS2005).

2.1.2.4 *Analysis of model performance using ROC curves*

The crystal structures were obtained from the RCSB Protein Data Bank and pre-processed using the Protein Preparation module in Maestro. The active compounds were prepared using LigPrep. Multiple tautomers and/or protonation states for each compound were generated within specified pH range (default setting: pH 7 \pm 2) in the Ionizer option in LigPrep. A set of 1,000 drug-like decoy compounds was obtained from Schrodinger library available for free downloaded from <http://www.schrodinger.com/>. The drug-like decoy set was prepared in the same way as the active compounds, including generation of multiple tautomeric forms and ionization states. Virtual screening was carried out with 26 active compounds (structures in Appendix 4) along multiple tautomeric and ionization states for each of the decay compounds. The docked compounds were ranked and

scored using GlideScore. Best scoring (lowest GlideScore) tautomer/ionization state of each compound was retained.

Analysis of model performance was carried out using Receiver operating characteristic (ROC) curves, and the performance of each crystal structure was compared. ROC curves were plotted using Microsoft Excel where the percentage rank of true positives (actives found) was plotted on the Y-axis against the percentage rank of false positives (decoys found) on the X-axis. The area under the ROC curve (AUC) was used to measure the overall performance of each model.

Results and Discussion

3.1 Structural studies of AKR1B14 His269Arg mutant

AKR1B14, a recent addition to the AKR1B subfamily has gained interest due to its PGF2 α synthase activity that is associated with luteolysis and parturition in mammals and also its broad substrate specificity [61, 91]. The crystal structure of AKR1B14 has been recently solved revealing the importance of a unique electrostatic and π -stacking interaction between the non-conserved residue His269 of AKR1B14 and the coenzyme NADPH [93]. Site-directed mutagenesis studies of this His269 to an arginine residue (corresponding residue in AKR1B1) in AKR1B14 had a significant effect on coenzyme binding (NADPH) leading to an increase in the K_m values. In an earlier study [93], site-directed mutagenesis of His269 in AKR1B14 to Arg showed a more than fourfold increase in the K_m value for NADPH compared to the wild-type enzyme (Table 3-1). Other mutations with Phe and Met residues also showed a decreased binding affinity.

Table 3-1: Site mutagenesis of His269 revealed the increase in binding affinity of NADPH. The values in parentheses represent fold increase in binding affinity compared to wild type (WT).

	WT	His269Arg	His269Phe	His269Met
K_m NADPH (μM)	1.5 ± 0.1	6.2 ± 0.5 (4)	10 ± 1 (7)	185 ± 13 (127)

This study was aimed to solve the crystal structure of the mutants in order to examine the structural differences in coenzyme binding. This study has been published and is attached as Appendix 1.

3.1.1.1 *Structure of the His269Arg mutant*

AKR1B14H269R was expressed by our collaborators (Akira Lab, Gifu University). The pCold IV expression plasmid (Takara) harbouring the cDNA for the His269Arg mutant enzyme was used to transform *Escherichia coli* BL21 (DE3) pLysS cells to express AKR1B14H269R and purified to homogeneity using three column chromatography steps (Q-Sepharose column (2 cm × 40 cm), Sephadex G-100 column (2.5 cm × 90 cm) and Red-Sepharose column (1.5 cm × 5 cm) in 10 mM Tris-HCl buffer, pH 8.0, containing 5 mM 2-mercaptoethanol, 0.5 mM EDTA and 20% (v/v) glycerol.

The obtained purified protein was used to set up crystals of the AKR1B14H269R-NADPH binary complex using the hanging drop vapor diffusion method in a crystallization buffer containing 0.1 M HEPES pH 7.5, 20% polyethylene glycol 4000 and 10% 2-propanol (optimization of Hampton Research Crystal Screen condition No. 41).

The crystal structure of the AKR1B14 His269Arg mutant in complex with NADPH was refined at 1.87 Å resolution with a final R cryst of 16.4% and R free of 23.2%. The backbone dihedral angles of 92% of the residues were in the favoured regions, and the remaining 8% were in the allowed regions of the Ramachandran plot. A summary of the data collection and refinement statistics is presented in Table 3-2.

The overall structure of the mutant protein was identical with AKR1B14 wild type (PDB: 3O3R) with an RMSD of 0.216 Å. The residues that participated in interactions with the NADPH cofactor were found to be identical to those observed in the AKR1B14 wild-type structure (PDB:3O3R). The side chain of the mutated Arg269 formed ionic interactions with the 2'-phosphate group in addition to the stacking interaction of its guanidinium group with the adenine ring of the NADPH analogous to the His residue in the wild-type (Figure 3-1).

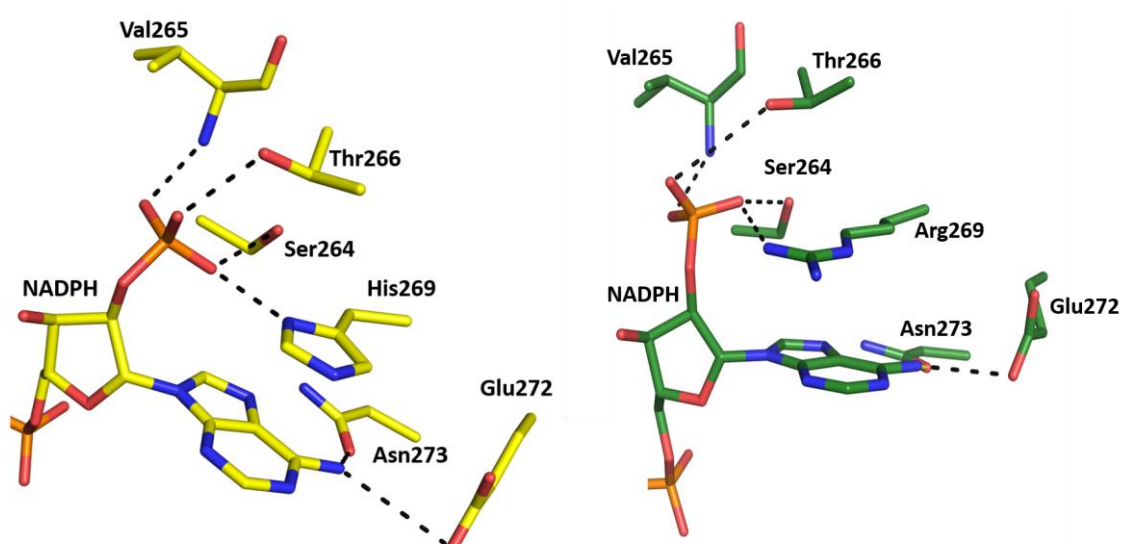


Figure 3-1: Interactions of the AKR1B14 wild type and AKR1B14 His269Arg mutant. Both AKR1B14 wild type (left) and AKR1B14 His269Arg mutant (right) make similar interactions with NADPH. Hydrogen bonds and ionic interactions formed by both are represented by black broken lines

Table 3-2: Data collection and refinement statistics. Values in parentheses are for the highest resolution shell.

Data collection and processing	
Space group	$P2_1$
Unit-cell parameters (Å, °)	$a = 50.85, b = 69.30, c = 87.95, \alpha = 96.0$
Radiation source	Rotating anode
Wavelength (Å)	1.54178
Diffraction data	
Resolution (Å)	30-1.87 (1.91-1.87)
No. of unique reflections (possible)	48259 (4159)
No. of unique reflections (measured)	46136 (3581)
Multiplicity	3.4 (2.8)
Completeness (%)	95.6 (86.1)
$\langle I/\sigma(I) \rangle$	20.8 (5.4)
R_{merge} (%)	3.7 (11.6)
Refinement statistics	
Resolution (Å)	30-1.87
Protein residues	630
Solvent molecules	668
NADPH molecules	2
R_{free} (%)	23.2
R_{cryst} (%)	16.4
R.M.S.D	
Bonds (Å)	0.021
Angles (°)	1.7
Ramachandran plot, residues in (%)	
Most favoured regions (%)	92
Allowed regions (%)	8
Luzzati mean coordinate error (Å)	0.21
Mean B factors (Å²)	
Protein	17.4
NADPH	16.2

The crystal structures of the AKR1B14 His269Arg mutant and AKR1B1 (PDB entry: 1PWL) complexed with NADPH [152], were also compared. The orientations of the Arg residues and adenosine 2'-phosphate moieties of NADPH were basically identical (Figure 3-2).

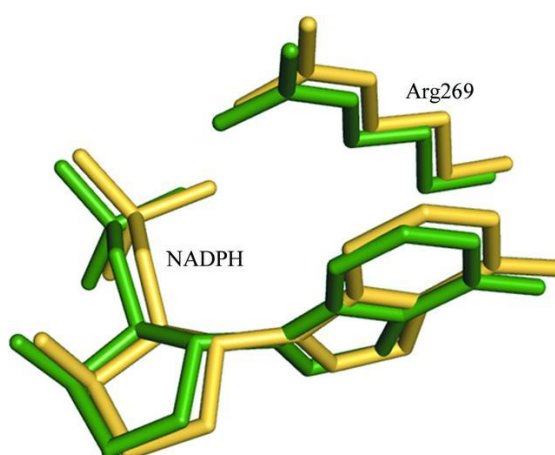


Figure 3-2: Superimposition of the crystal structures of the AKR1B14 His269Arg mutant (green) and AKR1B1 (gold) in the vicinity of the adenosine 2'-phosphate moiety of NADPH, showing the corresponding Arg269 side chains. The R.M.S.D. of non-H atoms was 0.52 Å.

The present crystal structure confirmed that the decrease in affinity on mutation arises from alteration of the interaction between the adenine ring of NADPH and the imidazole ring of His269 observed in the structure of the wild-type enzyme. His269 in the AKR1B14 wildtype forms π -stacking and π -cation interactions with adenine ring. The guanidium group in the Arg mutant can only form the π -cation and not the π -stacking interactions, which may explain the decrease in affinity of NADPH.

3.1.1.2 *Molecular docking studies in other mutants*

Molecular modelling studies were carried out to study the changes in NADPH K_m due to the other in vitro mutations AKR1B14His269Phe and AKR1B14His269Met described above (Table 3-4) [93] (due to difficulties in obtaining the crystals of AKR1B14His269Phe and AKR1B14His269Met).

In the model of His269Phe mutant AKR1B14, the phenyl ring of the mutated Phe269 was found to be oriented in a similar manner to the His269 imidazole ring of the AKR1B14 wild-type structure forming a π -stacking interaction with the adenine ring of the NADPH (Figure 3-3). However, the side chain of Phe269 lacked the additional hydrogen-bond interaction observed in the wild-type AKR1B14 between the 2'-phosphate group of NADPH and the ND1 of the imidazole ring of His269. This may serve to explain the sevenfold increase in the K_m value for NADPH for this mutant as previously described in the earlier mutagenesis studies [93].

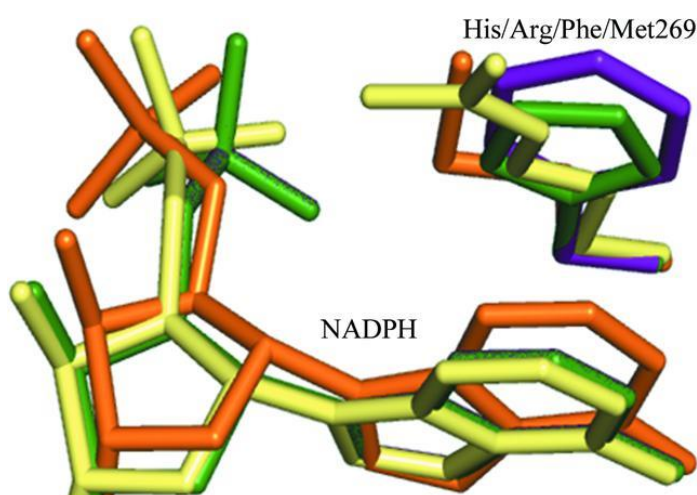


Figure 3-3: Superimposition of the models of wild-type (green), His269Arg (yellow), His269Phe (purple) and His269Met (orange) AKR1B14 in the vicinity of the adenosine 2'-phosphate moiety of NADPH. For clarity, only the corresponding side chains at position 269 are shown.

The energy-minimized structure of the AKR1B14 His269Met mutant illustrated that the largest loss in affinity for NADPH arising from the mutation resulted from the loss of both hydrogen-bonding and π -stacking interactions between His269 of the wild-type AKR1B14 and the coenzyme. Interestingly, the replacement of His269 in the wild-type enzyme by the non-aromatic residues Arg or Met, resulted in a shift in the 2'-phosphate group of the coenzyme, while the orientations of the coenzyme in the wild-type and His269Phe structures were virtually superimposable.

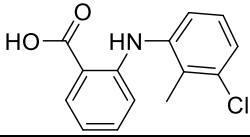
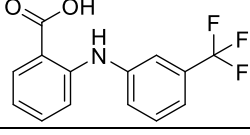
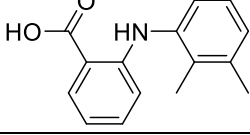
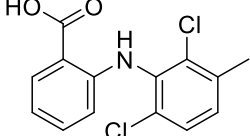
In summary, previous crystallographic and modelling studies of the binding of coenzyme to AKR1B14 confirmed that the π -stacking interaction between the imidazole ring of the nonconserved His269 and the adenine ring of the coenzyme and the hydrogen bond between ND1 of His269 and the 2'-phosphate group of the coenzyme are both important for binding of the coenzyme. While the replacement of His269 by Arg resulted in a fourfold increase in the K_m value for NADPH, the loss of the hydrogen-bond interaction in the His269Phe mutant and both π -stacking and hydrogen-bond interactions in the His269Met mutant were responsible for the sevenfold and 127-fold increases in the K_m value, respectively. Our models may serve to understand the underlying reasons for the increase in the K_m values and support the important role of nonconserved His269 in coenzyme NADPH binding.

3.2 Why is tolfenamic acid a potent and selective inhibitor of AKR1C3?

Non-steroidal Anti-inflammatory Drugs (NSAIDs) have been long investigated as potential inhibitors of AKR1C3. Many NSAID inhibitors have been found quite effective in the treatment of cancer and inhibit AKR1C3 with similar potencies [143, 153]. N-phenylanthranilic acids, the first described potent inhibitors of AKR1C3, are not very selective inhibitors of AKR1C3 [143]. The first described crystal structures of AKR1C3 bound to NSAID inhibitors flufenamic acid (PDB:1S2C) and indomethacin (PDB:1S2A) [67] have enabled rational design of inhibitors for AKR1C3. To date many analogues of flufenamic acid have been developed, however, none of them are selective towards AKR1C3 (Table 3-3).

Tolfenamic acid, an NSAID used to treat migraines is a structural analogue of flufenamic acid. In a recent study by Akira Hara's group (Gifu University Japan), it was revealed that tolfenamic acid was found to be three times more potent than flufenamic acid [133]. It was also observed that tolfenamic acid was 10-fold selective towards the AKR1C3 isoform. This study focused on studying the underlying structural reasons for the high potency of tolfenamic acid and also its selectivity towards AKR1C3 using *in silico* approaches.

Table 3-3: N-phenylanthranilic acid inhibitors of AKR1C3. Where the IC₅₀ values were not available it is represented by N.D.

Inhibitor	Structure	IC ₅₀ value (μM)			
		AKR1C1	AKR1C2	AKR1C3	AKR1C4
Tolfenamic acid [133]		0.71	0.57	0.017	53
Flufenamic acid [67]		N.D	0.37	0.051	N.D
Mefenamic acid [154]		N.D	N.D	0.3	N.D
Meclofenamic acid [154]		N.D	N.D	0.7	N.D

3.2.1.1 *Molecular docking of Tolfenamic acid in AKR1C3*

Tolfenamic acid was docked in the active site of the crystal structure of AKR1C3-NADPH-flufenamic acid complex (PDB: 1S2C). The top ranking pose was selected and compared with the crystal structure of AKR1C3 in complex with flufenamic acid [67]. It was found that tolfenamic acid adopts a similar pose to flufenamic acid in the active site of AKR1C3 with an RMSD of 1.78 Å (Figure 3-4).

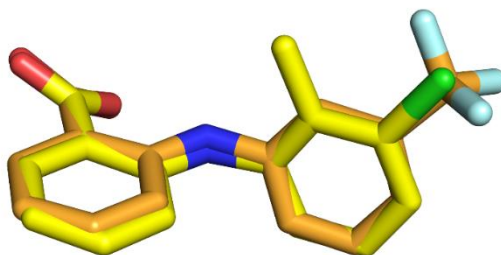


Figure 3-4: Docked pose of tolfenamic acid (yellow) superimposed on the crystal structure of AKR1C3 in complex with flufenamic acid (orange).

Tolfenamic docks adjacent to the nicotinamide ring of the cofactor, with the benzoic acid ring binding in a similar position as the benzoic acid ring of flufenamic acid. The carboxylic acid of tolfenamic acid interacts with the active sites residues Tyr55 and His117 and forms strong hydrogen bonds with both the residues (Figure 3-5). The similarities of the binding pose are consistent with the similar IC_{50} values towards AKR1C3 of 17 nM and 51 nM for tolfenamic acid and flufenamic acid, respectively. The recently available crystal structures of the other N-phenylanthranilic acids Mefenamic acid (PDB:3R43) and Meclofenamic acid (PDB:3R6I) were compared with the docking output of tolfenamic acid in AKR1C3 and it was observed that tolfenamic acid a similar binding pose to the other N-phenylanthranilic acid inhibitors.

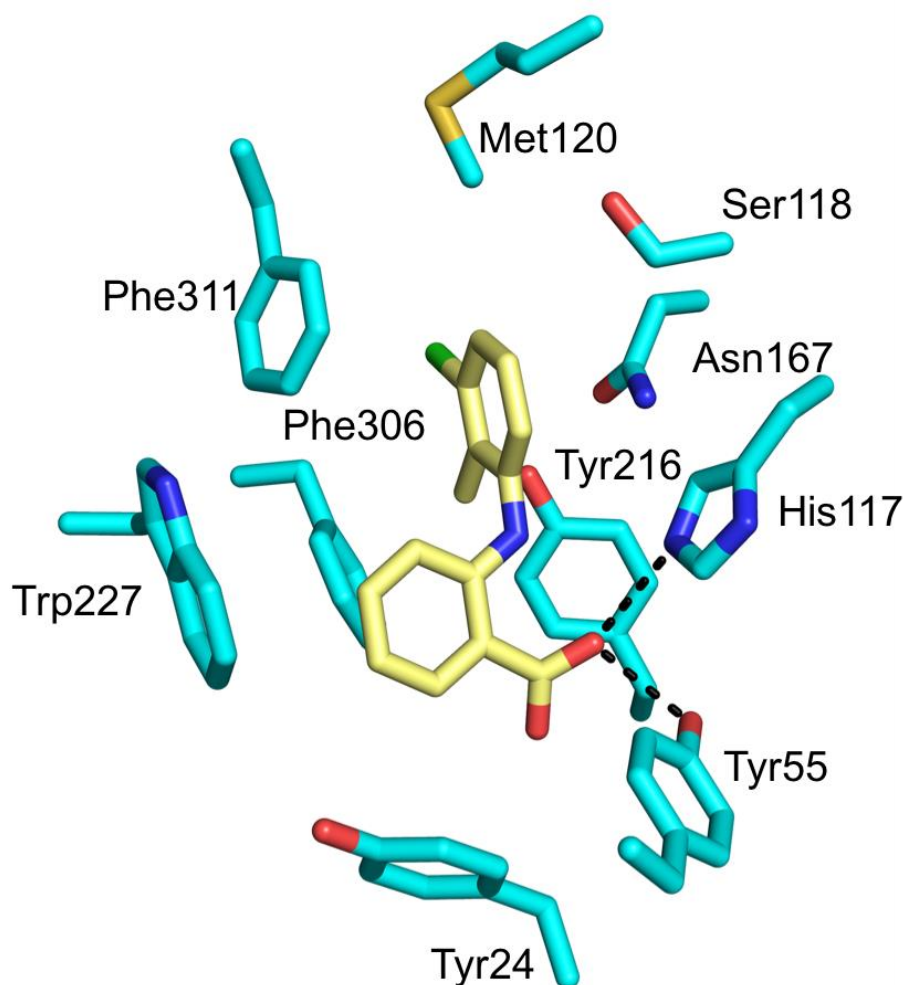


Figure 3-5: Interactions between the AKR1C3 and Tolfenamic acid. Hydrogen bonds and ionic interactions are represented by black broken lines

Although the trifluoromethyl substituent of flufenamic acid extends deep into the SP1 pocket compared to the smaller chloro substituent of tolfenamic acid, the additional methyl group present in tolfenamic acid interacts with hydrophobic residues (Phe311, Phe306, and Tyr216). These additional interactions may contribute to the better inhibitory potency of tolfenamic acid (Figure 3-6).

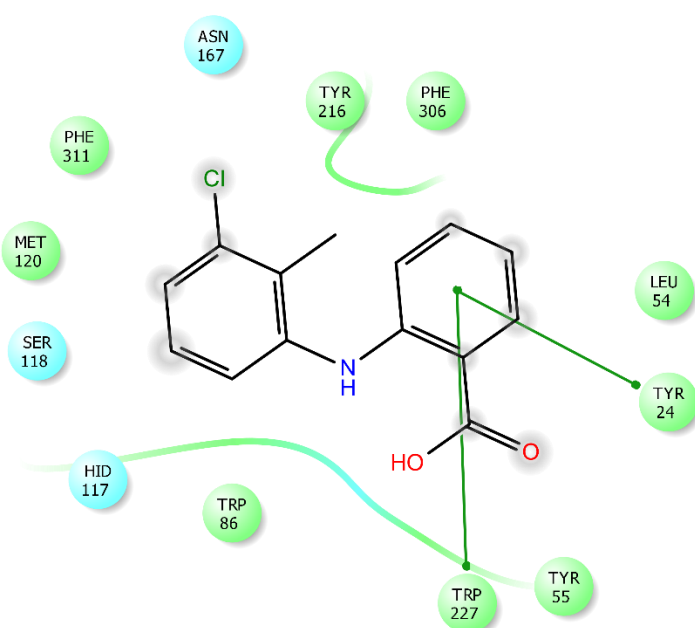


Figure 3-6: Schematic diagram of the residues making van der Waal's contact with Tolfenamic acid. Pi-stacking interactions are represented as green lines.

3.2.1.2 Molecular docking studies in other human AKR1C isoforms to understand the selectivity determinants of Tolfenamic acid

To identify the key residues that determine the inhibition selectivity of tolfenamic acid, docking was carried out in the other three human AKR1C isoforms (C1, C2 and C4). None of the obtained poses consisted of the carboxylate group occupying the oxyanion pocket and didn't adopt any similar binding modes to match the docked pose found in AKR1C3. Further analysis of the binding pocket revealed that the structural differences in the four isoforms may attribute to the higher selectivity in AKR1C3.

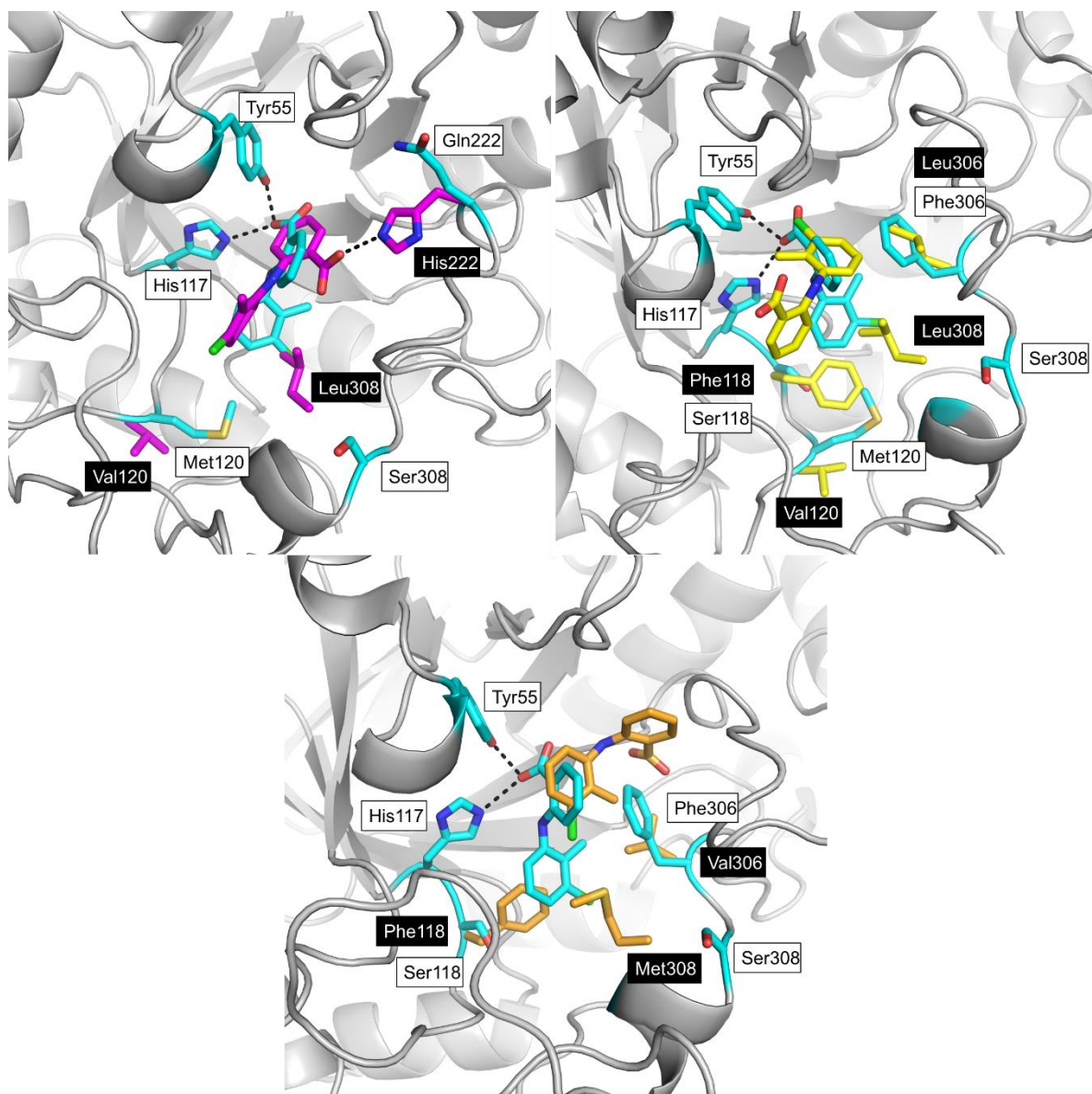


Figure 3-7: Superimposition of docked poses of tolfenamic acid in the other human isoforms AKR1C1 (top left) shown in magenta, AKR1C2 (top right) shown in yellow and AKR1C4 (bottom) shown in orange. The non-conserved residues that are important for binding in AKR1C3 are shown the white box, and the same residues in other are shown in the black box.

The binding pocket of AKR1C3 is larger than that of the other three isoforms which may dictate the inhibitor-substrate selectivity. In particular,

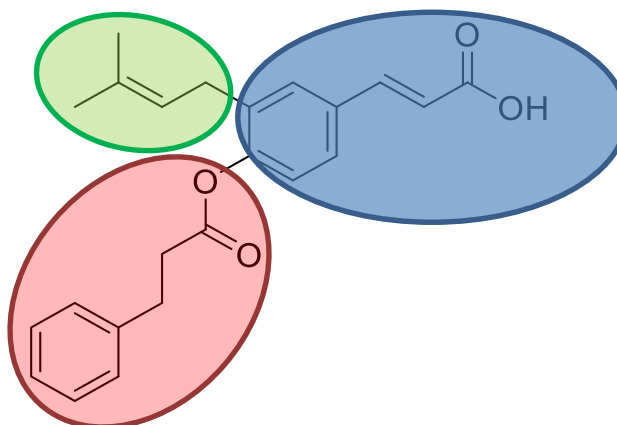
tolfenamic acid occupies the SP1 pocket, lined by residues Ser118, Gln167, Phe306, Phe311, and Tyr319 and partially occupies the SP3 pocket formed by Tyr24, Glu192, Ser217, Gln222, Tyr305, and Phe306.

Four key residues of the binding pocket, Ser118, Gln222, Phe306 and Ser308 are non-conserved. Ser118 is replaced by a bulky phenylalanine in the other three isoforms which restricts the binding of the 3-chloro-2-methylbenzene ring of tolfenamic acid in the other three isoforms. Gln222 is replaced with histidine in the AKR1C1 and AKR1C2 isoforms which prevents binding of the benzoic acid of tolfenamic acid in the binding pocket. The bulky aromatic residue Phe306 is substituted with aliphatic residues, leucine in AKR1C1 and AKR1C2 and with valine in the AKR1C4. Another residue Ser308 is replaced with leucine or methionine in the other three isoforms which occupies the binding pocket, thus preventing binding (Figure 3-7). Collectively, these four non-conserved residues appear to play a key role in imparting AKR1C3 selectivity to tolfenamic acid.

In summary, the modelling studies revealed that tolfenamic acid binds in a similar manner to the other inhibitors belonging to the N-phenylanthranilic acid class of NSAID inhibitors of AKR family. Future crystallographic studies may confirm this binding mode of tolfenamic acid in the binding pocket but to date have not been successful. Molecular modelling studies of tolfenamic acid in the three AKR1C human isoforms revealed that four non-conserved residues Ser118, Gln222, Phe306 and Ser308 may play a role in conferring isoform selectivity.

3.2.2 Molecular modelling studies of baccharin, an AKR1C3 inhibitor

Baccharin is a selective and potent inhibitor of AKR1C3, with an IC₅₀ value of 0.11 μ M. Baccharin exhibits more than 900-fold selectivity to AKR1C3 over the other three AKR1C isoforms (Figure 3-8) [140]. This study aimed to investigate the structural rationale for the selectivity of baccharin using molecular docking. The results of these findings have been published along with allied biochemical studies and are appended to this thesis (Appendix 2).



Inhibition of AKR1C isoforms by baccharin; IC ₅₀ value (μ M) or % inhibition at μ M			
AKR1C1	AKR1C2	AKR1C3	AKR1C4
(0%)	(0%)	0.11 \pm 0.01	(40 \pm 6%)

Figure 3-8: Structure of baccharin and its inhibitory potencies in the human AKR1C isoforms. The cinnamic acid moiety is shown in blue, the dihydrocinnamoyloxy is shown in red and the prenyl moiety is shown in green. Table shows the inhibitory values of baccharin on the four AKR1C isoforms.

3.2.2.1 *Molecular docking studies of Baccharin in the active site of AKR1C3*

Molecular docking studies of baccharin (Figure 3-8) in the AKR1C3-NADP⁺ complex (PDB 1S2C) was carried out in Glide as described in the methods Section 2.1.2.2. At the time of study only a few PDBs were available, none with cinnamic acids bound in AKR1C3. Hence the crystal structure of AKR1C3 in complex with flufenamic acid (PDB: 1S2C) was used to study binding mode of baccharin due to its high resolution. The docking solutions show a binding pose that has some unique features, distinct from all other reported structures. (Figure 3-9 A). The carbonyl group of the dihydrocinnamoyloxy ester moiety of baccharin presents in proximity to the oxyanion site residues His117 and Tyr55. The residues His117 and Tyr55 along with the cofactor NADPH are involved in the binding of baccharin with protons from either Tyr55 or His117 hydrogen bonding to the carbonyl group of the dihydrocinnamoyloxy moiety of baccharin.

The carboxylic acid group on the cinnamic acid moiety of baccharin forms a strong H-bond interaction with the side chain of the residues Ser118 and Ser87 (2.6 Å and 3.2 Å respectively) and the backbone carboxyl group of Met120 (3.4 Å) in the SP1 pocket. In addition to hydrogen bonding, baccharin was also involved in hydrophobic interactions of Met120, Phe306, Gln222, Trp227 and Phe311 and pi-pi stacking (edge to face) interactions with His117, Phe311 and Phe306 (Figure 3-9 B). The isoprenyl moiety occupies the SP3 pocket interacting with the hydrophobic residues.

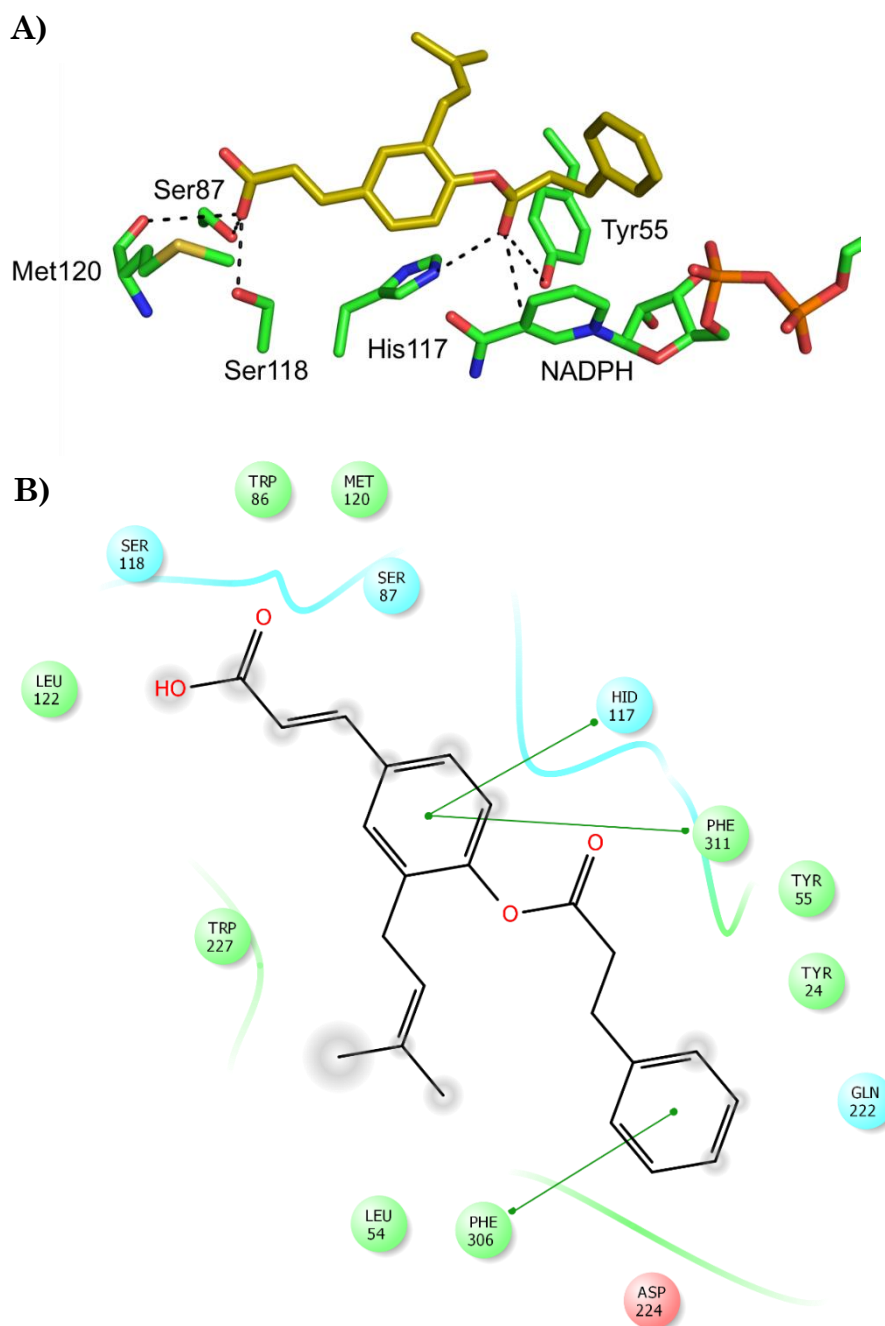


Figure 3-9: Interactions of Baccharin in AKR1C3. (A) Binding mode of baccharin (gold) in the AKR1C3- NADPH complex (green). Hydrogen bonds are represented as dotted lines with the interaction distances in Å. (B) Ligand Interaction Diagram showing the interacting residues within 4 Å of docked baccharin. Hydrophobic residues are represented in green, Polar residues in blue and charged residues are shown in purple (positive) and red (negative). Pi- stacking interactions between aromatic rings of baccharin and adjacent aromatic residues are represented by green lines.

3.1.1.1 Structural insights into high selectivity of baccharin towards AKR1C3

The underlying structural reasons for the high selectivity of baccharin was investigated by comparing the active residue sequences of AKR1C1-C4 to identify any key residues that contribute to selectivity. Some of the non-conserved residues that could contribute to selectivity are highlighted in Figure 3-10.

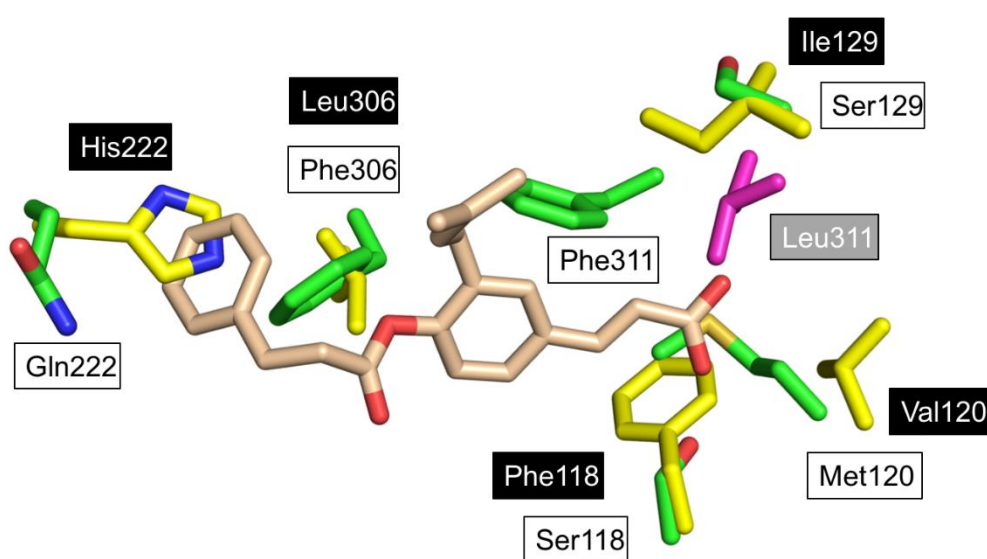


Figure 3-10: Differences in the key residues involved in inhibitor binding in AKR1C3 and the other three human isoforms. AKR1C3 (PDB: 1S2C) is shown in green, AKR1C1 (PDB: 3NTY) shown in yellow, and AKR1C4 (PDB: 2FVL) shown in cyan. AKR1C1 and AKR1C2 share more than 80% sequence similarity and since no major residue differences were found it is not shown here. The residues in the white boxes represent AKR1C3, and the black boxes represent AKR1C1 and the grey box represents AKR1C4.

The carboxyl group of baccharin is predicted to make a hydrogen bond with Ser118, which is a non-conserved residue present only in the AKR1C3 isoform and is substituted by phenylalanine in the other three isoforms. The π -stacking interaction between the benzene ring of the dihydrocinnamoyloxy moiety of

baccharin and Phe306, another residue unique to AKR1C3 is also believed to play a role in selectivity.

To test these binding models, site-directed mutagenesis (Table 3-4) of these two non-conserved residues Ser118 and Phe306 with the corresponding residues Phe and Leu present in AKR1C1 and AKR1C2 was carried out.

In addition, proximate non-conserved residues Met120, Gln222, and Ser129 were also subject to mutagenesis studies and were substituted with Val, His and Ile respectively that are present in the AKR1C1 and AKR1C2 isoforms. Phe311 undergoes an induced-fit conformation [67, 130] to accommodate various ligands in the binding pocket and mutated to Leu, which is unique to the AKR1C4 isoform. The inhibitory potency of baccharin at the mutated enzymes is summarized in Table 3-4.

Table 3-4: Site-directed mutagenesis of the residues carried out by Hara's lab (Gifu University)

Enzyme	K_i (nM)	Mu/Wt
wild type	56 ± 6	
Ser118Phe	850 ± 100	15
Met120Val	550 ± 70	10
Ser129Ile	105 ± 11	2
Gln222His	300 ± 50	5
Phe306Leu	46 ± 8	0.8
Phe311Leu	1200 ± 90	21

Mutation of Ser118 to Phe has a significant impact on the affinity of baccharin, consistent with the predicted role of the Serine in H-bonding to baccharin. The mutation Phe306Leu had no effect on the potency of baccharin. The mutations of Met120Val and Gln222His also had some impact on the affinity

of baccharin. However, the affinity of baccharin was highly impacted with the mutation of Phe311Leu.

3.2.2.2 *In silico mutagenesis studies*

In silico mutagenesis studies were conducted to determine if the mutations affected the predicted binding affinity of baccharin. The non-conserved residues in the AKR1C3 were mutated to match the residues present in AKR1C isoforms similar to the site-directed mutagenesis carried out by Prof. Akira Hara (Table 3-4).

Based on the available biochemical data, the mutation of phenylalanine to leucine at residue position 311 had the highest impact on the binding affinity and mutation of phenylalanine in 306 position to a leucine had the least effect on the affinity. Unfortunately, the molecular docking results did not agree with the biochemical data. The docked pose of baccharin in the AKR1C3 Phe311Leu mutant was similar to the docked pose of baccharin in AKR1C3 WT. The docking output of baccharin in AKR1C3 Phe306Leu mutant was vastly different compared to that of baccharin in wild-type leading to the loss of the important hydrogen bond with one of the catalytic residues Tyr55.

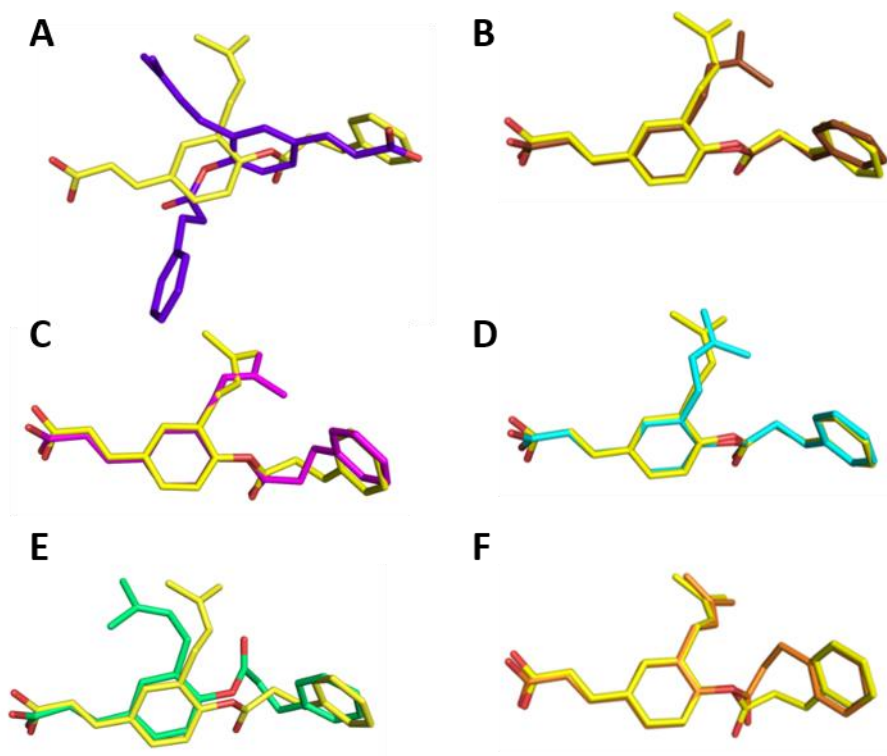


Figure 3-11: Superimposition of docking results of baccharin in mutants on docking results of baccharin in wild type. The baccharin docking in wild type is represented in yellow in all six images. A: Baccharin docked in Phe306Leu, B: Baccharin docked in Phe311Leu, C: Baccharin docked in Met120Val, D: Baccharin docked in Gln222His, E: Baccharin docked in Ser118Phe, F: Baccharin docked in Ser129Ile.

The mutation of serine in position 118 to a phenylalanine led to impairment of affinity as per the biochemical data. In molecular docking studies (Figure 3-11), it was observed that this mutation caused the carbonyl group to face away from the catalytic residues, thus leading to loss of binding with the catalytic residues H117 and Y55. The movement of the carbonyl may be due to interactions with the aromatic ring of the mutated Ser118Phe.

3.2.3 *Molecular docking studies of structural analogues of baccharin*

Baccharin is one of the most potent inhibitors of AKR1C3 with an IC_{50} = 0.11 μ M [155] and presents a starting point for the development of analogues with improved properties. Derivatives of baccharin were prepared by replacing the prenyl moiety of baccharin with aliphatic and aromatic ethers (list of compounds tested attached in Appendix 3). Two derivatives BA-25 and BA-28 (Figure 3-12) were equipotent with baccharin (IC_{50} = 0.11 μ M). This study aimed to carry out molecular docking studies of BA-25 and BA-28 to study the influence of the structural changes upon binding interactions.

3.2.3.1 *Molecular docking studies of BA-25 and BA-28*

Molecular docking studies of the baccharin analogues in the AKR1C3-NADP⁺ complex (PDB 1S2C) were carried out as for baccharin itself.

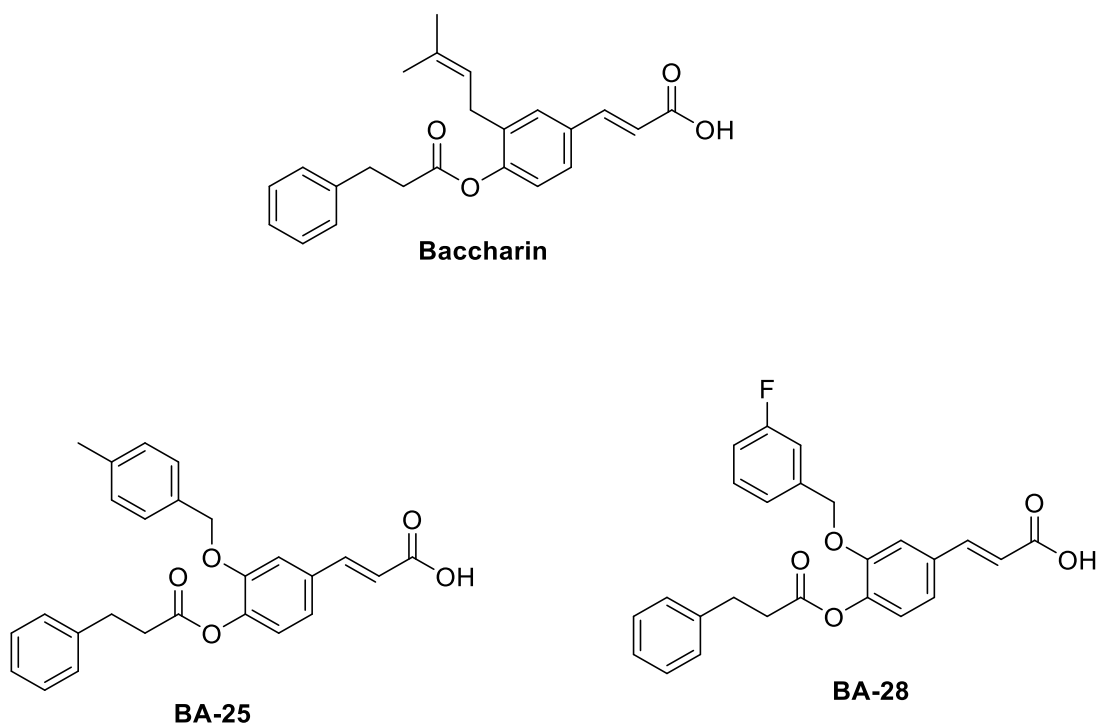


Figure 3-12: Structures of baccharin, BA-25 and BA-28.

Upon superimposition of the obtained poses of BA-25 and BA-28 on the docked pose of baccharin, it was observed that BA-25 and BA-28 were bound to AKR1C3 in a similar manner to baccharin (Figure 3-13) with the only difference in the 4-methylbenzyl and 3-fluorobenzyl ether substituents. BA-25 and BA-28 retained the interactions with the carbonyl group on the dihydrocinnamoyloxy moiety which is believed to contribute high inhibitory potency in baccharin (Figure 3-14).

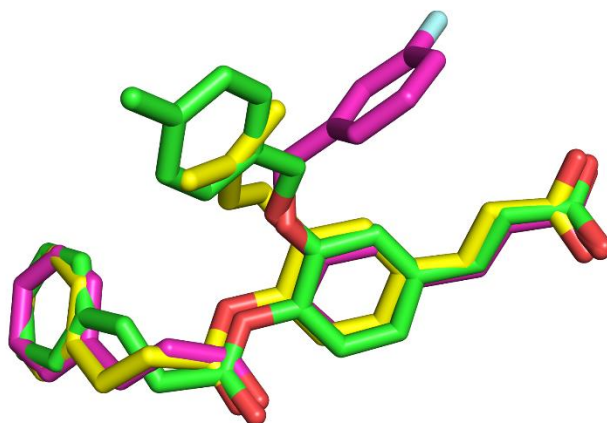


Figure 3-13: Superimposition of docked poses of BA-25 (green) and BA-28 (magenta) on the docked pose of baccharin (yellow).

Both the compounds also retained the carboxylate group interaction on the cinnamic acid moiety. The interaction of the non-conserved residue Ser118 and Met120 in AKR1C3 with the carboxylate group is believed to impart strong binding affinity as well as selectivity for baccharin in AKR1C3. Since, both BA-25 and BA-28 retained the hydrogen bond interactions, they may display similar inhibitory activity like baccharin (Figure 3-15 and Figure 3-16).

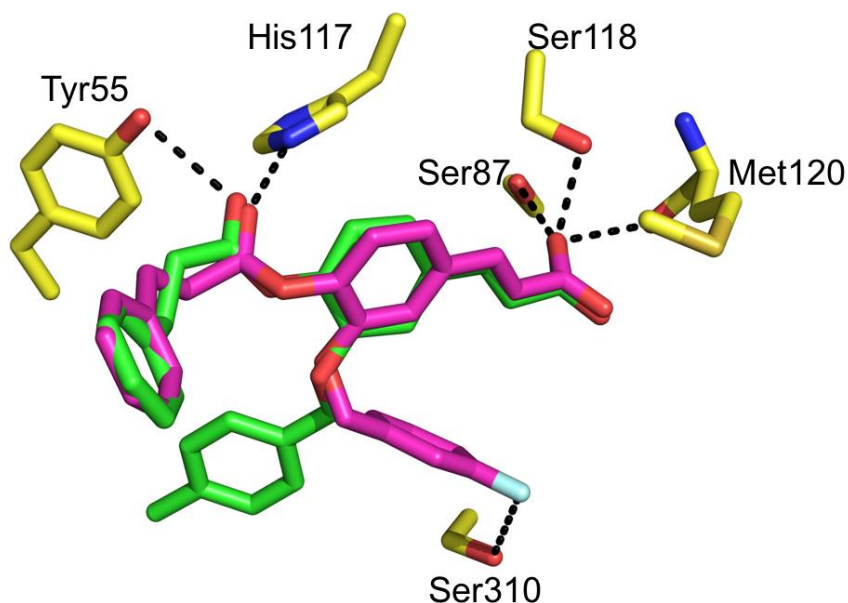


Figure 3-14: BA-25 and BA-28 make similar bonds as baccharin.

Based on our previous docking studies, it was revealed that the isoprenyl group of baccharin occupied the SP3 pocket and formed hydrophobic interaction with the residues in the pocket. The isoprenyl group is substituted with a 4-methylbenzyl in BA-25 which also occupies the SP3 pocket interacting with similar residues. However, extension of the 4-methylbenzyl also provides additional interactions such as the π -stacking and π -cation interaction with Arg226, a non-conserved residue which is replaced with a Pro in AKR1C1 and AKR1C2 and Leu in AKR1C4.

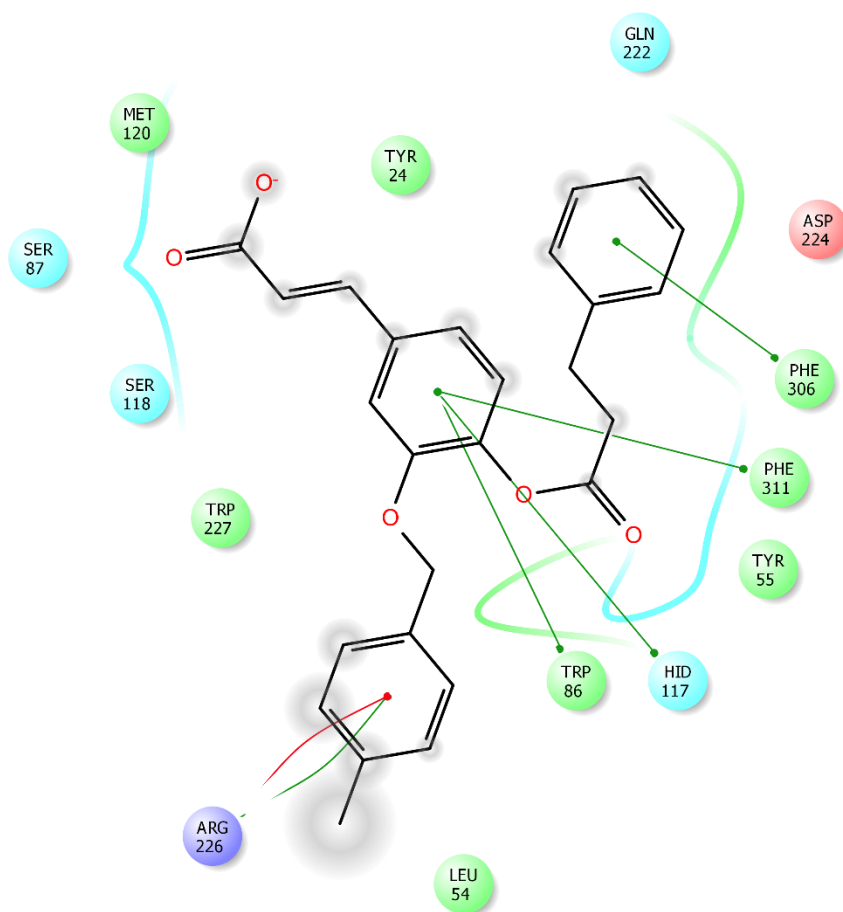


Figure 3-15: Interactions of BA-25 with AKR1C3. Hydrophobic residues are represented in green, Polar residues in blue and charged residues are shown in purple (positive) and red (negative). Pi- stacking interactions between aromatic rings of BA-25 and adjacent aromatic residues are represented by green lines and Pi- cation interactions are represented by red lines..

The introduction of 3-fluorobenzyl group changes the orientation of the BA-28. The fluoro group of the 3-fluorobenzyl moiety makes new interactions with Ser129 (3.8 Å). Ser129 is replaced by Ile in AKR1C1 and AKR1C2 and Leu in AKR1C4. The 3-fluorobenzyl moiety also interacts with Ser310 a non-conserved residue (3.8 Å). It is replaced by Ile in AKR1C1 and AKR1C2 and Phe in AKR1C4.

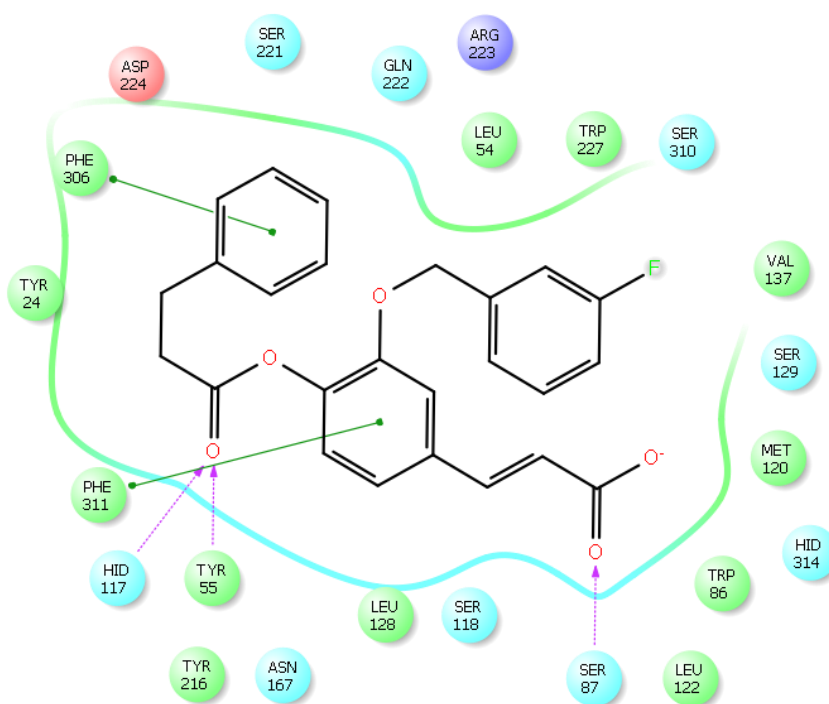


Figure 3-16: Interactions of BA-28 with AKR1C3. Pink dashed lines represent hydrogen bond with the residues in the binding pocket. Hydrophobic residues are represented in green, Polar residues in blue and charged residues are shown in purple (positive) and red (negative). Pi-stacking interactions between aromatic rings of BA-28 and adjacent aromatic residues are represented by green lines and Pi- cation interactions are represented by red lines

BA-25 and BA-28 may exhibit similar inhibitory potencies as baccharin due to the similar binding modes; however, the selectivity of BA-25 and BA-28 is unknown. The interactions of the carboxylate group of the cinnamic acid moiety along with interactions of the carbonyl group of the dihydrocinnamoyloxy moiety are important for high inhibitory activities of BA-25 and BA-28 and also baccharin. The role of these groups in potency has been subsequently validated by Zang *et al.* [156]. In the study, 15 synthetic analogues of baccharin were developed by modifying or removing the prenyl group as well as esterification of the cinnamic acid group and it was concluded that these modifications led to the decrease in inhibitory potency and selectivity to AKR1C3.

In a recent report by Endo *et al.* [157], a novel inhibitor 3-(3-hydroxybenzyloxy)-4-(dihydrocinnamoyloxy)cinnamic acid (K_i 6.4 nM) has been described. The inhibitor was designed based on the docking results of BA-25 and BA-28 as described above. 3-(3-hydroxybenzyloxy)-4-(dihydrocinnamoyloxy)cinnamic acid is highly selective towards AKR1C3 and exhibits similar interactions to BA-25 and BA-28. Although the selectivity profiles of the BA-25 and BA-28 are not determined, we hypothesize that both of the compounds may exhibit similar or higher selectivity towards AKR1C3 over other three isoforms due to the similarity in binding retaining the important interactions.

3.2.4 *Influence of protein structure as a starting point for virtual screening for AKR1C3 inhibitors*

The initial goal of this study was to discover novel compounds exhibiting significant binding affinities for the active site of AKR1C3 using virtual screening approaches. Virtual screening has emerged as an important tool in drug discovery and development and encompasses screening large libraries of compounds and categorizing the structures that bind to a drug target *in silico*. However, the virtual screening paradigm is known to be strongly influenced by a range of arbitrarily selected parameters which can impact notably on success.

3.2.4.1 *Evaluation of the AKR1C3 starting structure on docking outcomes*

Virtual screening was carried out to assess the ability of the protein template that had been utilized in the studies of tolfenamic acid and baccharin (above) (PDB:1S2C[67]) to identify known AKR1C3 inhibitors in a library of drug-like decoys. 26 compounds (Appendix 4) sampled from different classes of AKR1C3 inhibitors were selected based on the potencies and combined with 1000 decoy compounds obtained from the Schrodinger website. The library with both known inhibitors and decoys were docked in the active site of AKR1C3 using a similar approach as described in the previous section (HTVS omitted).

Receiver Operating Characteristic (ROC) curves, a technique first described by Triballeau *et al.* [158] was employed to rank the performance of our docking protocol. The ROC is a fundamental tool for any evaluation of a test and determines the cutoff value. This method entails docking of a **decoy set** of inactive compounds enriched with compounds with known activity against the biological

target. Receiver operating characteristic (ROC) curves compare the sensitivity of a given docking/scoring combination (y-axis) versus specificity (x-axis) across a range of values. The obtained Area's Under the Curve (AUC) can be calculated which determines the overall performance of the test. The values of AUC determines the efficiency of the virtual screening workflow and its value range between 0 and 1.0. AUC values of 0.5 and lower represent poor performance due to the inability of the model to pick active compounds over inactive compounds. Higher values (0.6 and higher) indicate the ability of the model to differentiate between active and decoy compounds.

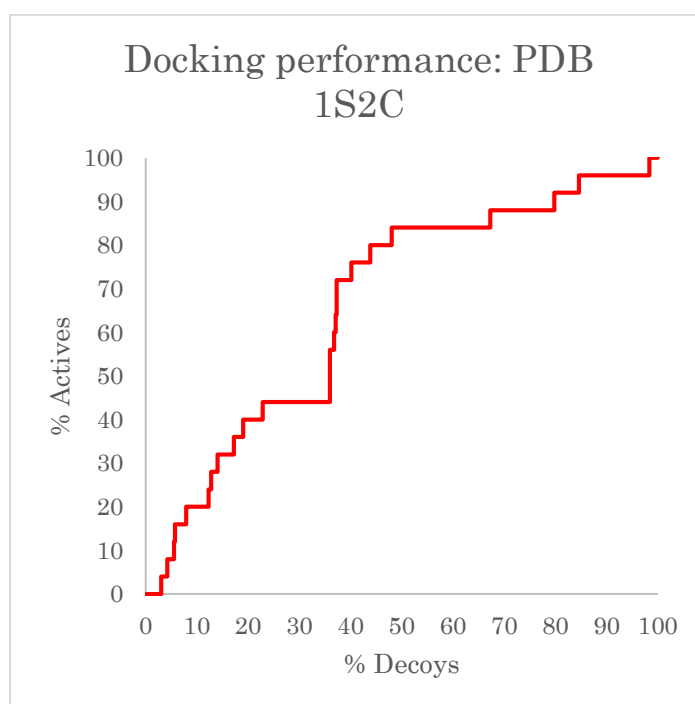


Figure 3-17: Assessment of docking performance of the model protein (PDB:1S2C) used in previous docking protocols.

The ROC curve generated for our model protein PDB 1S2C had an AUC of 0.676 implying it is not efficiently able to distinguish between active and inactive compounds (Figure 3-17).

3.2.4.2 *Identification of ideal model protein for virtual screening using ROC curves*

During the course of this study, Brožič *et al.* [159] carried out a virtual screening and identified two novel inhibitors. They used a different model protein (PDB: 1S2A) and a different docking program (FlexX 3.1) for their study. Since our choice of protein template was arbitrary, the next step was to evaluate our docking procedure against a range of available proteins to identify a model protein for future docking studies. A good measure of an ideal model protein is its ability to distinguish between active and non-active compounds.

The virtual screen carried out above was repeated using five different starting protein structures. Note that in 2012, when this study was carried out, 16 crystal structures of AKR1C3 were available in the PDB database. Currently, there are more than 30 structures of AKR1C3 in complex with various inhibitors. The six crystal structures were selected based on their resolution and included AKR1C3 co-crystallized with various inhibitors (Table 3-5). The results are summarized in Table 3-5 and Figure 3-18.

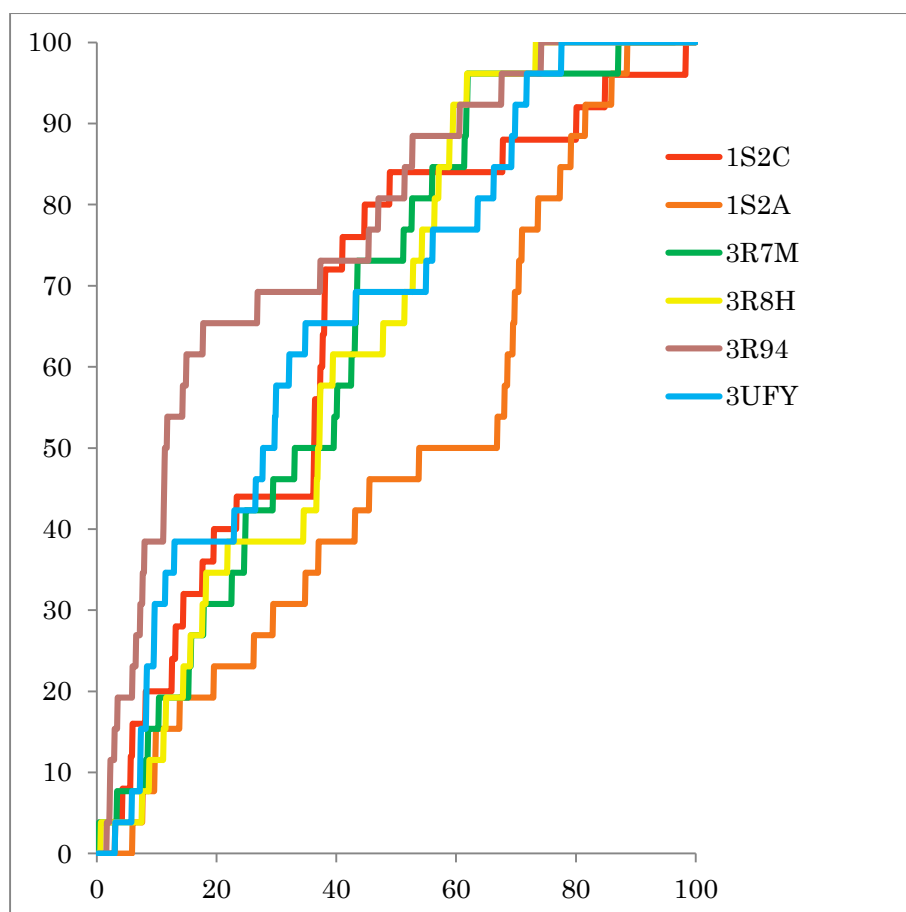


Figure 3-18: Identification of ideal model for use in molecular modelling studies using ROC curves.

Table 3-5: Performance of the six models analysed in the study.

PDB ID	RESOLUTION (Å)	INHIBITOR	AUC
1S2C	1.8	Flufenamic acid	0.676
1S2A	1.7	Indomethacin	0.519
3R7M	2.1	Sulindac	0.66
3R8H	1.9	Zomepirac	0.665
3R94	2.01	Flurbirprofen	0.791
3UFY	1.9	Naproxen	0.69

The AUC of the six structures was compared to evaluate the performance and determine a preferred starting model for virtual screening. The screen obtained from PDB 3R94 performed the best in discriminating the active

compounds over the decoys with an AUC of 0.791. Of the other five proteins, 1S2A fared poorly with a low score of 0.519. The other four models (including 1S2C) had AUC values between 0.66 – 0.69.

The reason of the low performance of 1S2A was analysed by superimposing the structures over the other five models, and it was observed that the two residues Phe306 and Phe311 in the structure 1S2A adopt a different conformation compared to the models 3R94, 1S2C, 3UFY and 3R7M (model 3R8H adopts similar conformation). According to Flanagan *et al.* [154] Trp227, Phe306, and Phe311 adopt various conformations based on the bound ligands and display a significant side chain flexibility which is the case in the models 1S2A and 3R8H. The different conformation of Phe306 and Phe311 opens up the SP3 pocket for the binding of the ligands. The opening of this pocket may also account for the ability of some of the decoy compounds to bind in the binding site which may be indicative of the poor performance of model 1S2A.

4 Conclusions, limitations and future outcomes

This chapter evaluated the structural studies of two aldo-keto reductases AKR1B14 and AKR1C3.

Previous structural studies revealed the importance of a non-conserved residue (His269) in coenzyme binding and site-directed mutagenesis confirmed the role with a decrease in binding affinities with mutations to the residue. The results obtained in Section 3.1 present the crystal structure of AKR1B14 His269Arg mutant and molecular modelling studies of AKR1B14 His269Phe and AKR1B14 His269Met mutant. Analysis of the loss of affinities was due to loss of the π - π (face to face) stacking as well as π - cation interactions between the adenosine moiety of the coenzyme NADPH and the residue His269. Both of these interactions contributed equally in the better binding of the coenzyme NADPH and were validated by our structural studies.

AKR1C3 is implicated in various cancers, and many pharmacological small molecule inhibitors have been described that inhibit AKR1C3 however they lack specificity. There are various NSAID inhibitors of AKR1C3 reported to date; however tolfenamic acid, a structural analogue of a known potent inhibitor flufenamic acid (presented in chapter 3.2.1) remains the most potent and selective inhibitor of AKR1C3 known to date. Our analysis has allowed understand the differences in the binding pocket of AKR1C3 that contribute to the differences in binding affinities between Tolfenamic acid and flufenamic acid. We have also identified four key residues which may play a critical role in imparting selectivity of Tolfenamic acid in AKR1C3. The structural information obtained could be used

for the development of future selective and potent inhibitors. Baccharin, a natural product inhibitor and its analogues presented in Section 3.2.2 and 3.2.3 represent a new class of cinnamic acid inhibitors of AKR1C3 with high potency as well as selectivity. SAR studies of baccharin revealed the importance of six non-conserved residues that are believed to play a crucial role in imparting selectivity in baccharin. An attempt to replicate the influence of site-directed mutagenesis on baccharin inhibition by *in silico* mutagenesis and docking analysis failed. This may cast some doubt on the docking solution, and emphasizes the value that a crystallographically determined structure would have in dictating future work.

This study finally aimed to evaluate the docking protocols and examine the influence of template protein structure during virtual screening. Our analysis has identified that conformations of the residues that line the binding pocket contribute to the performance of model proteins in their ability to choose active compounds amongst a library of decoys. The structure PDB 3R94 was identified as an improved protein template for future virtual screening studies.

Further work could not be conducted on this project due to a change in supervisory arrangements. However, this work has set a stepping stone to the identification of new inhibitors of AKR1C3. For example, two recent reports have revealed further work pursuing analogues of baccharin based on the published findings described above [156, 157]. In a separate study, structural studies of two NSAID inhibitors belonging to the N-phenylanthranilic acid inhibitors (Meclofenamic and Mefenamic acid) were described by Flanagan *et al.* [154]. Although neither of these compounds is as selective as tolafenamic acid, the

findings of this study also agree with the experimentally bound orientation of meclofenamic and mefenamic acid in the active site of AKR1C3. These findings could be used in the future design of potent and selective inhibitors of AKR1C3.

Section B

***Class II PI3KC2 β as a novel
cancer target***

Chapter 1: Introduction to PI3Ks

1.1 Overview of PI3K family

Phosphatidylinositide 3-kinases (PI3Ks) are a conserved family of enzymes that catalyse the phosphorylation of the D3 position of inositol ring of the phosphoinositide lipids. PI3Ks play key roles in various cellular functions such as cell growth, proliferation, differentiation, apoptosis, cytoskeletal organization and intracellular trafficking [160-164]. PI3K has also been shown to be up-regulated in diseases associated with neoplasia and alterations in PI3K dependent pathways may lead to cancer [163, 165-167]. PI3Ks were first discovered by Cantley and associates in 1988 and have been associated with various diseases such as cancer, cardiovascular diseases, allergy, inflammation and diabetes and thus present as potential therapeutic targets [168-170].

1.2 Classification of PI3K family

The PI3K family consists of eight mammalian isoforms which have been grouped into three classes (class I, II and III) based on their subunit structure, substrate specificity and regulation [160, 170-172]. Further members of the PI3K superfamily are the class IV PI3Ks, which are structurally related but show protein kinase activity and lack lipid kinase activity.

1.2.1 Class I PI3K

Of the three classes of PI3Ks, most of the intracellular functions have been attributed to class I members which have been studied in much detail. Members of class I PI3K consist of a catalytic subunit involved in phosphorylation of PtdIns,

PtdIns-4-P *in vitro* and PtdIns4, 5-bisphosphate *in vivo* (Table 1-1). All members of class I PI3K possess a ~ 110kDa (p110) catalytic sub-unit [160]. The class I family is further subdivided into subclasses based on the regulatory subunits and mechanism of activation.

Table 1-1: Phosphorylation of phosphoinositides catalysed by PI3Ks

	PI3K subunit (catalytic)	Substrates	Products
Class I A	p110 α , p110 β , p110 δ	PI(3)P, PI(4,5)P2	PI(4,5)P2, PI(3,4,5)P3
Class I B	p110 γ	PI(3)P, PI(4,5)P2	PI(4,5)P2, PI(3,4,5)P3
Class II	C2 α , C2 β , C2 γ	PI, PI(3)P	PI(3)P, PI(4,5)P2
Class III	C3	PI	PI(3)P

1.2.1.1 **Class IA**

The three class I A catalytic subunits namely p110 α , p110 β and p110 δ (denoted as PI3K α , PI3K β and PI3K δ) are encoded by their specific genes: PIK3CA, PIK3CB, and PIK3CD. These class I A isoforms interact with Src homology 2 (SH2) domain of regulatory adaptor proteins (p85 α , p85 β , and p55 γ) thus facilitating the translocation of PI3Ks from the cytosol to the membrane where their lipid substrates are present [160, 173-175]. Of the three isoforms, PI3K p110 α and PI3K p110 β are widely distributed in mammalian tissues; whereas, PI3K p110 δ is mostly found in leukocytes [160, 176].

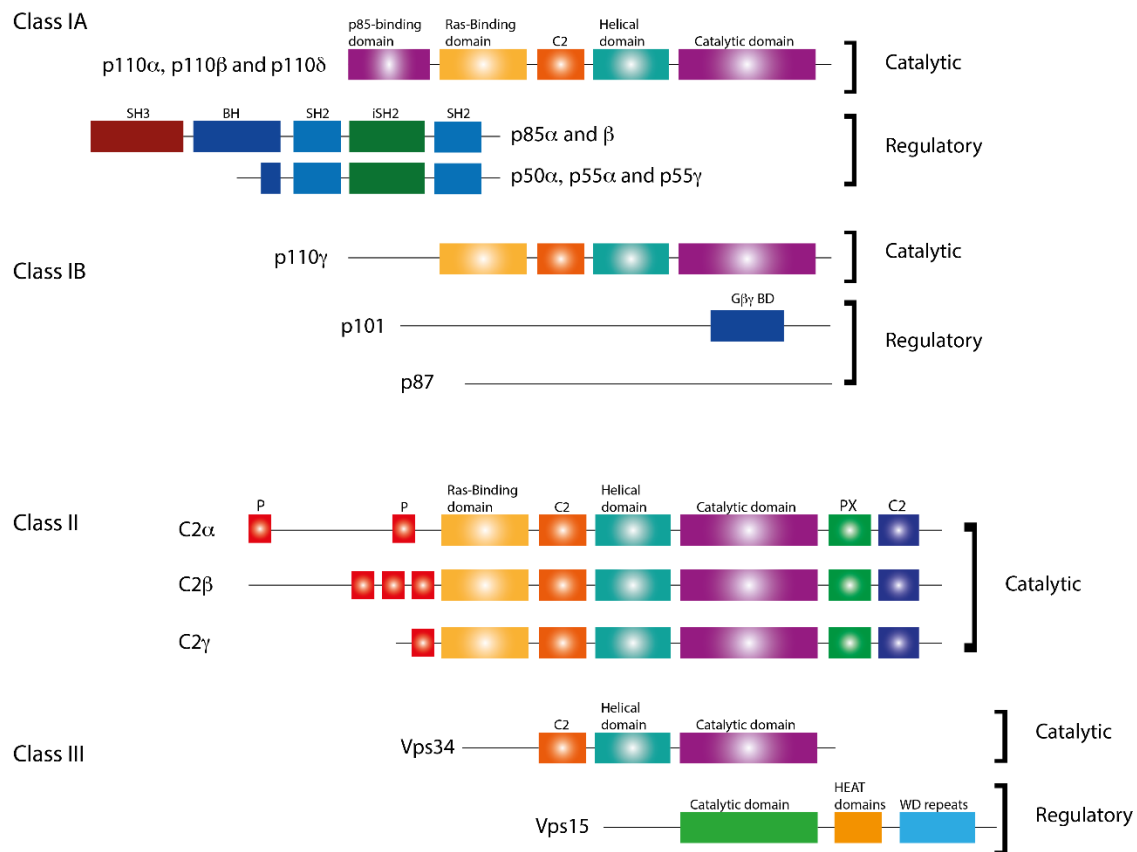


Figure 1-1: Classification of PI3Ks. The catalytic core is relatively conserved among all eight isoforms. The class I PI3Ks consist of adapter proteins that associate with regulatory subunit. Class II proteins lack the regulatory subunits but consist of additional PX and C2 domains in their catalytic subunit. Class III PI3Ks consist of Vps34 catalytic subunit which binds to Vps15 regulatory subunit (Adapted from Vanhaesebroeck *et al.* [177]).

The catalytic subunit of class IA PI3Ks are made up of five domains: an N-terminal adaptor binding domain (p85 binding domain), Ras binding domain (RBD), C2 domain, a helical domain and catalytic kinase domain. The C2 domain, helical domain and the catalytic domain encompass the PI3K core (Figure 1-1) [178]. The regulatory subunit consists of three domains: the N-SH2 domain, the inter SH2 (p110 binding) domain and the C-SH2 domain. N-termini of p85 (p85 α and p85 β) have extensions which are hypothesized to play a role in additional

signalling including an SH3 domain, Proline-rich region and a BCR homology (BH) domain that interacts with small GTPases such as Rho, Ran and Rab [179, 180].

The three isoforms have various functions. The PI3K p110 α isoform is associated with cancer prognosis and cell survival. The gene that encodes for PI3K α (p110 α) isoform is believed to be one of the most frequently mutated oncogenes in human tumors. The PI3K p110 α isoform is also associated with associated with glucose intolerance and insulin resistance, thus playing a major role in the development of Type 2 diabetes mellitus [181, 182] [183] [184]. PI3K p110 β plays a role in platelet aggregation and thrombosis and promotes cell proliferation. Studies also indicate that PI3K p110 β plays a role in phagocytosis and ROS production in macrophages and neutrophils [185, 186]. PI3K p110 δ is essential for B-cell development and T-cell differentiation. Any deletions or mutations in PI3K p110 δ gene affects antibody production [187, 188]. PI3K p110 δ is also associated with diseases such as chronic lymphocytic leukemia and asthma [189, 190].

1.2.1.2 ***Class IB***

Class IB PI3K consists of a sole catalytic subunit p110 γ along with two different regulatory subunits (p101 and p84/p87) [179, 191, 192]. The class IB PI3Ks are activated by GPCRs (G-protein coupled receptors) unlike class IA PI3Ks, which are activated by tyrosine kinase mediated signals. The catalytic subunit of p110 γ is similar to class IA PI3Ks and consists of the RBD domain and the PI3K core made up of C2 domain, helical domain and catalytic domain; however, it lacks the adaptor binding domain. The regulatory subunits p101 and

p84/p87 lack the SH2 domains (or any domains) and are not homologous to any other proteins (Figure 1-1) [193].

PI3K γ upon activation with GPCRs, regulate various inflammatory and immune functions via macrophages, neutrophils, and lymphocytes, mast cell reactivity [194, 195]. Mouse phenotypic analyses have also revealed PI3K γ is involved in platelet aggregation and T-cell function [196] [197]. PI3K γ also regulates the control of vascular tone and heart contractility [198, 199]. According to Fougerat *et al.* [200] it also plays a key role in mediating the progress of atherosclerosis.

1.2.2 ***Class II PI3K***

Compared to the class I PI3Ks, not much is known about the class II PI3K members and their precise physiological significance or cellular functions still need to be defined. Class II PI3Ks were primarily identified in *Drosophila melanogaster* using a PCR-based approach. Three isoforms of class II PI3Ks have been identified namely: PI3K-C2 α , PI3K-C2 β and PI3K-C2 γ . PI3K-C2 α and PI3K-C2 β were first cloned from the U937 and MCF-7 cultured cell lines respectively. A third isoform PI3K-C2 γ was identified simultaneously in human, mouse and rat [201-205].

Class II PI3Ks are larger than class I PI3Ks with a molecular weight of 170-210 kDa. Although they share 45-50% similarity with class I PI3K, they do not appear to utilize regulatory subunits. All the three isoforms consist of both a PI3K core kinase core domain and a Ras binding domain (Figure 1-1); they differ at the C-terminus, which consists of an additional C2 domain that is believed to

bind to phospholipids *in vitro* in a Ca^{2+} independent manner. The three isoforms differ from each other in the N-terminal region that is also not homologous to any known protein [203, 206, 207].

In vitro, the class II PI3Ks phosphorylate PtdIns (PI) to generate PtdIns (3)P (PIP) as well as PtdIns(4)P and PtdIns(4,5)P₂ (PIP₂). The by-product PtdIns (3)P is considered to play a crucial role in the insulin signalling pathway [208, 209].

PI3KC2 α is believed to play a key role in cell growth, and survival and also has been linked to insulin secretion, glucose homeostasis and transport [202, 210]. Recently, a study by Yoshioka *et al.* [211] has revealed that PI3KC2 α is associated with angiogenesis and vascular barrier function. Northern-blot analysis carried out by Domin *et al.* [201] revealed that PI3KC2 α was widely expressed in heart, placenta and ovary. PI3KC2 α is believed to be associated with neuroexocytosis and smooth muscle cells contraction. PI3KC2 α is generally localized in the trans-Golgi and is believed to play a role in membrane trafficking via clathrin activation [212-215]

PI3KC2 β is highly expressed in thymus and placenta and is involved in cell growth, survival, migration and cell cycle progression [216]. PI3K-C2 β participates in LPA-mediated cell migration [217]. It has been shown that T cell receptor on CD4 + T cell could activate PI3KC2 β and plays a crucial role in calcium-activated potassium channel (KCa3.1) activity in immune cells. This KCa3.1 channel is responsible for Ca^{2+} influx that leads to T cell activation [218]. PI3KC2 β was also found to be involved in PKB activity [219]. PI3KC2 β is overexpressed in certain

types of cancers such as acute myeloid leukemia (AML), brain tumors and neuroendocrine tumors and inhibiting this enzyme may reduce proliferation and survival in cancer cells [220]. This chapter will focus on studies of PI3KC2 β to elucidate its role in cancer as well as identify new and selective inhibitors of PI3KC2 β .

Very little is known about the third human isoform PI3KC2 γ , however, it is believed to be involved in homing of leukemic cells. Northern-blot studies have revealed that it is present in the liver prostate, breast and salivary glands [205].

1.2.3 *Class III PI3K*

Class III PI3Ks are the oldest known PI3Ks. They are sometimes referred to as Vps34 (vacuolar protein sorting protein 34) as they were first identified in a screen for proteins involved vesicle-mediated vacuolar protein sorting in *Saccharomyces cerevisiae* [221]. Vps34 homologues are found in all eukaryotes, including humans [222]. Unlike class I and II PI 3-kinases, class III PI3Ks can only phosphorylate PtdIns to generate PtdIns(3)P and are implicated in endosome fusion during intracellular trafficking events [170]. They are also believed to be involved in autophagy in yeast, amino acid sensing [223, 224]. The human Vps34 consists of a single 100 kDa catalytic subunit which share a common PIK and kinase core domain and a single 150 kDa regulatory subunit Vps15/p150 [225].

1.2.4 *Class IV PI3Ks*

PI3-related kinases (sometimes also referred to as class IV PI3Ks) are a family of Ser/Thr-protein kinases that exhibit sequence similarity to PI3Ks. They consist of six members which are involved in various biological process. Some of the

proteins belonging to this class include ataxia telangiectasia mutated (ATM), ataxia telangiectasia and Rad3 related (ATR) protein kinases, DNA-dependent protein kinase (DNA-PK) and mammalian target of rapamycin (mTOR). An overview of the class IV PI3Ks and their similarities are discussed in detail by Lempiäinen *et al.* [226].

1.3 PI3Ks in signalling pathways

PI3Ks play a crucial role in various signal transduction cascades that regulate cell growth, survival and cell migration. The class I PI3Ks upon activation by their respective receptors (either tyrosine kinase or G-protein coupled receptor) phosphorylate inositol lipids at the 3 position of the OH group of phosphatidylinositide-4,5-bisphosphate (PIP₂) to generate phosphatidylinositide-3,4,5-trisphosphate (PIP₃). The generated product, PIP₃ acts a second messenger and activates a number of downstream signalling pathways which are involved in various cellular functions, such as cell growth, glucose metabolism, cell motility and cell survival. Any abnormalities in this PI3K pathway can assist in the propagation of diseases such as cancer. Phosphatase enzymes such as the phosphatase and tensin homolog (PTEN) dephosphorylate PIP₃ to PIP₂; terminate the PI3K signalling cascade [227-230].

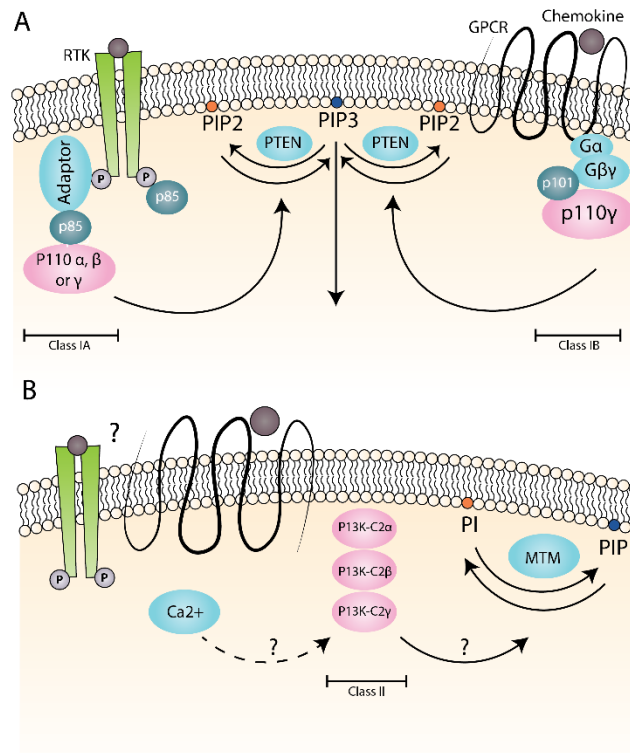


Figure 1-2: PI3K signalling pathway by different classes of PI3Ks. A) Conversion of PIP2 to PIP3 by class I PI3Ks via activation through tyrosine kinases or GPCRs. B) Class II PI3Ks are believed to convert PI to PIP, however exact mechanism of activation and signalling still remains unclear (Adapted from Thorpe *et al.* [231]).

The signalling mechanism of the class II PI3Ks is not very well understood, however, it is hypothesized that the members of class II PI3Ks are activated by a range of different stimuli (such as growth factors, hormones, phospholipids and calcium). Class II PI3Ks phosphorylate phosphatidylinositides (PI) as well as phosphatidylinositide-4-phosphate (PI4P) *in vitro*, nevertheless, *in vivo*, they prefer to phosphorylate PI to generate phosphatidylinositides-3-phosphate (PI3P) (Figure 1-2). PI3P is believed to be involved in cellular functions such as glucose transport, endocytosis, cell migration and survival. The class II PI3K signalling is inactivated by Myotubularins (MTM) which dephosphorylates PI3P to PI [231].

The class III PI3Ks are activated by stimuli such as amino acids, glucose and phosphorylate phosphatidylinositides to generate phosphatidylinositides-3-phosphate and thus play vital roles in phagocytosis, autophagy and endosomal trafficking. These enzymes are also inactivated by Myotubularins [231].

1.4 PI3K and cancer

The role of class I PI3Ks in cancer through their signalling pathways has been well established. Alterations in the PI3K pathway are most commonly found in all human tumours especially the PIK3CA gene which encodes the PI3K catalytic isoform p110 α which has been found to be the second most frequently mutated oncogene [165, 232, 233]. Mutations associated with the PIK3CA gene have been implicated in various cancers such as breast, colon, and endometrial cancers and glioblastomas [165].

The precise role of class II PI3Ks in cancer is yet to be determined. However, it has been reported that PI3KC2 β is expressed in high levels in various epithelial cell-derived cancers [234] and microarray studies have confirmed that PI3KC2 β is upregulated in cancers [235]. This upregulation also contributes to the activation of PKB (a known oncogene) as well as increased expression of Bcl2 genes involved in AML [219, 236].

1.5 Inhibitors of PI3K in Cancer Research and Therapy

Due to their role in various key cellular processes and many human diseases, PI3Ks have gained attention as potential therapeutic drug targets. Current drug discovery has aided in unearthing many potent and selective small molecule inhibitors.

1.5.1 *First-generation PI3K inhibitors*

Wortmannin (Figure 1-3), is a steroid metabolite of the fungi *Penicillium wortmannii* was the first PI3K inhibitor identified while studying its potent anti-proliferative and anti-inflammatory activity in neutrophils [237]. Wortmannin inhibits the class I PI3K isoforms irreversibly with an IC_{50} in the low nanomolar range across isoforms ($IC_{50} = 1\text{--}10\text{ nM}$). Although it potently inhibits the class II enzyme PI3KC2 β ($IC_{50} = 1.6\text{ nM}$), it is not as active against PI3KC2 α ($IC_{50} = 420\text{ nM}$). The inhibition of class III PI3Ks is species dependent, nevertheless it inhibits the human isoform with an IC_{50} of about 10 nM [178, 238]. In an attempt to identify natural product inhibitors of PI3Ks, Eli Lilly initiated a screening in the early 1990's which led to the discovery of quercetin and myricetin. Both quercetin and myricetin are polyphenolic flavonoids and inhibit class I PI3Ks with an IC_{50} of $3.8\text{ }\mu\text{M}$ and $1.9\text{ }\mu\text{M}$ respectively [239, 240].

LY294002, a synthetic inhibitor and analogue of quercetin was developed by Eli Lilly in 1994. LY294002 is a reversible, ATP-competitive PI3K inhibitor. The IC_{50} of LY294002 against class I PI3K isoforms was found to be in the low micromolar range [241-243]. It also inhibits the class III PI3K at $3.5\text{ }\mu\text{M}$. LY294002 however, does not inhibit the class II PI3Ks as potently as its counterparts (v. PI3KC2 α $27\text{ }\mu\text{M}$; v. PI3KC2 β $10.4\text{ }\mu\text{M}$) [244]. Due to its reportedly high selectivity, LY294002 has formed the basis of a pharmacological lead compound and thus played a central role in the design of newer classes of PI3K inhibitors.

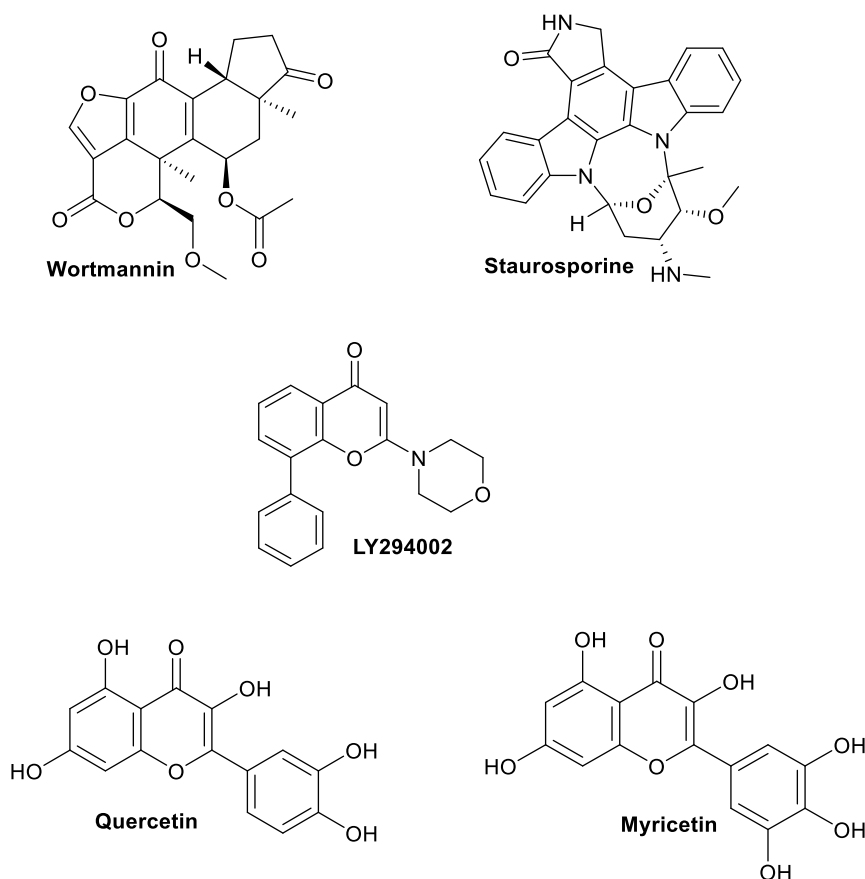


Figure 1-3: Structure of the first generation PI3K inhibitors.

1.5.2 *New-generation PI3K inhibitors*

Over the last decade, many potent inhibitors of PI3Ks have been identified based on optimisation of the first generation inhibitors or from compound screens. Compounds have been identified that inhibit all classes of PI3Ks (PAN-PI3K inhibitors) or are selective towards a particular class of PI3Ks. Some of the identified inhibitors are currently being evaluated in clinical trials. A detailed list of all the PI3K inhibitors and their current stage of clinical development has been recently reviewed by Wymann [245].

1.5.2.1 *Structural determinants of inhibitor binding*

With numerous crystal structures of the class I PI3Ks in complex ATP, as well as with various inhibitors has provided a robust template for understanding the structural features that contribute to binding of inhibitors in the active site. Crystallographic studies by Walker et al. (2000), revealed the important residues that determine or influence the inhibitor binding. All the PI3Ks adopt a common fold with a canonical ATP-binding pocket located near the kinase ‘hinge’ that connects the bi-lobed catalytic core structure. The adenine ring of the ATP forms hydrogen bonds with the hinge region and the ribose and triphosphate groups of ATP extend into the substrate binding site consisting of conserved residues essential for catalysis. The majority of the PI3K inhibitors discovered so far are ATP-competitive and occupy the ATP binding site. Some of the potent PI3K inhibitors project into a deeper hydrophobic pocket known as the ‘affinity pocket’ that is not occupied by ATP and interact with the residues that line this pocket (Figure 1-4). It is believed that interactions of the inhibitors with the residues in this region may play a crucial role in the increase in binding affinities of the potent inhibitors [246]. Some of the inhibitors also induce the formation of the ‘selectivity pocket’ which is located at the entrance of the ATP binding site.

As previously mentioned, not much is known about the class II PI3Ks and currently there is no structural information available for these isoforms. However, preliminary studies have pointed towards similarity of structural domains between class I and class II PI3K isoforms including the ATP-binding architecture [177].

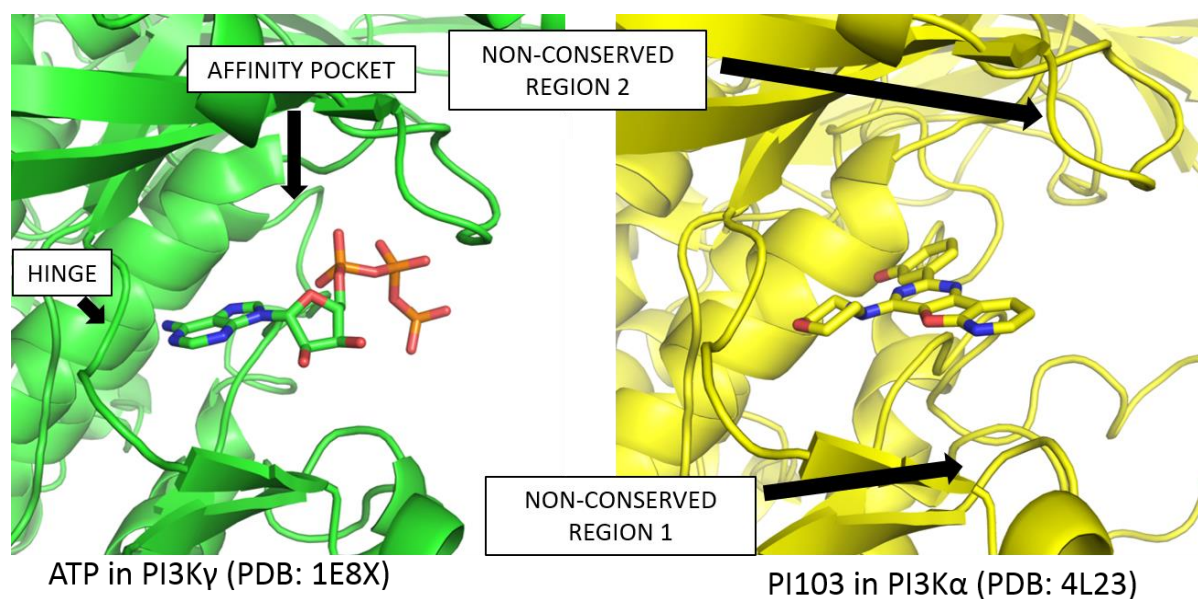


Figure 1-4: ATP binding site in PI3Ks. Comparison of ATP bound in PI3K along with ATP-competitive inhibitor PI103 bound in the ATP-binding site.

1.5.3 *Inhibitors of class II PI3K β*

In an attempt to elucidate the selectivity of PI3K inhibitors towards the class I isoforms, some of the inhibitors were also tested for potential “off-target” activity while assessing the activity against various isoforms including the class II PI3Ks [244, 246-248]. Some of the reported inhibitors that showed inhibition against PI3K β have been shown in Table 1-2 (Structures shown in Figure 1-5). Most of the inhibitors that inhibited PI3K β are the PAN-PI3K inhibitors.

Table 1-2: IC₅₀ values (μM) for reported PI3K inhibitors [249]

Inhibitor	Class I				Class II		Class III
	<i>PI3Kα</i>	<i>PI3Kβ</i>	<i>PI3Kδ</i>	<i>PI3Kγ</i>	<i>PI3KC2α</i>	<i>PI3KC2β</i>	
ZSTK474	0.016	0.044	0.0046	0.05	> 100	0.18	> 100
PI-103	0.008	0.088	0.048	0.15	1.0	0.026	2.3
PIK93	0.039	0.59	0.12	0.016	16	0.14	0.32
PIK90	0.011	0.35	0.058	0.018	0.047	0.064	0.83
PIK124	0.023	1.1	0.34	0.054	0.14	0.37	10
GDC0941	0.003	0.033	0.003	0.075	> 100	0.59	> 100
NVP-BEZ235	0.004	0.075	0.007	0.005	0.034	0.044	0.45
LY294002	0.55	11	1.6	12	27	10.4	3.5

In a recent study, two compounds PI701 (YM185453) and PI702 (YM182832) developed by Yamanouchi Pharmaceutical Co. Ltd., were tested against members of the PI3K family and inhibited the class II PI3KC2 β [250]. These two compounds exhibit high selectivity towards PI3KC2 β (IC₅₀ = 0.53 μM and 0.63 μM respectively).

In another report by Freitag *et al.* [251], the core structure of a known class I PI3K inhibitor XL147 was modified and developed two small molecule inhibitors, Freitag-26 and Freitag-30. Both of these compounds inhibit class II PI3K members PI3KC2 β and PI3KC2 γ with high selectivity for PI3KC2 β (80-fold selectivity for Freitag-26 and 10-fold selectivity for Freitag-30). With the four selective inhibitors

as promising leads, more work needs to be done in developing novel inhibitors of PI3KC2 β that are not only selective but potent as well.

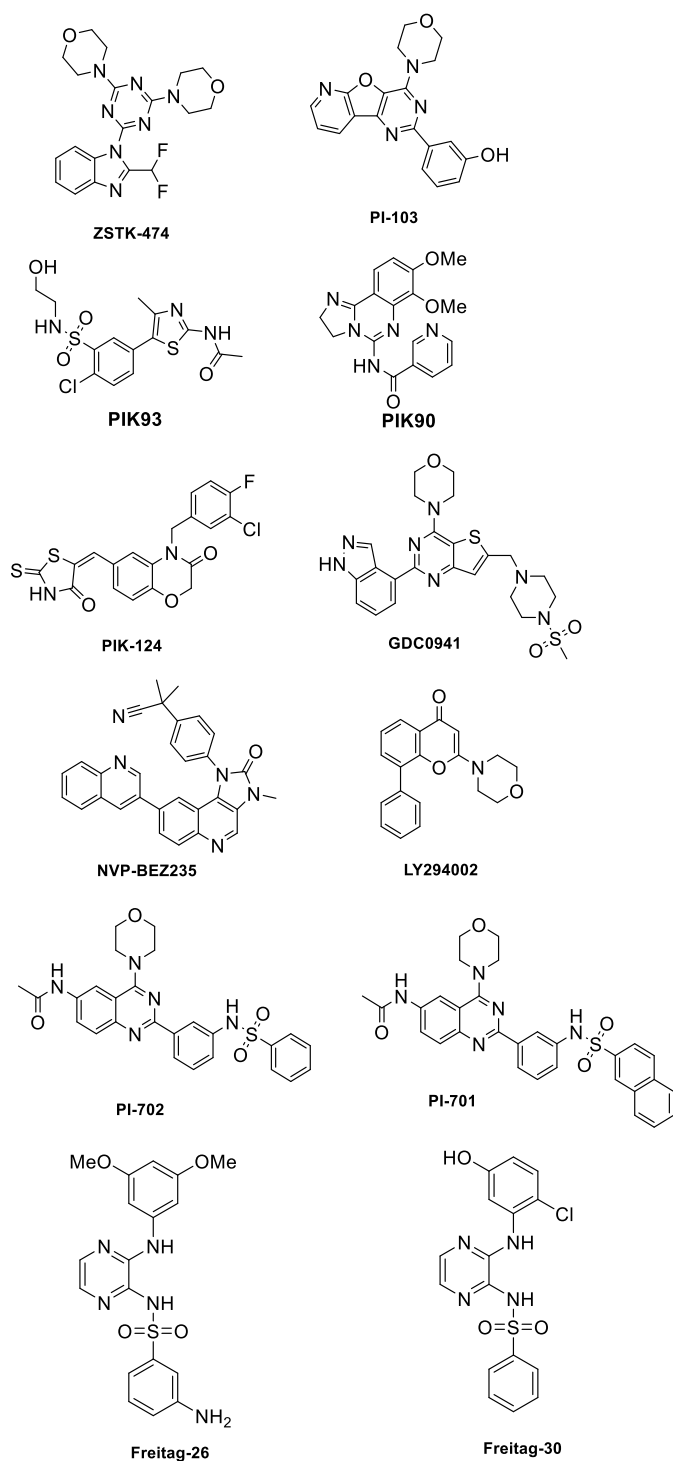


Figure 1-5: Chemical structures of the reported class II PI3K inhibitors. Class II PI3KC2 β selective inhibitors PI-701 and PI702 have been identified recently.

1.6 Rationale and Aims

Twenty years since their discovery, numerous efforts have been made in defining the roles of PI3Ks. Nevertheless, these advances have been predominantly focussed on the class I and class III PI3Ks and not much information is known about the class II PI3K members and their precise physiological significance and cellular functions. The class II PI3Ks are emerging as an important class of signalling enzymes with potential therapeutic applications. There is a growing body of evidence suggesting a role for Class II PI3KC2 β in cancer, although the exact role in cancer signalling pathway is yet to be defined.

There are numerous compounds that selectively inhibit the Class I PI3K isoforms, some of which have even advanced to clinical trials. The class II PI3Ks have been neglected due to the chronology of their discovery, and not much progress has been made to identify selective inhibitors of Class II PI3Ks. As previously mentioned, the currently known inhibitors were initially identified as a result of class II PI3Ks as a potential “off-target” activity while screening for class I inhibitors. Hence, development of isoform-selective inhibitors of class II PI3Ks may aid in understanding the class II PI3K signalling pathways as well as their cellular roles. Dissecting the exact roles of class II PI3K isoforms has been hampered by a lack of information on the structural features of class II PI3Ks. Hence developing a usable homology model may aid in understanding the structural features, in particular the residues that may play a key role in binding of small molecule PI3K inhibitors. The structural information could facilitate rational design of novel isoform-selective inhibitors for class II PI3Ks.

Chapter 2: Materials and Methods

2.1 Computational studies

2.1.1 Sequence alignment and selection of template

Protein sequences of the eight mammalian PI3Ks were retrieved from the UniProtKB database (www.uniprot.org/) [252]. Clustal Omega [149] was used to align the sequences to determine percentage identity as well as study the alignment. Based on the analysis, potential template proteins were identified, and the crystal structures for homology modelling purposes were selected representing each class and subclass of the PI3Ks.

2.1.2 Generation of PI3KC2 β homology models

Five homology models were generated using Prime Structure Prediction available from Maestro version 9.1, (Schrödinger, LLC, NY). The crystal structures of the templates from each class (apo and holo from class IA and IB and class III PI3K) were acquired from RCSB Protein Data Bank (<http://www.rcsb.org>). The structure was edited to incorporate amino acids encompassing the catalytic domain only. Selected loops were refined using extended sampling and then minimized.

2.1.3 Molecular modelling studies

All of the docking was carried out using Glide version 5.6 in the Maestro interface version 9.1, (Schrödinger, LLC, NY) using the default settings for all programs unless otherwise stated. The generated homology models and the crystal structures used in docking were prepared using the Protein Preparation module

in Maestro, which optimizes the geometry of the amino acid residues. In order to eliminate any potential bond length and bond angle biases in the structures, all of the ligands used in the studies were subjected to a full minimization prior to the docking using LigPrep. The ligands were docked flexibly using the “Extra Precision” (XP) mode of Glide [253]. The docked compounds were then examined visually in greater detail using the Pose Viewer module of Maestro. The figures showing the docked model were generated using PyMOL (DeLano Scientific).

2.2 Biochemical analysis

2.2.1 Generation of the recombinant vector

2.2.1.1 Recovery of cDNA of PI3KC2 β

The human, wild type cDNA of PI3KC2 β cloned from U937 [238] was kindly provided by Arcaro lab (University of Bern). The filter paper containing the cDNA was soaked in a microfuge tube containing 50 μ L of elution buffer (10 mM Tris-Cl, pH 8.5) for 10 min and briefly centrifuged to obtain the plasmid DNA as the supernatant.

2.2.1.2 Transformation of DH5 α cells (heat-shock method)

5 μ L of the recovered plasmid DNA was added to a microfuge tube containing 100 μ L of competent DH5 α cells and incubated on ice for 30 min. The cells were then heat-shocked for 90 s at 42 °C and immediately chilled ice for 2 min. 300 μ L of LB medium was added to the cells and incubated for 30 min. The entire culture was then plated onto an LB plate containing ampicillin and incubated at 37 °C overnight.

2.2.1.3 *Isolation of recombinant plasmid DNA*

A single colony was selected and grown in 2 mL LB-amp for 6 h then expanded to 10 mL LB-amp and allowed to grow for 16 h at 37 °C. The overnight bacterial culture was pelleted by centrifugation at 13,000 rpm (16,060 x g) using Heraeus Biofuge for 5 min at room temperature (15–25 °C). The plasmid DNA was isolated using Qiagen miniprep kit following the manufacturer's instructions. Briefly, the cell pellet was resuspended in 250 µL Buffer P1 (50 mM Tris-Cl, pH 8.0, 10 mM EDTA, 100 µg/mL RNase A). 250 µL Buffer P2 (200 mM NaOH, 1% SDS (w/v)) was added and mixed thoroughly till the solution turned clear. 350 µL Buffer N3 was added and mixed thoroughly. The entire sample was centrifuged for 10 min at 13,000 rpm (16,060 x g). The obtained supernatant was carefully transferred onto the QIAprep spin column and centrifuged for 60 s (discarding the flow-through). 0.5 mL Buffer PB containing guanidine hydrochloride and isopropanol was added to wash the spin column and centrifuged for 60 s discarding the flow-through. The QIAprep spin column was washed by adding 0.75 mL Buffer PE and centrifuged for 60 s discarding the flow-through. The QIAprep spin column was centrifuged for 1 min to remove any residual wash buffer. The QIAprep column was placed in a new, clean 1.5 mL microcentrifuge tube and 50 µL Buffer EB (10 mM Tris-Cl, pH 8.5) was added and centrifuged for 1 min to elute the DNA.

2.2.1.4 *Restriction enzyme digestion of the insert PI3KC2β and vector pFastBac HTC*

The pcDNA vector containing the PI3KC2β insert was excised from the pcDNA vector using XbaI and EcoRI. As the size of the cut plasmid was similar to the

insert, further digestion by RsrII was performed (Table 2-1). The recipient vector pFastBac HTC was subjected to digestion by XbaI and EcoRI.

Table 2-1: Restriction digestion conditions for cleaving PI3KC2B insert from pcDNA (A), further cleavage of the vector to enable distinction of the insert (B) and pFastBac HTC (C).

A) pcDNA vector with PI3KC2β insert	
DNA (PI3KC2 β in the pcDNA)	60 μ l
XbaI	2 μ l
EcoRI	2 μ l
10x Buffer (H)	8 μ l
10x BSA	8 μ l
B) Further cleavage of pcDNA vector	
Vector (pcDNA)	50 μ l
RsrII	2 μ l
dH ₂ O	2 μ l
10x Buffer (H)	6 μ l
C) pFastBac HTC	
Vector (pFastBac HTC)	28 μ l
XbaI	2 μ l
EcoRI	2 μ l
10x Buffer (H)	4 μ l
10x BSA	4 μ l

Both the digested samples were then mixed with 2 μ L loading dye and loaded onto 0.8% agarose gel to confirm the presence of insert using electrophoresis unit (Bio-Rad) at 80 V and 53 A. The 1 kb DNA ladder was added in one of the gels as a marker of molecular weights.

2.2.1.5 *Gel purification*

The insert and the vector DNA were excised from the agarose gel using a scalpel and transferred into a microfuge tube. The Qiagen gel purification kit was used to extract the insert and the vector DNA. Based on the weight of the gel slice, 3 times the volumes of buffer QG was added and incubated at 50 °C with intermittent vortexing till the gel slice completely dissolved (approximately 15 min). Next, 1X volume of isopropanol was added to the samples and mixed. The

samples were then loaded onto the QIAquick spin column placed in a 2 mL collection tube and centrifuged for a minute. The flowthrough was discarded and 0.5 mL Buffer QG was added to the QIAquick column and centrifuged for 1 minute. The flowthrough was discarded and the QIAquick column was washed with 0.75 mL Buffer PE. After 2-3 minute incubation, the samples were centrifuged for 1 min. A second spin was also carried out to remove residual wash buffer. Next, the QIAquick column was placed in a new, clean 1.5 mL microcentrifuge tube and 50 μ L Buffer EB (10 mM Tris-Cl, pH 8.5) was added to elute the insert or the vector.

2.2.1.6 *Ligation of pFastBacHTC vector and insert*

After isolating both the insert and vector DNA, the samples were placed in new tubes in various concentrations as described in Table 2-2 and incubated for 5 min at 50 °C followed by cooling on ice. This was followed by addition of 1 μ L ligase buffer and 1 μ L T4 DNA ligase and incubation at 16 °C for 3-4 h.

Table 2-2: Conditions for ligation of pFASTBac HTC with PI3C2B insert

Dilution	Insert (PI3KC2 β)	Vector (pFastBac HTC)	dH ₂ O	Total
Negative control	0 μ L	1 μ L	7 μ L	8 μ L
1:1	1 μ L	1 μ L	6 μ L	8 μ L
3:1	3 μ L	1 μ L	4 μ L	8 μ L
6:1	6 μ L	1 μ L	1 μ L	8 μ L

2.2.1.7 *Transformation and isolation of DNA*

5 μ L of ligation mix was added to a microfuge tube containing 50 μ L of competent DH5 α cells and transformed as described in Section 2.2.1.2. Three single colonies were picked from the plate with 6:1 insert: vector ratio, cultured in 2 mL LB containing ampicillin by incubating at 37 °C for 5 h. The entire 2 mL

culture was transferred into a tube containing 10 mL LB containing 100 µg/mL ampicillin and incubated overnight at 37 °C. The cells were harvested and the DNA was isolated using the Qiagen miniprep kit method as described in Section 2.2.1.3. The concentration of the obtained DNA was measured using a Nanodrop spectrophotometer (Thermo-Scientific) and the DNA samples were stored at -20 °C.

2.2.1.8 *Confirmation of presence of the insert by restriction analysis and DNA sequencing*

The insert length was confirmed by restriction digestion of the plasmid containing the PI3KC2B (Table 2-3). Restriction digest was mixed with 2 µL loading dye and loaded onto 0.8% agarose gel to confirm the presence of DNA using electrophoresis.

Table 2-3: Double digestion of pFastBac HTC containing PI3KC2B to confirm fragment sizes

Restriction digestion of DNA	
DNA	2 µL
XbaI	1 µL
EcoRI	1 µL
10X buffer (H)	1 µL
10x BSA	1 µL
dH₂O	4 µL

To confirm the sequence of the insert, DNA was sent to Micromon DNA sequencing facility, Monash University.

2.2.2 Generation of recombinant bacmid

2.2.2.1 Generation of DH10bac competent cells

The DH10Bac cells were cultured in 100 mL LB containing kanamycin (50 µg/mL), tetracycline (10 µg/mL) at 37 °C/ 225 rpm until OD₆₀₀ was about 0.6-0.8. 50 mL of the culture was transferred into sterile falcon tubes and cooled on ice for 10 min and centrifuged at 5000 x g for 15 min at 4 °C. The pellet was resuspended in 10 mL of ice-cold 0.1M CaCl₂ and incubated on ice for 10 min. The cells were centrifuged at 5000 x g for 15 min at 4 °C and the cell pellet was resuspended in 2 mL of 0.1M CaCl₂ containing 20% (v/v) glycerol, aliquot into microfuge tubes (250 µL per tube) and stored at -70 °C for future use.

2.2.2.2 Transformation DH10Bac E. coli competent cells with pFastBac plasmids

The pFastBac HTC vector containing the PI3KC2β was transformed into the DH10Bac based on the protocol described in Bac-to-Bac® Baculovirus Expression System (Version D, Invitrogen). For each transformation, 5 µL of pFastBac HTC plasmid DNA (1ng) was added to 100 µL of the competent DH10Bac cells and incubated on ice for 30 min. The cells were then subjected to heat-shock for 45 s at 42 °C without shaking and immediately chilled on ice for 2 min. 900 µL of LB Medium (room temperature) was added to the cells and incubated at 37 °C, with shaking at 225 rpm for about 4 h. 300 µL of the culture was plated on an LB agar plate containing 50 µg/mL kanamycin, 7 µg/mL gentamicin, 10 µg/mL tetracycline, 100 µg/mL X-gal, and 40 µg/mL IPTG and incubated for 48 h at 37 °C. Another LB agar plate containing 50 µg/mL kanamycin, 7 µg/mL gentamicin, 10 µg/mL

tetracycline, 100 µg/mL X-gal, and 40 µg/mL IPTG was plated with 300 µL 1:10 dilution of the cells and incubated for 48 h at 37 °C.

2.2.2.3 Recombinant phenotype verification using blue/white colony screening

After the 48 h incubation, the plates were screened for the presence of single, large white colonies for phenotype verification. 10 white colonies were selected and re-streaked on fresh LB agar plates containing 50 µg/mL kanamycin, 7 µg/mL gentamicin, 10 µg/mL tetracycline, 100 µg /mL X-gal, and 40 µg /mL IPTG and incubated overnight at 37 °C.

2.2.2.4 Isolation of recombinant bacmid DNA

A single, isolated bacterial colony was inoculated into 2 mL of LB medium containing 50 µg/mL kanamycin, 7 µg/mL gentamicin, and 10 µg/mL tetracycline and grown in a 37 °C for 4-5 h. The entire 2 mL culture was transferred into 10 mL of LB medium containing 50 µg/mL kanamycin, 7 µg/mL gentamicin, and 10 µg/mL tetracycline and incubated overnight at 37 °C shaking at 225 rpm.

The cells were then centrifuged at 4,000 rpm (3220 x g) for 15 min and the cell pellet was resuspended in 200 µL of Solution I (50mM Tris-HCl pH8.0, 10mM EDTA 100µg/mL ribonuclease) followed by 200 µL of Solution II (200mM NaOH, 1% SDS (w/v) and incubated for 5 min at room temperature. 200 µL of Solution III (3M Potassium acetate pH 5.5) was added while gently mixing and cooled on ice for 5 to 10 min. The sample was then centrifuged for 10 min at 13,000 rpm (16060 x g) and the supernatant was carefully transferred to a fresh microcentrifuge tube containing 0.8 mL of isopropanol and placed on ice for 5 to 10 min. The sample

was centrifuged for 15 min at 13,000 rpm (16060 x g) and the supernatant carefully removed, taking care not to disturb the pellet.

The cell pellet was washed three times with 0.5 mL of 70% ethanol and mixed by inversion to wash the pellet and recovered by centrifugation for 5 min at 13,000 rpm (16060 x g) between each wash. The pellet was air-dried for 5 to 10 min at room temperature, before being dissolved in 40 µL of 1X TE Buffer (pH 8.0) and stored at 4 °C for future use.

2.2.2.5 *PCR analysis of the recombinant Bacmid DNA*

To analyse the recombinant Bacmid DNA, PCR reaction was performed to amplify the region of interest and verified using gel electrophoresis. PCR reaction was performed with P-17 and PT-18 primers or with internal PI3K C2beta oligos (PT44 and PT-18, to reduce the size of PCR product). The reaction mixture was prepared using the recipe as described below (Table 2-4). 19 µL reaction mix was mixed with 1 µL of DNA for PCR analysis, and the PCR products were analysed on 1% agarose gel.

Table 2-4: PCR reaction mixture and cycle conditions

Reaction Mixture	
40µL	10 x Taq buffer
4µL	10mM dNTPs
4µL	5' primer, 1:10 dilution (5' bacmid specific, M13F, PT-17 or PT-44)
4µL	3' primer, 1:10 dilution (3' bacmid specific, M13R, PT-18)
2µL	Taq polymerase
156µL	dH ₂ O

Step	Time	Temperature	Cycles
Initial	3 min	93°C	1
Denaturation			
Denaturation	45 s	94°C	35
Annealing	45 s	55°C	
Extension	45 s	72°C	
Final Extension	7 min	72°C	1

2.2.3 Production of the recombinant baculovirus

2.2.3.1 Recovery of cryopreserved Sf9 cells

1 mL of frozen Sf9 cells were thawed in a 37 °C water bath and added to a tube containing 20 mL of 1X Sf-900™ II SFM media (Life technologies) and incubated at 27 °C in a shaker (140 rpm) overnight. The cells were then centrifuged at 550 x g for 5 min (to remove residual DMSO) and the pelleted cells were resuspended in 20 mL of fresh 1X Sf-900™ II SFM media and incubated for 48 h.

2.2.3.2 Culturing Sf9 cells (cell viability)

Suspension cultures of Sf9 cells were cultured and maintained at cell density 1-8 x 10⁶ cells/mL in a sterile bottle at 27 °C in a shaker (140 rpm). Oxygenation was achieved by lightly loosening the cap of the bottle. The cells were counted twice a week and passaged. The cell viability was determined by staining with

0.2% Trypan blue and counting the cell viability on a haemocytometer using the following equation:

$$\% \text{ viable cells} = [1.00 - (\text{Number of blue cells} \div \text{Number of total cells})] \times 100$$

2.2.3.3 *Cryopreservation*

The Sf9 cells were checked for cell viability (found to be >96%) using 0.2% Trypan blue as described earlier. Cells were centrifuged to remove media and were resuspended in Sf-900™ II SFM media containing 10% DMSO. The cells were aliquot in 1 mL cryotubes and placed in cryofreezing container overnight at -70 °C. These tubes were transferred to liquid nitrogen container for future use.

2.2.3.4 *Transfection of insect cells with recombinant bacmid DNA*

The recombinant bacmids containing the PI3KC2β (Section 2.2.2.4) were used to transfect the Sf9 cells to produce the recombinant baculovirus using the Bac to Bac Expression system. In a 6-well plate (Corning® Costar® cell culture plates, Sigma–Aldrich), the Sf9 cells were seeded in 2 mL of fresh Sf900 medium and incubated for at least an hour for the cells to allow the cells to adhere to the bottom surface of the wells. Following this incubation, the media was aspirated off and replaced with 800 µL 1X Sf-900™ II SFM media. For each transfection, 2-8 µg of bacmids DNA mixed with 6 µL of cellfectin reagent (Life Technologies) was added to each well and incubated for 5 h at 27 °C. After 5 h, the entire mixture in all the wells was removed and replenished with 2 mL of fresh 1X Sf-900™ II SFM media and further incubated for 72 h at 27 °C.

2.2.3.5 *Isolation of P1 viral stock*

Post transfection the medium from each well containing the recombinant virus was harvested by centrifuging at 550 x g for 5 min to remove the cells and cell debris. The P1 virus was stored at 4 °C.

2.2.3.6 *Amplification of the viral stock*

The P1 virus (100 µL- 200 µL) was then used to infect a 2 mL well of Sf9 cells (cell density 1×10^6 cells/mL) for 72 h in order to amplify the virus to produce P2 virus. P2 virus was re-amplified to produce P3 virus stock using 100 µL-250 µL P2 virus and infect a 2 mL well of Sf9 cells (cell density 1×10^6 cells/mL) for 72 h. The viral stocks were harvested following centrifugation at 550 x g for 5 min.

2.2.3.7 *Viral plaque assay*

The titre of the baculovirus stock was determined using the viral plaque assay. 2 mL of Sf9 cells (cell density 1×10^6 cells/mL) along with Sf900 medium containing Pen-Strep was dispensed in each well of a 6-well plate and allowed to adhere for at least 15 min at room temperature. Once the cells were adhered the medium was aspirated and 200 µL of virus solution (Serial 1:10 dilutions of P2 and P3 virus solution were made by diluting 900 µL SF900 medium with dilutions of 10^{-3} , 10^{-4} , 10^{-5} , 10^{-6} , 10^{-7} viral dilutions along with control) was added and incubated for an hour at 28 °C. As a negative control, one of the wells consisted of medium alone. Following the incubation, the virus solution was removed, and 1.5 mL of agar solution was added and allowed to set at room temperature. Agarose overlay solution was prepared by adding 5 mL of the 4% agarose was melted in the microwave and cooled to 37 °C in a 50 mL tube and 15 mL of 1.3X Sf900

medium containing pen-strep was added just prior to use. Once the agarose overlay was set, 1.5 mL of SF900 medium containing pen-strep was added, and the 6-well plate was incubated at 28 °C for around 5 days. The plates were checked for plaques by staining with neutral red (1 mg/mL water), and the viral titre was calculated as follows:

$$\text{Titre (pfu/mL)} = \text{No. of plaques} / (\text{dilution factor} \times \text{Volume of diluted virus/well})$$

2.2.4 *Expression and Purification of PI3KC2β*

400 mL of Sf9 cells at a cell density of 2×10^6 cells/mL were infected with 40 mL of the P3 virus and incubated for 48 h at 27 °C at 140 rpm. The cells were harvested at 3000 rpm (1811 x g) for 15 min.

The obtained pellet was re-suspended in 20 mL lysis buffer (50 mM Na_2HPO_4 , 300 mM NaCl, 10 mM imidazole, 1% Tween-20, & Complete Protease Inhibitors (Roche, 1 tablet/50 mL) pH 8.0) and sonicated four times for 5 secs with 5 secs rest. The sample was then centrifuged at 15000 rpm (30000 x g) for 30 min at 4 °C. The obtained supernatant was loaded onto 0.5 mL of Ni-NTA beads and incubated on a shaker for at least 1h at 4 °C. The sample along with the beads was centrifuged at 3000 rpm (1811 x g) at 4 °C for 5 min remove supernatant. The beads were washed twice with 0.5 mL wash buffer (50 mM Na_2HPO_4 , 300 mM NaCl, 10 mM imidazole, pH 8.0.) and PI3KC2β was eluted using 0.5 mL of elution buffer (50 mM Na_2HPO_4 , 300 mM NaCl, 350 mM imidazole, pH 8.0) into 6 different tubes.

Fractions containing the PI3KC2 β protein were pooled and dialysed against 2 L of 50 mM Tris-HCl pH 7.5, 300 mM NaCl at 4°C for 16h. PI3KC2 β protein stocks were made 20% (v/v) glycerol and 2 mM DTT and stored in aliquots at -80 °C.

2.2.5 *Protein separation by SDS-PAGE*

The purified protein samples were separated and analyzed using PolyAcrylamide Gel Electrophoresis (PAGE) in the presence of SDS and DTT. Each of the samples were mixed with 2x SDS loading buffer (20 mM Tris-HCl pH 6.8, 30% Glycerol [v/v], 4% SDS [w/v], 0.01% bromophenol blue [w/v], 10mM DTT) and heated to 95 °C for 5 min prior to separation on the 8% acrylamide gel. The gel was stained using Coomassie Brilliant Blue solution (50% methanol [v/v], 10% acetic acid [v/v] in water with 1 g/L of Brilliant Blue R250) for 1 h at room temperature on a shaker and washed in de-staining solution (40% methanol [v/v], 10% acetic acid [v/v] in water) for 3-4 h at room to visualize the protein bands. The purity of the bands and the molecular weights were calculated using the GelAnalyzer software (version 2010a, gelanalyzer.com).

2.2.6 *Western blot*

Following electrophoresis, the gels were subject to electrophoretic transfer onto nitrocellulose membrane at 60 V for 2 h in transfer buffer (25 mM Tris, 190 mM glycine, 20% methanol [v/v]). Following the blotting, the membrane was blocked with Odyssey® Blocking Buffer (LI-COR Biosciences) for 1 h at RT in a small tray on a rocker. This was followed by incubation with 1:500 dilution of primary rabbit anti-human PI3KC2 β antibody (Santa Cruz Biotech) in PBST for

1 h at RT. Membranes were washed three times in PBST and incubated with anti-rabbit secondary antibody used at 1:2000 (LI-COR Biosciences) for 1 h at RT. Membranes were washed three times in PBST followed by detection using Odyssey® Infrared Imaging System (LI-COR Biosciences).

2.2.7 *Enzyme assays*

To determine the PI3K enzyme activity, a luminescence-based kinase activity assay (Kinase-Glo Assay platform, Promega) was used. The assay measures the decrease in ATP concentration during the kinase reaction. The amount of purified enzyme used was optimised experimentally to obtain a linear relationship between enzyme concentration and activity. The reaction mixture consisting of 20 mM HEPES pH 7.5, 5 mM MgCl₂, PI substrate (180 µM) and 10 µM ATP was added to the enzyme and incubated at RT for 1 h to initiate the kinase reaction. The ATP remaining was measured by incubating reaction mixture with an equal amount of Kinase-Glo reagent (Promega) for 15 min. The luminescence was measured using a Fluostar plate reader (BMG Labtech).

2.2.8 *Inhibition assays*

The PI3K inhibitors were dissolved at 10 mM in dimethyl sulfoxide (DMSO). Inhibitors were diluted in 20% (v/v) DMSO at the indicated concentrations (JP 7-126: 2 µM to 0.004 µM; JP 7-118: 100 µM to 0.2 µM; JP 7-108: 500 µM to 0.1 µM) to generate an inhibitor concentration versus enzyme activity curve. Assays were repeated for each compound in three separate assays each performed in duplicate. Individual dose–response curves were generated, and IC₅₀ values were determined

using GraphPad Prism version 5.00 for Windows, (GraphPad Software, San Diego California USA) and reported as Mean \pm SEM (n=3).

Chapter 3: Results and Discussion

3.1 Development of homology models of PI3KC2 β : insights for the development of isoform-selective inhibitors of PI3KC2 β

3.1.1 Introduction

In the absence of crystal structures, homology models serve as useful tools in structure-based drug discovery and drug design. Homology modelling, also referred to as comparative modelling, utilises experimentally determined protein structures as templates to predict the three-dimensional structure of the target protein with a similar amino acid sequence. Development of a useful homology model can aid in understanding the structural features. This study focusses on the generation of a homology model of PI3KC2 β to understand the key structural attributes that could aid in the rational design of class II PI3KC2 β inhibitors.

3.1.2 Protein sequence comparison of human PI3Ks to identify a suitable template protein for development of homology model of PI3KC2 β

The quality of homology models relies heavily on the sequence similarity between the primary target sequence and the sequence of the template protein. Therefore the initial step is to identify the proteins with

available three-dimensional structures that are related to the target sequence [254]. The protein sequences of the catalytic domains of the eight human isoforms of PI3Ks were compared to identify a suitable template for developing a model of PI3KC2 β . The protein sequences of the overall catalytic subunits of the class I and III PI3Ks were used to compare the sequences. CLUSTAL-Omega, software available from European Bioinformatics Institute (EMBL-EBI) was used for sequence alignment [149].

The sequence comparison of the eight human PI3K sequences revealed that PI3KC2 β shares highest sequence identity with the other class II PI3K members PI3KC2 α (47%) and PI3KC2 γ (36%) (Table 3-1). Against the remaining isoforms, the homology is \sim 28% (Table 3-1). The results of the alignment are shown in Appendix 5.

Table 3-1: Sequence identity of the catalytic sub-unit of PI3KC2 β with the catalytic subunits of the eight human PI3K isoforms.

Class	Enzyme (catalytic sub-unit)	Sequence identity (%)
Class I	p110 α	28.54
	p110 β	27.5
	p110 δ	27.25
	p110 γ	28.5
Class II	C2 α	46.96
	C2 γ	36.25
Class III	hVps34	27.72

A sequence identity greater than 30% is generally accepted as the requirement for developing efficient homology models [254]. However, as none of the proteins with available X-ray structures share greater than 30% identity, it was decided to examine a suite of structural templates. The templates chosen included class IA PI3K p110 α , class IB PI3K p110 γ as well as a class III PI3K structure. Templates were chosen to represent both apo (without ligand) and holo (with a ligand) structures to compare the influences of ligand-induced changes in the binding pocket.

Two homology models were developed based on the crystal structures of class I A PI3K p110 α . The first homology model (model 1) was developed using the co-ordinates of apo-PI3K p110 α (PDB: 4TUU) as a template [255]. The second model (model 2) was developed using the co-ordinates of murine PI3K p110 α in complex with the inhibitor PIK-108 (PDB: 4A55) as a template. A notable feature in template PDB: 4A55 is that the binding of ligand PIK-108 induces a conformational change in one of the key residues (Met702) in the binding pocket of class I PI3Ks by opening up the binding pocket to accommodate the ligand [256]. For class IB PI3K p110 γ again, two models were generated using the apo and holo structures (model 3 and model 4 respectively). The apo structure (PDB: 1E8Y) was one of the first PI3K crystal structures and exhibits a high resolution of 2 Å [257], and the holo structure consists of a PI3K p110 γ bound to a selective PI3K p110 γ inhibitor AS605240 (PDB: 2A5U) [258].

Model 5 was developed using the co-ordinates of the only human class III PI3K crystal structure available (PDB: 3LS8) (Tresaugues *et. al*, unpublished data; DOI: 10.2210/pdb3ls8/pdb). Notably, the class III PI3K has, in common with PI3KC2 β , a Phe residue in the binding site aligned with the methionine residue (Met702) described above which is common to class I PI3Ks.

In conclusion, five homology models were generated based on the three sub-classes of PI3K (Class I A and IB as well as class III). Each of the generated homology models was assessed using Ramachandran plot analyses and the backbone phi and psi angles were found to be in the expected regions. A summary of the templates used for the generation of homology models is presented in Table 3-2.

Table 3-2: Five homology models developed using the co-ordinates of available crystal structures of class I and class III PI3Ks. The templates were chosen based on the resolution of the structure, presence of the ligand and differences in the binding site.

Homology Model	PDB ID	Crystal Structure	Resolution	Ligand
<i>Model 1</i>	4TUU	PI3K p110 α	2.6 Å	None (Apo structure)
<i>Model 2</i>	4A55	PI3K p110 α	3.5 Å	PIK-108
<i>Model 3</i>	1E8Y	PI3K p110 γ	2.0 Å	None (Apo structure)
<i>Model 4</i>	2A5U	PI3K p110 γ	2.7 Å	AS605240
<i>Model 5</i>	3LS8	hVps34	2.2 Å	3-[4-(4-Morpholinyl)thieno[3,2-d]pyrimidin-2-yl]-phenol

The five generated models all appeared to be plausible at the level of tertiary structure and in fact exhibited high similarity to each other with an RMSD <3Å, varying largely only in the loop regions (Figure 3-1). The

binding pockets of the five models were also quite similar to each other with only slight movement of the protein backbone. Model 5, based upon the class III Vps34 showed a distinct difference in conformation at the hinge which also manifested as a displacement of the residue Glu1136 (Figure 3-1). One of the residues, Phe1057 exhibited different conformations across the five models, consistent with the variable positioning of the corresponding residue in the template proteins.

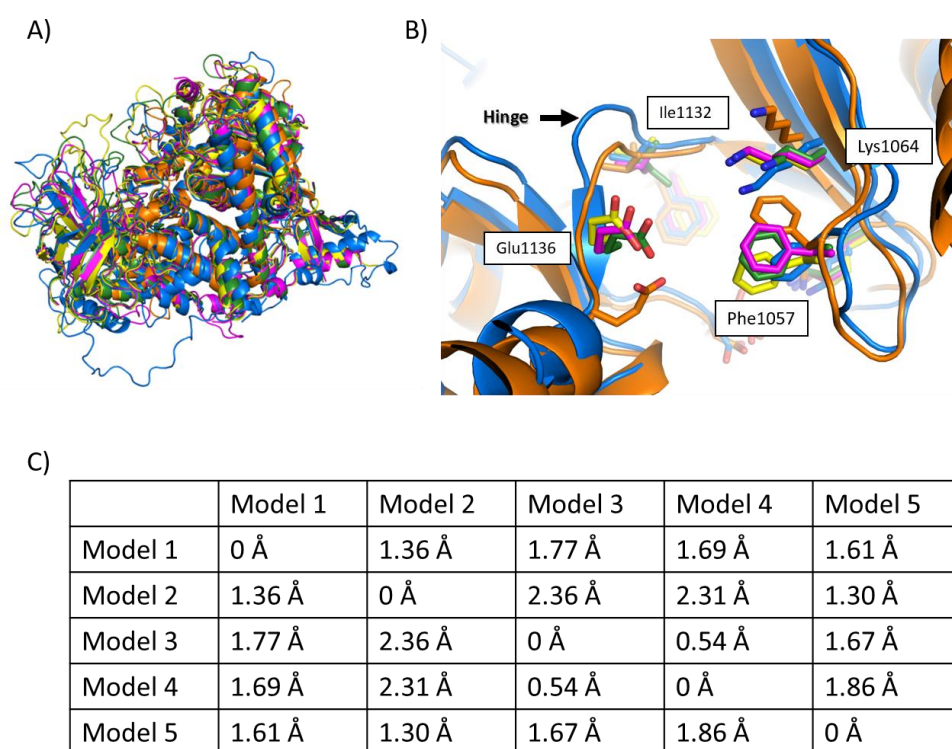


Figure 3-1: The five generated homology models : A) Superimposition of the five models (models 1: blue, model 2: magenta, model 3: green, model4: yellow and model 5: orange). The overall structure is conserved in all the generated models with a few differences in the loop regions. B) Close-up of the binding pocket of PI3KC2 β shows different conformations of the residues. For clarity, only the residues that vary are shown. The hinge loop also exhibits a minor movement only in model 5 as shown. C) The RMSD values of the models when superimposed on each other indicate that the models are quite similar to each other.

A number of non-conserved residues in the binding pocket of class I PI3Ks have been shown to contribute to the isoform selectivity of inhibitors within the Class I isoforms, while others are conserved across the series. [259], Sequence analysis of the corresponding residues in all eight human PI3K isoforms reveals that some residues are conserved within class I PI3Ks, but they vary in class II and III isoforms. The non-conserved residues lining the ATP-binding pocket may contribute to the differences in ligand binding affinity or isoform selectivity (Figure 3-2).

Table 3-3: The non-conserved residues in binding site of the eight mammalian PI3K isoforms

PI3K Isoform	Region 1			Region 2					
	1136	1138	1140	1056	1057	1058	1061	1064	1065
PI3K α	H	I	Q	I	M	A	K	R	W
PI3K β	E	I	D	Y	M	K	M	K	W
PI3K δ	D	I	N	F	M	K	M	K	W
PI3K γ	T	I	K	V	M	K	K	K	W
PI3KC2 α	D	L	Q	F	F	N	A	V	K
PI3KC2 β	E	L	K	Y	F	N	A	V	K
PI3KC2 γ	V	L	K	Y	F	N	A	L	K
PI3KC3	P	A	V	L	F	K	L	M	Q

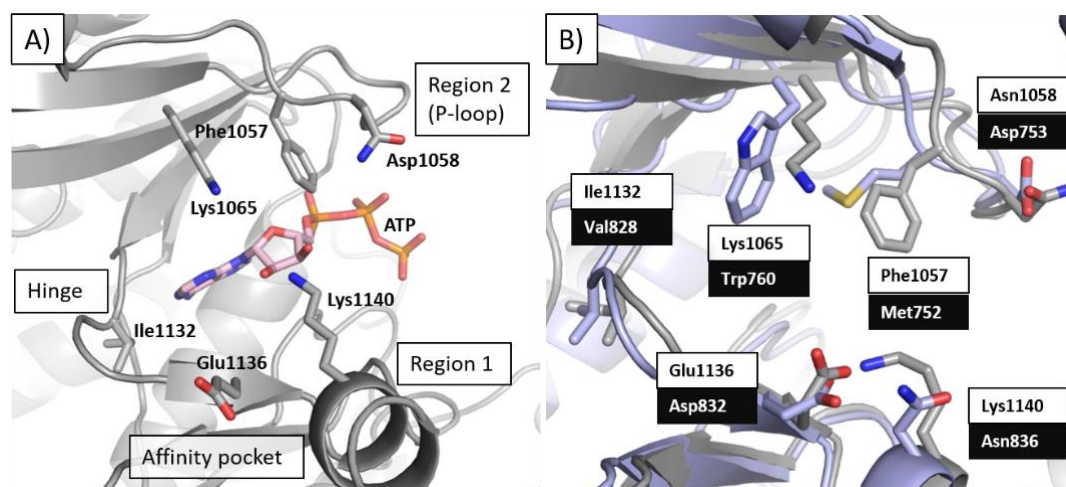


Figure 3-2: Close-up of PI3KC2 β binding pocket. A) The binding site of PI3KC2 β (model 3 shown) superimposed on the crystal structure of PI3K p110 γ in complex with ATP. Some of the residues belonging to region 1 (1136-1140 in PI3KC2 β) and region 2 (1057-1065) as shown are believed to confer selectivity. B) The non-conserved residues belonging to region 1 and region 2 are shown in the text boxes. The residues in black text boxes correspond to the residues in the crystal structure of PI3K p110 δ (PDB: 2WXL).

The P-loop, which is believed to associate with the phosphates of ATP, is quite heterogeneous among the PI3Ks. This loop (also referred to as region 2 in previous literature [260]) has been previously shown to be flexible when binding to ATP and other ligands [260]. Two key residues in the P-loop (Met752 and Trp 760 in class I PI3K δ) are modified in class II PI3Ks and replaced with a phenylalanine and a lysine respectively (Figure 3-2).

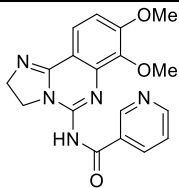
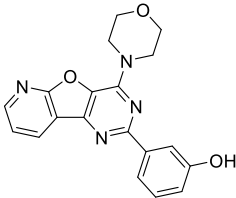
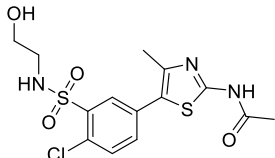
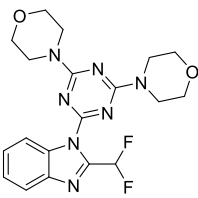
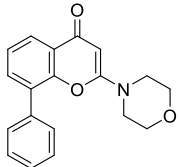
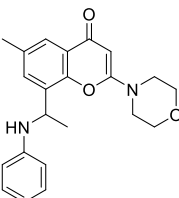
3.1.3 *Docking of known PI3KC2 β inhibitors into homology models*

Molecular docking was used to assess the ability of the five generated PI3KC2 β models to recapitulate likely binding poses of ligands previously

co-crystallised with other isoforms. The key assertion was that potent inhibitors would adopt the same binding pose in PI3KC2 β as in Class I or Class III enzymes for which they also held activity.

Six PI3K inhibitors (PIK-90, PIK-93, PIK-108, PI-103, ZSTK-474 and LY294002) were selected for docking simulations based on the availability of crystal structures of these inhibitors co-crystallized with either class I or class III PI3Ks, also noting differences in the inhibitory potencies at PI3KC2 β as well as their structural diversity. We wanted to identify which if any of the homology models could accommodate ligands that inhibited PI3KC2 β in a similar binding mode to the available crystal structure.

Table 3-4: List of the selected inhibitors chosen for validation.

Inhibitor	PI3KC2 β	PDB ID	Structure
PIK-90	0.064	2CHX	
PI-103	0.026	4L23	
PIK-93	0.14	2CHZ	
ZSTK-474	0.180	2WXL	
LY294002	10.4	1E7V	
PIK-108	> 100	4A55	

3.1.3.1 *Molecular docking studies in the homology model of PI3KC2 β*

Each of the selected compounds was docked in the binding pocket of each of the generated homology models and are discussed individually here.

3.1.3.1.1 ***PI-103***

Among the set of inhibitors chosen in the study, PI-103 exhibits the highest inhibition of PI3KC2 β with an IC₅₀ of 26 nM comparable to its potency at PI3K p110 α (IC₅₀ of 8 nM). In the crystal structure in PI3K p110 α (PDB:4L23), PI-103 adopts a flat conformation and the hydroxyl group of the phenol moiety interacts via H-bonds with an aspartyl residue of the affinity pocket [261]. Docking studies of PI-103 in the binding pocket of PI3KC2 β revealed that the binding pose of PI-103 (Figure 3-3) in the active site was similar to the crystal structure in only two of the generated models model 1 and model 5 (RMSD 1.32 and 2.09 Å respectively). Interestingly, in Model 1 the acidic phenol group sat in the affinity pocket but was flipped to interact with a lysine residue.

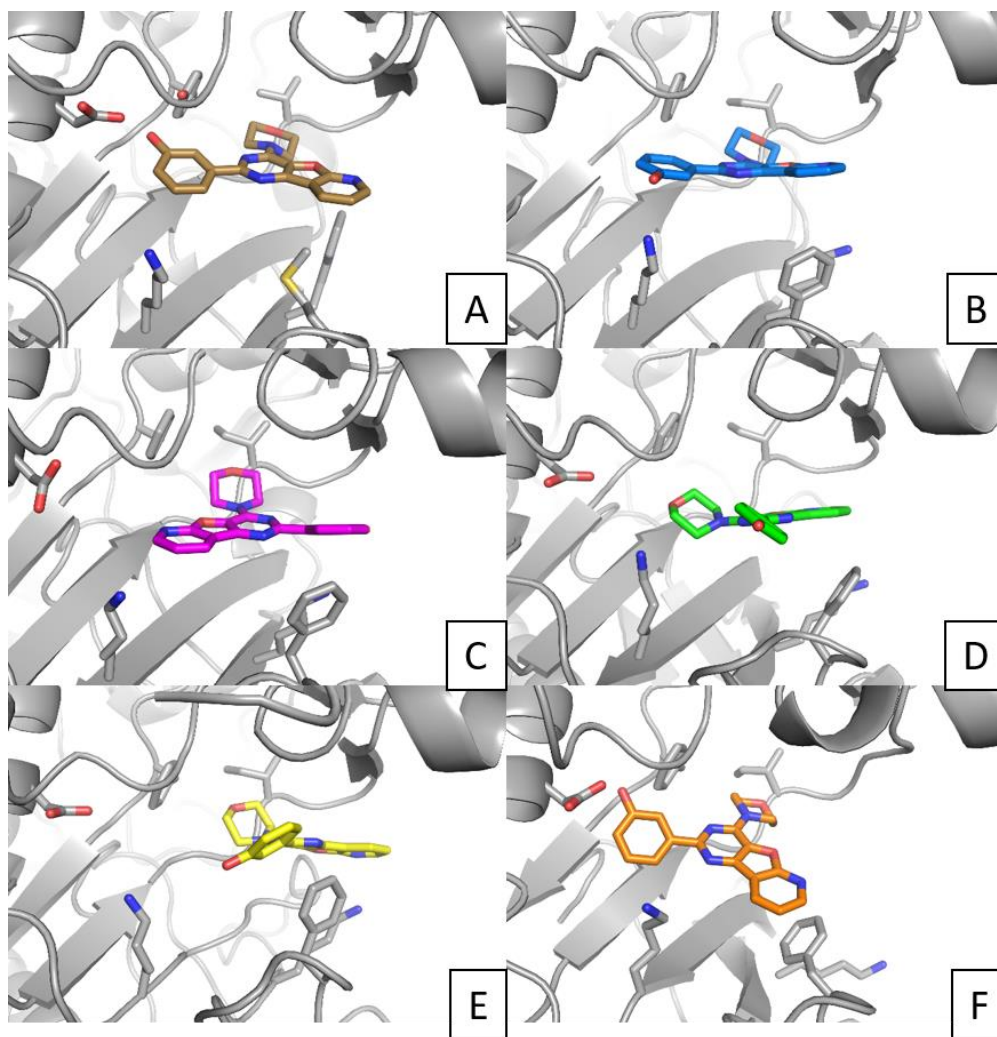


Figure 3-3: Docked poses of PI-103 in the five generated models and the crystal structure. A represents PI-103 co-crystallized in PI3K p110 α (PDB: 4L23). B to F (clockwise) represent the PI-103 docked in model 1: blue, model 2: magenta, model 3: green, model 4: yellow and model 5: orange.

3.1.3.1.2 *PIK-90*

PIK-90 is a potent inhibitor of all PI3Ks and inhibits PI3KC2 β with an IC₅₀ of 64 nM. Docking studies of PIK-90 in the five generated homology models revealed that model 1, model 2 and model 5 were able to present PIK-90 in a similar orientation as the reported crystal structure with RMSD values of 1.95 Å, 1.76 Å and 1.45 Å respectively.

In the co-crystal with PI3K p110 γ (PDB: 2CHX), PIK-90 makes a hinge interaction via its imidazole nitrogen and extends its 3-pyridinylcarboxamide deep into the affinity pocket. Docked into model 1, 2 and 5, the same interactions are produced. Models 4 and 5 show flipped poses, with no strong interaction with the affinity pocket (Figure 3-4).

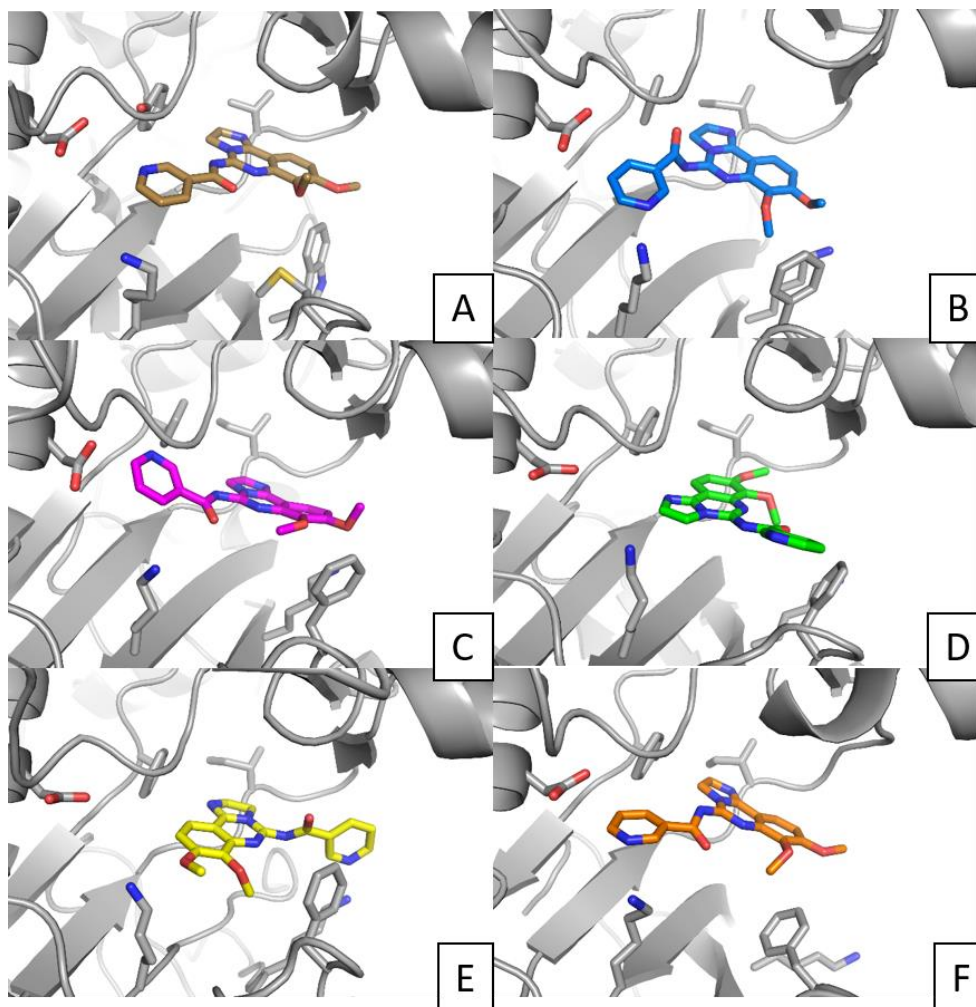


Figure 3-4: Docked poses of PIK-90 in the five generated models and the crystal structure. A represents PIK-90 co-crystallized in PI3K p110 γ (PDB: 2CHX). B to F (clockwise) represent the PIK-90 docked in model 1: blue, model 2: magenta, model 3: green, model 4: yellow and model 5: orange.

3.1.3.1.3 *PIK-93*

PIK-93 has an IC₅₀ of 140 nM versus PI3KC2 β compared to 16 nM versus PI3K p110 γ , with which it has been co-crystallized (2CHZ). Docked into the five generated homology models, a comparable pose to the crystal structure was achieved only in model 4 and model 5 with an RMSD of 2.5 Å and 1.64 Å (Figure 3-5). It is important to note that model 4 was originally built from the co-ordinates of 2CHZ, illustrating the ability of the homology model to template the parent ligand's binding site. The other three models failed to reproduce the crystal structure and exhibited high RMSD values (>10 Å).

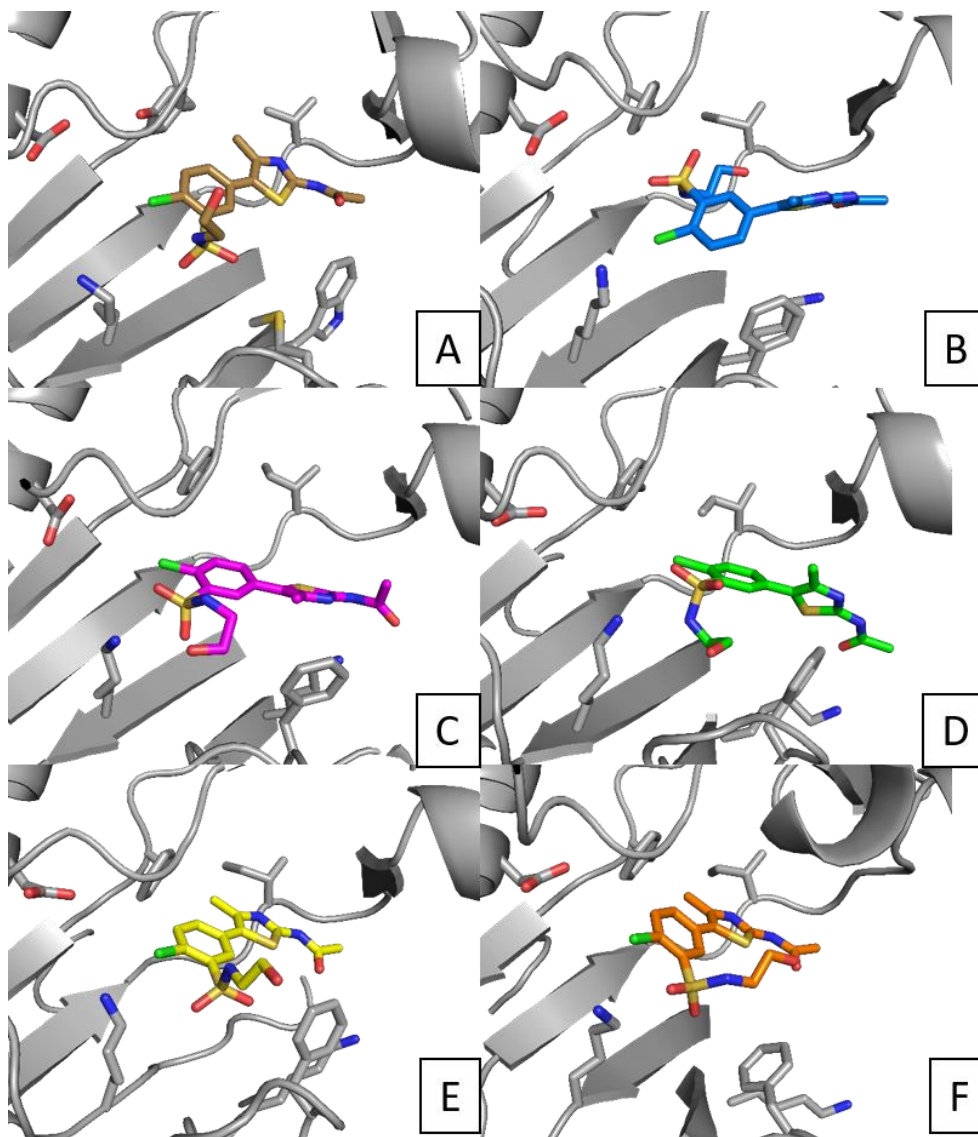


Figure 3-5: Docked poses of PIK-93 in the five generated models and the crystal structure. A represents PIK-93 co-crystallized in PI3K p110 γ (PDB: 2CHZ). B to F (clockwise) represent the PIK-93 docked in model 1: blue, model 2: magenta, model 3: green, model 4: yellow and model 5: orange.

3.1.3.1.4 *ZSTK-474*

ZSTK-474, a selective pan-class I PI3K inhibitor is a moderately potent PI3KC2 β inhibitor with an IC₅₀ of 180 nM. The ZSTK-474 bound in the crystal structure (PDB: 2WXL) consists of the benzimidazole group

extending into the affinity pocket [262]. The outputs of ZSTK-474 docked in the five generated models failed to reproduce the pose of ZSTK474 found in the crystal structure with the exception of homology model 1 which was able to imitate the crystal structure (from PI3K p110 δ , PDB 2WXL) with an RMSD of 1.21 Å (Figure 3-6). An interesting feature of these docking results is the apparent unwillingness of the models to accommodate the benzimidazole moiety in the affinity pocket. It should be noted that the first reported docking studies of ZSTK474 into Class I isoforms (PI3K p110 γ) equally failed to replicate the mode of binding shown crystallographically [263].

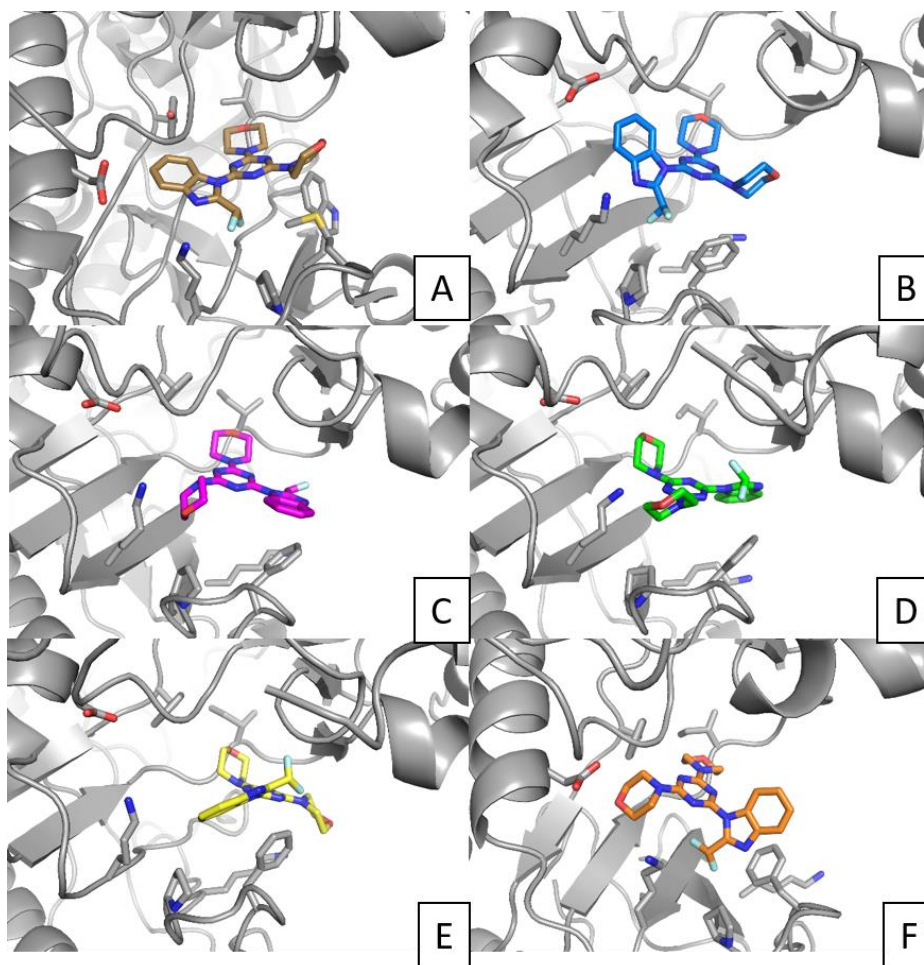


Figure 3-6: Docked poses of ZSTK-474 in the five generated models and the crystal structure. A represents ZSTK-474 co-crystallized in PI3K p110 α (PDB: 2WXL). B to F (clockwise) represent the ZSTK-474 docked in model 1: blue, model 2: magenta, model 3: green, model 4: yellow and model 5: orange.

3.1.3.1.5 **LY294002**

LY294002, another pan-PI3K inhibitor also inhibits PI3KC2 β with an IC₅₀ of 10 μ M. Docking studies of LY294002 in the five models resulted in similar binding of the docked poses to the crystal structure for models 1, 3 and 5 with RMSD 0.73 Å, 0.48 Å, 1.95 Å (Figure 3-7).

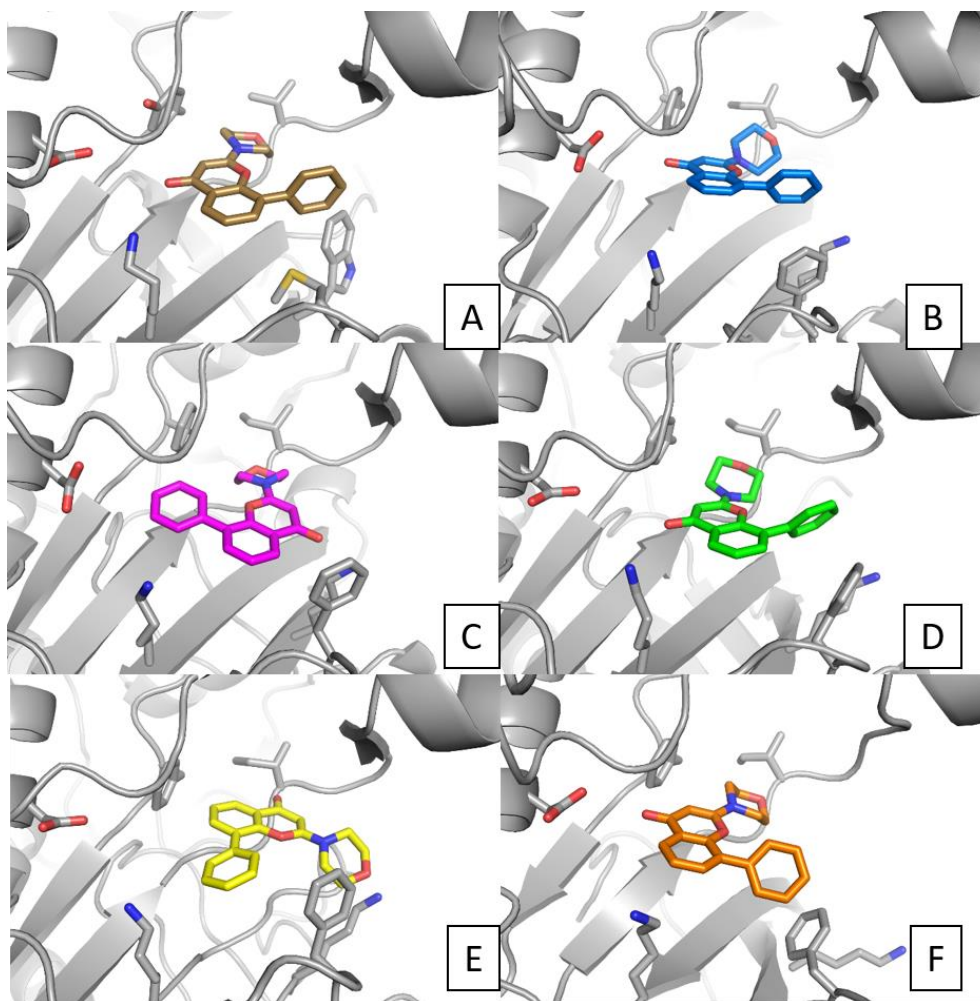


Figure 3-7: Docked poses of LY294002 in the five generated models and the crystal structure. A represents LY294002 co-crystallized in PI3K p110 γ (PDB: 1E7V). B to F (clockwise) represent the LY294002 docked in model 1: blue, model 2: magenta, model 3: green, model 4: yellow and model 5: orange.

3.1.3.1.6 *PIK-108*

PIK-108 does not inhibit PI3KC2 β so in principle acts as a negative control and should not be able to dock readily into any of the models. However, it was revealed that models 3, 4 and 5 could accommodate PIK-108 in a comparable pose to the crystal structure of class I PI3K p110 α (PDB 4A55). The obtained RMSD values of the PIK-108 docked in model 3, 4 and

5 were found to be 2.23 Å, 1.69 Å and 2.13 Å respectively. Note though that the placement of the pendant phenylaminoethyl group, crucial to its potent PI3K p110 β selectivity is not reproduced. Indeed model 2, which templates the PI3K p110 α -PIK108 co-crystal, failed to generate poses that matched the crystal structure as shown in Figure 3-8.

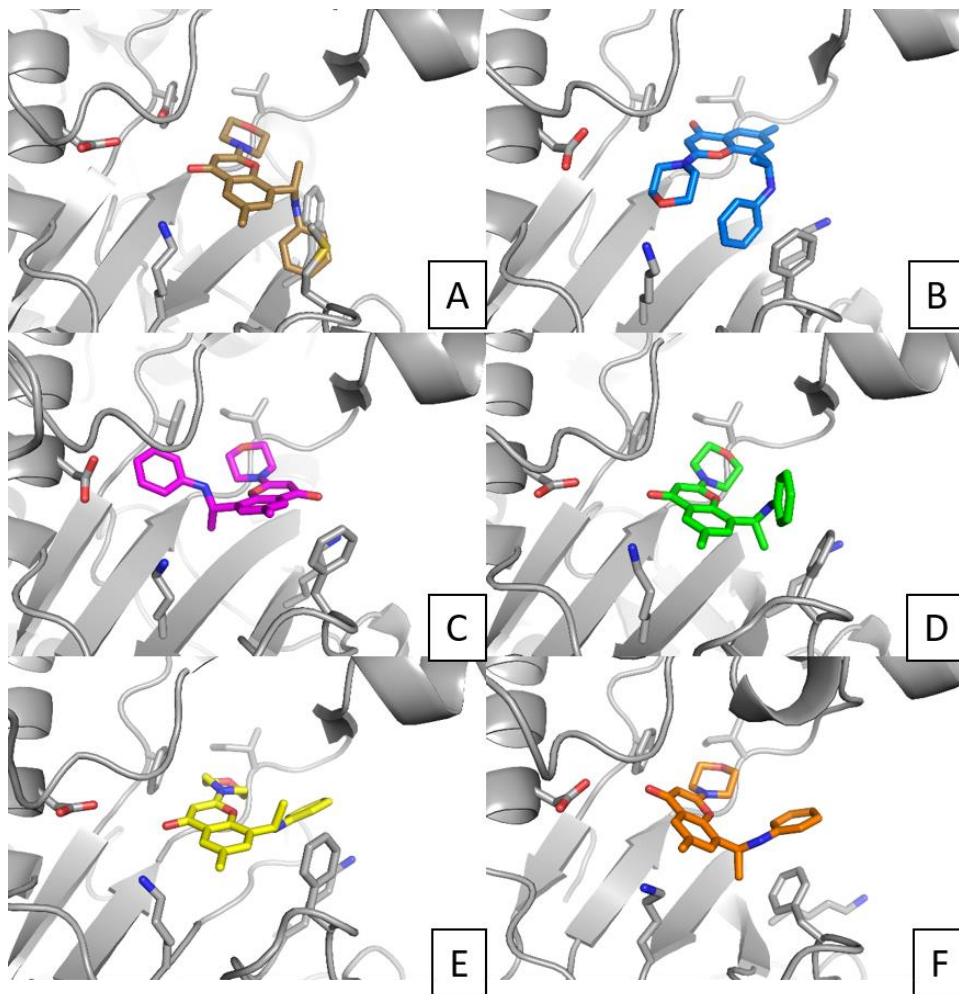


Figure 3-8: Docked poses of PIK-108 in the five generated models and the crystal structure. A represents PIK-108 co-crystallized in PI3K p110 α (PDB: 4A55). B to F represent (clockwise) the PIK-108 docked in model 1: blue, model 2: magenta, model 3: green, model 4: yellow and model 5: orange.

In the crystal structure, binding of PIK-108 induces a conformational change of methionine (Met772) residue in the active site opening up a

specificity pocket in class I PI3Ks (Figure 3-9). Replacement of the methionine residue with a bulky and rigid residue such a phenylalanine may contribute to the profound loss of binding affinity.

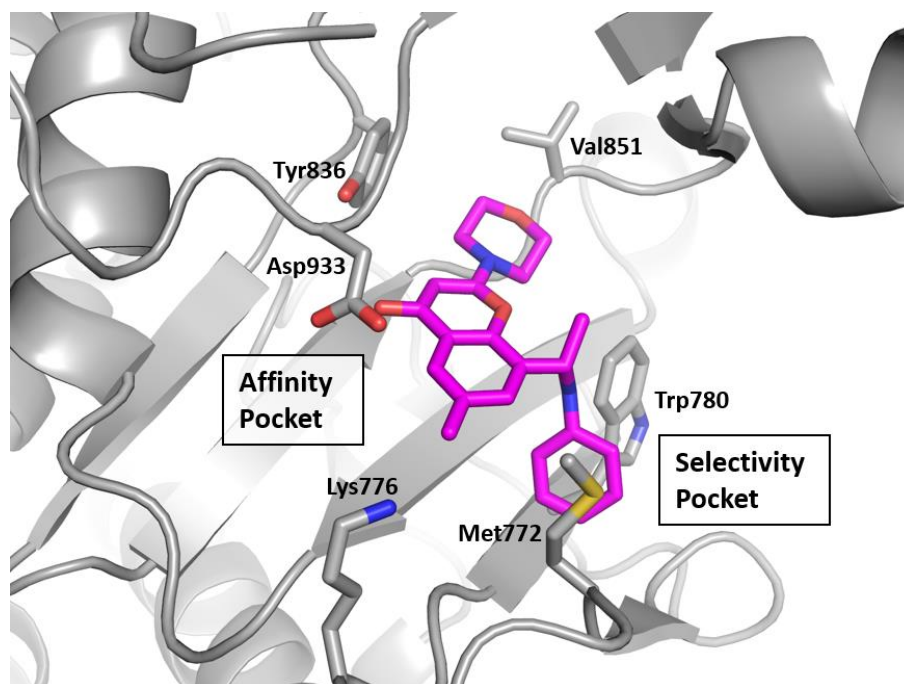


Figure 3-9: PIK-108 (magenta) induces a conformational change in the one of the residues Met772 in the binding pocket of class I PI3Ks (PDB: 4A55) by forming a selectivity pocket.

The results of these collected docking experiments, show that the five models have a differing capacity to accommodate binding of PI3KC28 inhibitors (Table 3-5) in spite of what appeared to be only modest differences between them (as measured by RMS calculations). Of the five models, model 5 based on the co-ordinates of class III hVps34 was able to recapitulate the bound ligands in crystal structure for five out six inhibitors tested; the only exception was ZSTK474.

Table 3-5: Docking summary of the validation studies of the six inhibitors (RMSD cutoff 3 Å).

	MODEL 1	MODEL 2	MODEL 3	MODEL 4	MODEL 5
PI-103	YES	NO	NO	NO	YES
PIK-90	YES	NO	NO	NO	YES
PIK-93	NO	NO	NO	YES	YES
ZSTK-474	YES	NO	NO	NO	NO
LY294002	NO	YES	YES	NO	YES
PIK-108	NO	NO	YES	YES	YES

This is somewhat surprising, given that the poses of ligands to be matched were in general derived from Class I co-crystals. Based on these results, it seems important that the Class II and III isoforms appear to have more in common at the catalytic site, than can be derived from measuring percentage homology. Pivotaly, it would seem that the correct presentation of the phenylalanine residue (F1057), shared by both class II and class III PI3Ks but aligned to a methionine in class I PI3Ks, plays a vital role in the ability of ligands to bind PI3KC2 β . The placement of the phenylalanine residue in model 5 (which is based class III hVps34) might be contributing to the binding poses with low RMSD to crystal structures. This also highlights the possible importance of this particular residue in the prospective development of new PI3KC2 β inhibitors.

Equally it would appear that the ability for ligands to access the affinity pocket of PI3KC2 β is a feature that might determine binding or otherwise. Typically, unsuccessful docking (with respect to matching the x-ray pose) was associated with the absence of any strong interaction with the

affinity pocket. This is suggestive that there may be a key difference between class I PI3K and PI3KC2 β in the affinity pocket that could dictate affinity.

3.1.4 Molecular docking of PI-701 and PI-702: insights into development of isoform-selective inhibitors of PI3KC2 β

Recently, two inhibitors, PI-701 and PI-702, were reported that selectively inhibit PI3KC2 β [250]. While only moderately potent, the selectivity they show is an important benchmark for the development of Class II inhibitors. These compounds show structural analogy to PI103 and related compounds, but possess a 6-acetamidoquinazoline scaffold. Based on the analogy to PI103 and related compounds, it was initially hypothesised that the naphthalene sulphonamide group of PI-701 and the benzene sulphonamide of PI-702 would occupy the affinity pocket, mimicking the phenol group of PI-103. The assumption then would be that these bulky groups would be accommodated in PI3KC2 β but not class I PI3K.

In an attempt to understand the reasons for the selectivity shown by these inhibitors, both (Figure 3-10) were docked in homology models of PI3KC2 β (model 5), being the most reliable model from the study above.

The obtained docking results were quite different to that expected, in that the binding pose is flipped by comparison to PI103, with the acetamidophenyl group occupying the affinity pocket of PI3KC2 β and making hydrophobic interactions with the residues lining the affinity

pocket. The morpholino group makes the expected backbone interactions with the Ile1125 residue lining the hinge region. The sulphonamide on the other hand now projects away from the catalytic site with sufficient space to accommodate even a bulky naphthyl ring. The docking poses of PI-701 and PI-702 were similar to each other with differences only in the phenyl and naphthyl groups (Figure 3-11).

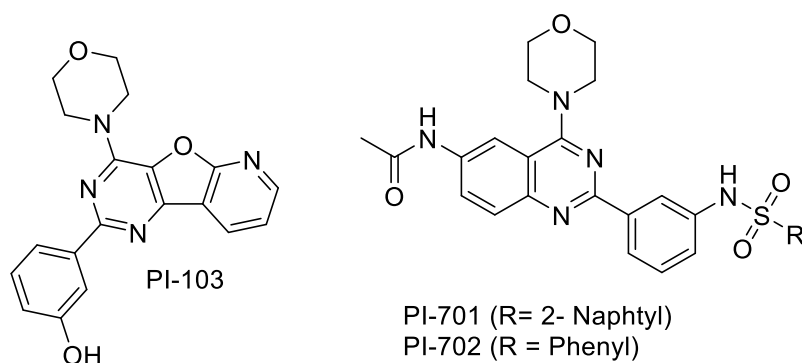


Figure 3-10: Chemical structures of PI-701, PI-702 and PI-103

a)

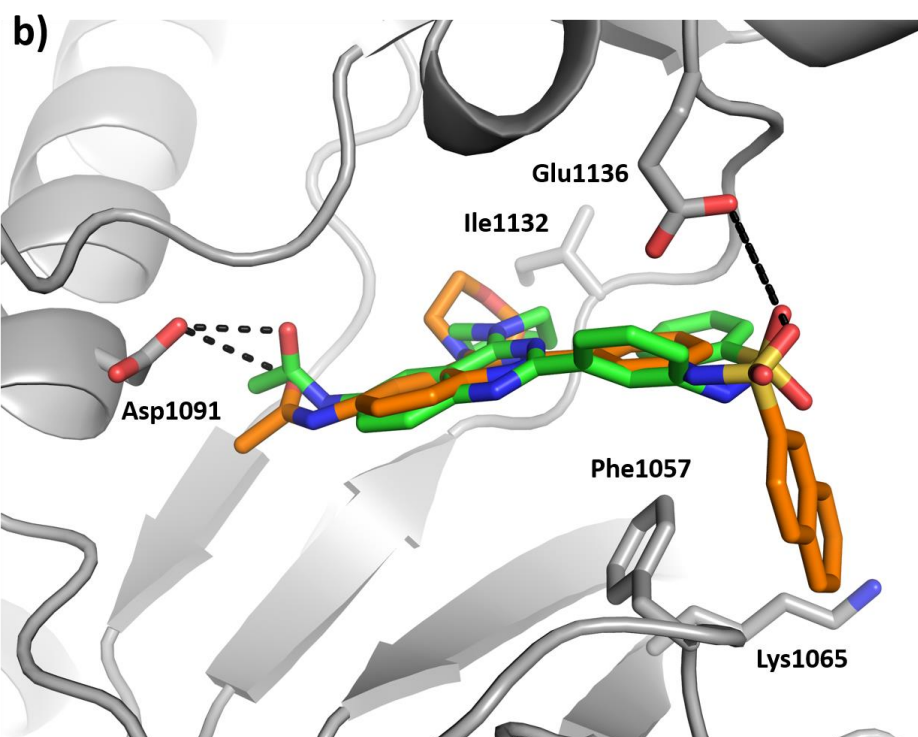
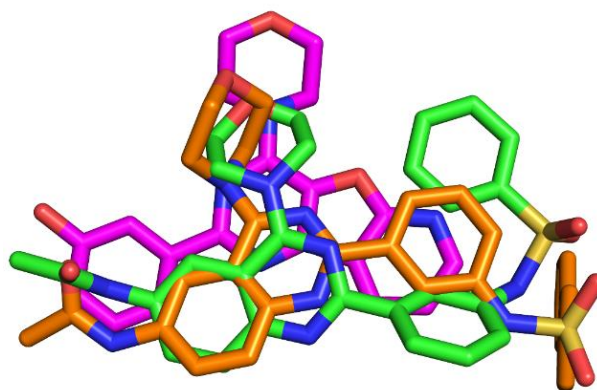


Figure 3-11: The docked poses of PI-701 (orange) and PI-702 (green) superimposed on PI-103 in magenta as shown in (a). The morpholino oxygen of both PI-701 and PI-702 interacts with residues of hinge region similar to PI-103.(b) Interactions of PI-701 (orange) and PI-702 (green) in PI3KC2 β .

As compared to PI-103, the acetamidoquinazoline of PI701 and PI702 have more capacity to fill the affinity pocket than the corresponding

benzothiophene group. The acetamido group of the both the inhibitors interact with Asp1091, a conserved residue via hydrogen bonding. The sulphonamide groups of PI701 and PI702 are able to engage in hydrogen bonding with a non-conserved residue Glu1136. Of the other PI3K isoforms, that Glu is present only in PI3K p110 β .

In summary, the molecular docking studies of PI701 and PI702, suggest that these molecules derive their unique selectivity profile via the combination of a unique interaction with the PI3KC2 β affinity pocket and a relatively selective interaction with the Region 1 binding site glutamic acid residue. These findings could be supported by further analogue design and may drive the design novel and more potent and selective inhibitors.

3.2 Inhibition studies of class I PI3K inhibitor ZSTK474 and its structural analogues against class II PI3KC2β

3.2.1 Introduction

The class II PI3KC2β is upregulated in cancers such as epithelial cell-derived cancers, acute myeloid leukemia (AML), brain tumors and neuroendocrine tumors [220, 234, 235] and compounds inhibiting PI3KC2β are of therapeutic interest. Most of the existing PI3KC2β inhibitors have been identified as off-targets while screening for compounds that inhibit Class I PI3Ks. Consequently, there are only two known selective inhibitors of PI3KC2β [250].

As described in the previous section, molecular modelling using docking into a PI3KC2β homology model had identified the affinity pocket of the catalytic site as a region that might engender selective interactions. We had hypothesized that the selectivity shown by compounds PI701 and PI702 had its origins in a specific ability to bind the PI3KC2β affinity pocket.

To further our understanding of the role of the affinity pocket in dictating selectivity for or against PI3KC2β, structure activity of ZSTK474 analogues against PI3KC2β was attempted. In our laboratories, numerous structural variants on the difluorobenzimidazole moiety of ZSTK474 had been prepared and were available to study. In order to conduct the study, we needed to prepare and characterize recombinant PI3KC2β.

The Bac-to-Bac baculovirus expression system was utilised to express the PI3KC2 β using insect cells. This system has been previously established for successful expression of class I PI3Ks by our lab and also offers various advantages over bacterial/yeast expression systems in terms of protein folding and posttranslational modifications like disulfide bonds and has higher expression compared to mammalian cells [264]. The first step involved generation of a recombinant vector. The insect cell expression vector pFastBac (HTC) was chosen as vector to harbour the PI3KC2 β insert. The pFastBac vectors are non-fusion vectors which have been identified to yield higher levels of expression (compared to other vectors) and facilitate easy transfer of the gene of interest into bacmid DNA. DH10Bac, a particular strain of *E. coli* was used in the production of the recombinant bacmid DNA. The DH10 Bac cells harbor a baculovirus shuttle vector (bacmid) and helper plasmids that are involved in the transposition reaction resulting in the generation of a recombinant bacmid. The recombinant bacmid was then used to infect insect cells (Sf9) in order to generate baculovirus for subsequent expression of the recombinant PI3KC2 β protein.

3.2.2 Cloning, expression, purification and Characterization of PI3KC2 β

3.2.2.1 Generation of recombinant vector consisting of PI3KC2 β insert

The pcDNA3 plasmid containing the PI3KC2 β insert was obtained from Dr Alexandre Arcaro (University of Bern, Switzerland) and subjected

to restriction enzyme digestion by EcoRI and XbaI to isolate the PI3KC2 β insert. Since the pcDNA3 vector and the PI3KC2 β insert are the same size (~5 kb), a second digestion with RsrII, which cleaves only the pcDNA3 vector was carried out to facilitate gel purification of the PI3KC2 β DNA fragment as described in Section 2.2.1.3 and 2.2.1.4.

The gel-purified PI3KC2 β DNA and the pFastBac HTC vector were digested with EcoRI and XbaI and analysed on an agarose gel (see section 2.2.1.5). Both purified DNA fragments were of the expected MW of approximately 5 kb. Subsequently the PI3KC2 β insert was ligated into the pFastBac plasmid using T4 DNA ligase and transformed into DH5 α competent cells followed by isolation and purification of the recombinant plasmid (Section 2.2.1.6).

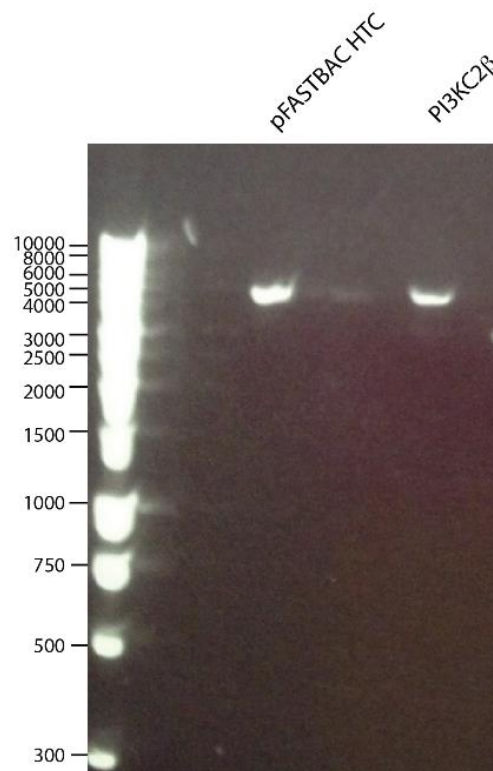


Figure 3-12: Agarose gel confirming the MW of the PI3KC2 β insert and the pFASTBAC HTC. The insert and vector were digested with EcoRI and XbaI and analysed using agarose gel to confirm the MW of about 5kb.

The PI3KC2 β insert was successfully sub-cloned into pFASTBAC (HTC) vector which incorporates a N-terminal His-tag. To confirm, an EcoR1/Xba1 double digest was performed to release the expected 5kb fragment of PI3KC2 β and analysed on an agarose gel (Figure 3-12). The nucleotide sequence of the insert was confirmed to encode a full-length protein with no errors using DNA sequencing.

3.2.2.2 *Production of baculovirus containing the PI3KC2 β insert*

To express PI3KC2 β in insect (Sf9) cells, bacmid DNA was generated by transforming DH10Bac cells with pFastBac HTC vector containing the

PI3KC2 β insert (Section 2.2.2.2). DH10Bac is a particular strain of *E. coli* encompassing a baculovirus shuttle vector (bacmid) which can be propagated in both *E. coli* and insect cells. The successful uptake of the insert by the DH10Bac cells was analysed by blue/white colony screening as well as PCR analysis. Due to difficulty in obtaining full-length product (large size of the product can lead to a decrease in the PCR efficiency), an internal oligo was used (please refer to methods Section 2.2.2.5 for details). The PCR products were run on agarose gel and confirmed the presence of the PI3KC2 β insert at expected MW of 5kb (Figure 3-13).

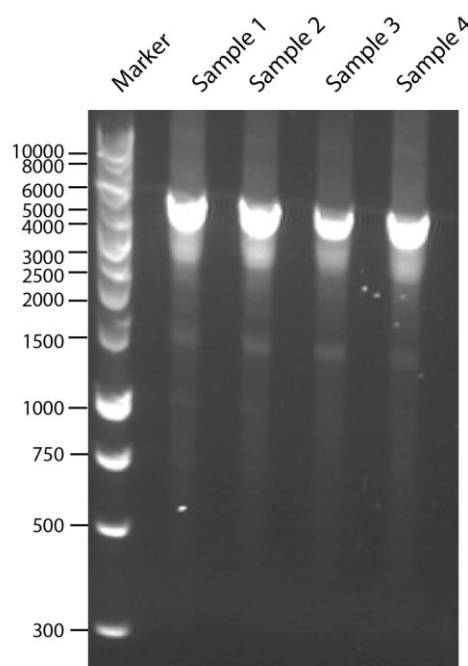


Figure 3-13: Agarose gel confirming the presence of the recombinant bacmid containing PI3KC2 β in the samples. The PCR products using the primer PT18 and an internal oligo PT46 were analysed on an agarose gel (Samples 1 – 4, Lanes 2-5) and were at the expected MW of around 5Kb.

Bacmid DNA was used for expression by transfecting Sf9 cells with bacmids DNA using Cellfectin reagent for efficient transfection of insect

cells. The baculovirus stocks were amplified in order to obtain a high titre recombinant baculovirus for infecting the Sf9 cells for protein expression as described in Section 2.2.3.6. The quantity of the viral titre was tested by plaque assay and was found to be 4.5×10^8 pfu/mL which lies in the optimal range as specified by Bac to Bac expression system manual (Invitrogen).

3.2.2.3 *Expression and purification of PI3KC2 β*

To optimise the expression of PI3KC2 β , several variables were tested related to the production and purification protocols. Firstly, small scale cultures were used to determine the amount of P3 virus (Section 2.2.3.6) required for optimum expression of the PI3KC2 β . Initial tests included using 250 μ L, 500 μ L and 1 mL of P3 virus per 10 mL culture. However, the small scale expression did not yield any detectable band using SDS-PAGE. However, a band corresponding to PI3KC2 β could be visualised using Western blotting with a PI3KC2 β -specific polyclonal antibody. To verify the quality of virus plaque assays were performed and found to be 4.5×10^8 pfu/mL. A larger scale expression was set up by adding 30 mL P3 virus to 200 mL culture and a faint band corresponding to PI3KC2 β could be visualised.

To enable further scale up, 1 L culture was set up to express PI3KC2 β however there was no significant improvement in protein expression. This could be due to poor aeration in the flask used for scale up. A truncated version of PI3KC2 β (155-end) was also expressed in an attempt to increase

the yields, however, there was no noticeable increase in PI3KC2 β expression.

At the end of optimisation trials, it was decided to use a 400 mL culture of Sf9 cells with 40 mL virus added at a multiplicity of infection (MOI) of 5.2 (Section 2.2.4). The presence of an N-terminal His-tag on the PI3KC2 β protein enabled a one-step purification using Ni-NTA affinity chromatography. The cell extract containing recombinant PI3KC2 β was loaded onto the Ni-NTA resin, extensively washed and eluted from the resin using Imidazole (350 mM). 0.5 mL fractions were collected and analysed by SDS-PAGE as described below.

3.2.2.4 *Electrophoresis and immunoblotting*

The purity of the obtained eluted fractions containing PI3KC2 β was analysed using SDS-PAGE and staining with Coomassie blue (Figure 3-14 A). This revealed the presence of PI3KC2 β in two of the eluted fractions; however, there were numerous contaminant proteins also present in the sample. The presence of these contaminant proteins is a reflection of the low expression level of the PI3KC2 β protein. The purity of full-length PI3KC2 β purified was also found to be low (around 15% by SDS-PAGE using GelAnalyzer software) despite using the 6-His tag. The molecular weight of the PI3KC2 β was calculated to be 188 kDa (expected 186 kDa) from the SDS-PAGE by using the R_f (relative migration) of the protein standards and generating a calibration curve of R_f versus log MW. Western blot was also carried out to validate the presence of PI3KC2 β using a rabbit

anti-PI3KC2 β as primary antibody (Figure 3-14B) and indicated a molecular weight of 184 kDa. In conclusion, the protein purified was confirmed as PI3KC2 β by SDS-PAGE and Western blot.

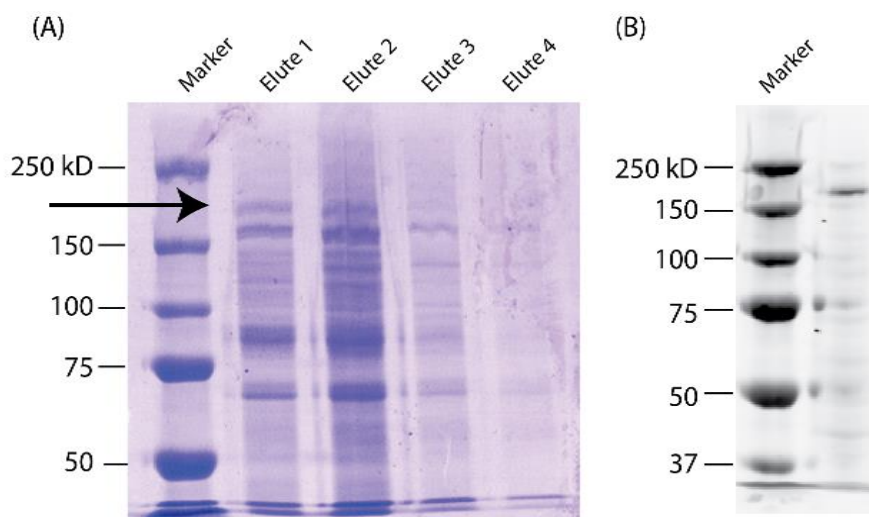


Figure 3-14: Coomassie stained SDS-PAGE gel and Western blot of purified PI3KC2 β . SDS-PAGE (A) lanes 2 and 3 (Elute 1 and 2) showed a higher molecule weight band (top band - marked with an arrow) corresponding to expected MW of PI3KC2 β (expected 186 KDa). To confirm the identity of PI3KC2 β , the gel was probed in an immunoblot (B) using rabbit anti-PI3KC2 β antibody confirming the presence of PI3KC2 β at the MW of around 184 KDa.

Despite best efforts to obtain higher yields including multiple new transfections, expression of the truncated PI3KC2 β containing only the catalytic domain and various scale up volumes (50 mL, 400 mL and 1.5 L), the expression levels were comparatively lower than the class I PI3Ks (based on results of previous work by our group). Commercially available preparations of PI3KC2 β protein have had similar levels of purity from one

step purifications. For example, the Millipore full-length his tagged PI3K C2 β protein has a purity of only 40%. The large size of the protein might contribute to the low expression. Further purification to yield cleaner product was precluded by low yields of the protein. It is also possible that PI3KC2 β -interacting cellular proteins were co-purified in the procedure. The other major bands in the gel could be identified using mass spectrometry to further optimise the purification.

3.2.2.5 *Enzymatic characterization of PI3KC2 β*

The purified fractions of PI3KC2 β were dialysed as described in Section 2.2.7 to remove the imidazole that interferes with PI3K enzyme activity. The fractions were stored in aliquots containing 1 mM DTT and 20% (v/v) glycerol at -80°C until used for the enzyme assay. To verify the catalytic activity of PI3KC2 β , a luminescence-based kinase assay was carried out (Section 2.2.7). PI3Ks catalyse the phosphorylation of various phosphoinositols in the presence of Mg and ATP. The amount of ATP remaining after the kinase reaction directly correlates to the luminescent signal as determined by the reaction of ATP with a luciferase and a luminescent substrate. Luminescence is inversely related to kinase activity.

The enzymatic activity of PI3KC2 β was measured using class I PI3K p110 α as a positive control. Although the expression levels of purified PI3KC2 β were found to be lower than class I PI3Ks, it showed higher activity towards PI at different dilutions tested compared to Class I PI3K p110 α (Figure 3-15). However, this may be attributed to the fact that PI

has been identified as the natural substrate for class II PI3Ks whereas the class I PI3Ks prefer PIP2 [230, 265, 266]. Since the enzyme activity was found to be linear with respect to enzyme activity up to the addition of the equivalent of 1 μL of the enzyme, all subsequent assays used less than this in order to maintain the linear relationship between activity and amount of enzyme.

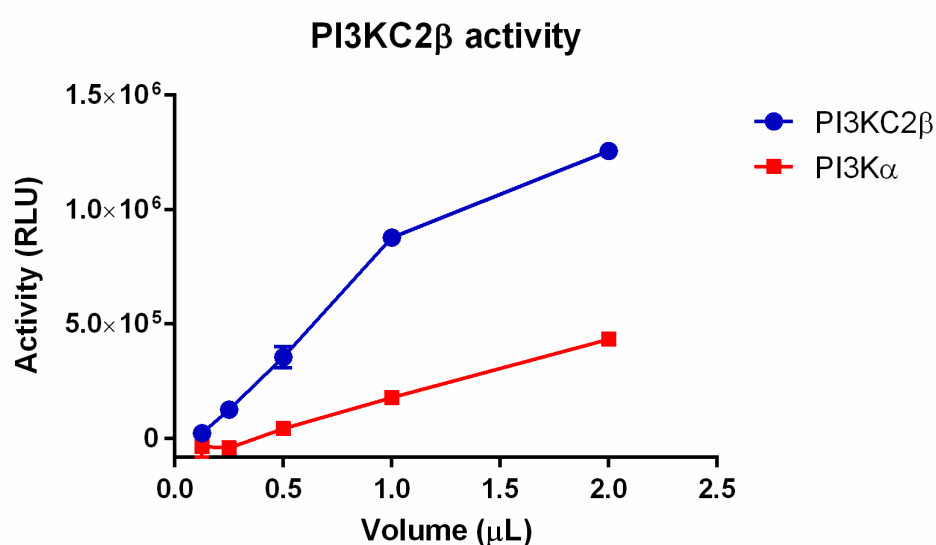


Figure 3-15: Enzymatic activity of PI3KC2 β and PI3K p110 α measured using luminescence (RLU- relative luminescence units) vs. ATP consumption assay. The purified PI3KC2 β (Blue circles) showed a volume-dependent increase in activity using PI and ATP as substrates at all volumes tested (0.5 to 2 μL). The activity is compared to class I PI3K p110 α (Red squares) which was used as a positive control.

3.2.3 Inhibitory activity of ZSTK474 against the class II

PI3KC2 β

ZSTK-474, a potent class I PI3K inhibitor of class I PI3Ks was reported to moderately inhibit PI3KC2 β with an IC₅₀ of 180 nM based on a study by Kong *et al.* [267].

The potency of ZSTK-474 inhibition was tested against PI3KC2 β using the PI3K luminescent assay. As shown in Figure 3-16, ZSTK-474 inhibited PI3KC2 β in a dose-dependent manner, and the IC₅₀ value was calculated using non-linear regression analysis.

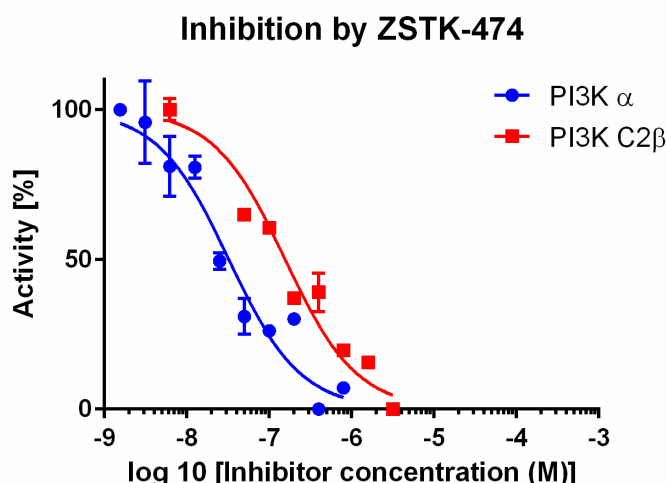


Figure 3-16: Determination of ZSTK-474 inhibition of PI3K activity as measured using a luminescent ATP consumption assay with PI as the substrate. Using a curve of inhibitor concentration versus enzyme activity IC₅₀ values were calculated as described. IC₅₀ values for PI3K p110 α (Blue circles, IC₅₀ = 33.5 nM) and PI3KC2 β (Red squares, IC₅₀ = 142 nM) were determined from duplicates of three independent assays (n=3, values represented as mean \pm SEM).

The inhibition potency of ZSTK-474 was also tested against class I PI3K p110 α and was found to be consistent with the previously reported

data [267], and the dose-response curve is also shown in Figure 3-16. ZSTK-474 inhibits PI3K p110 α with an IC₅₀ of 33.5 nM and PI3KC2 β with IC₅₀ of 142 nM. Although, ZSTK-474 exhibits 4-fold more potent inhibition for PI3K p110 α , it presents a promising lead for drug design of novel PI3KC2 β inhibitors.

3.2.4 *Inhibitory activities of ZSTK-474 analogues:*

In previous work, our group had examined the structure activity of ZSTK474 with respect to the difluorobenzimidazole group and have examined a number of structural variants. The eleven structural analogues of ZSTK-474 (structures shown in Figure 3-17) were tested for their inhibitory potencies against PI3KC2 β , and their selectivity profiles were compared against class I PI3K p110 α .

In an initial screen of compounds at 10 μ M, the influence of substitution on potency was readily apparent. Potencies ranged from a maximum of 73% to 5% inhibition, noting that all the compounds were less potent than ZSTK474 at that dose (~80% taken from Figure 3-18).

JP 7-126 showed the highest inhibition of ~70% against PI3KC2 β , followed by JP 7-42 with ~ 60% inhibition of PI3KC2 β . Compounds JP 7-160, JP 7-92, JP 7-108 has no or little inhibition towards PI3KC2 β . The remaining six compounds had weak/moderate inhibition of PI3KC2 β with their inhibition percentages ranging from 18% - 37%.

The same eleven compounds were tested against PI3K p110 α . All the compounds showed superior inhibition at PI3K p110 α with inhibition percentages ranging from 39% - 80% but there appeared some variations in selectivity at this one dose. Compound JP 7-118, which exhibited moderate inhibition of PI3KC2 β at 30%, was found to be highly selective towards PI3K p110 α with more than 90% inhibition. JP 7-126, which demonstrated the highest inhibition of PI3KC2 β , was also found to inhibit PI3K p110 α with 80% inhibition. MM 5-162 had the least inhibition in both the PI3K isoforms (Figure 3-18).

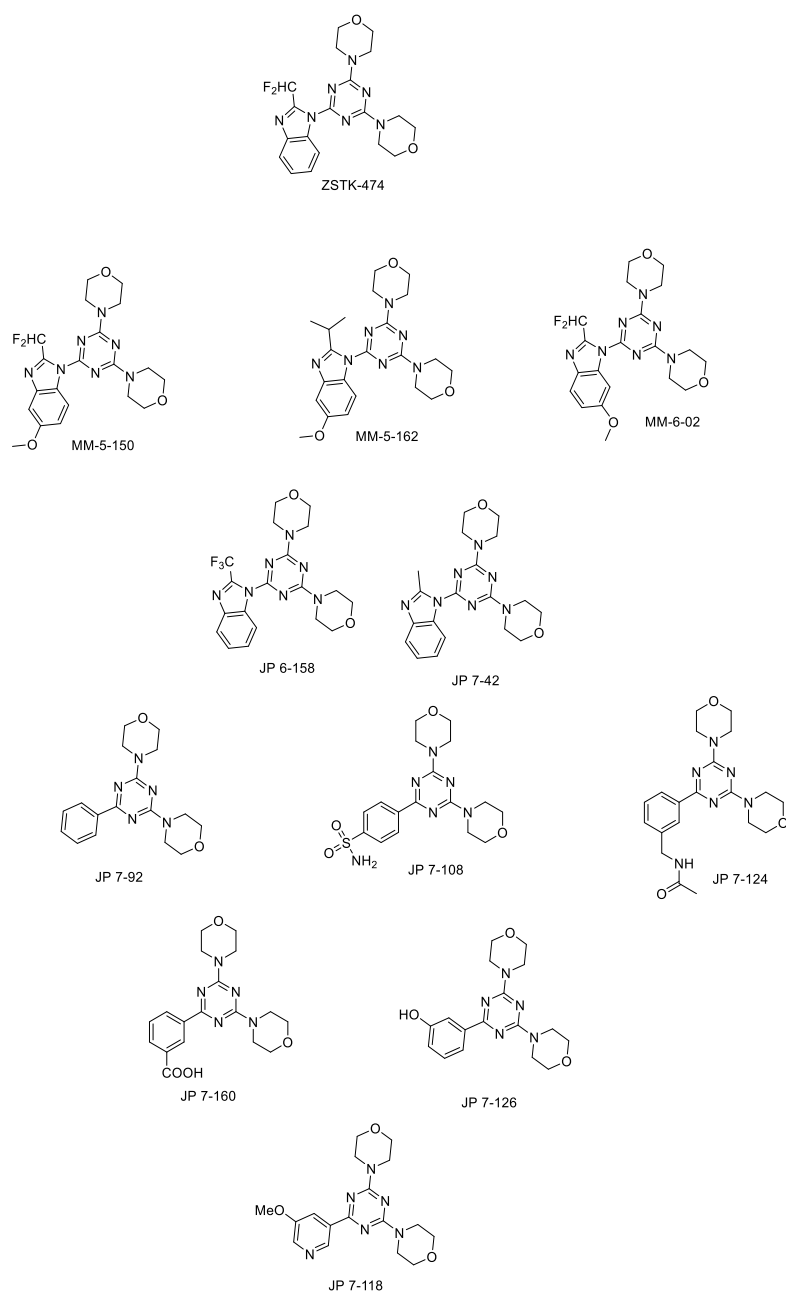


Figure 3-17: Chemical structures of the structural analogues of ZSTK-474

Inhibitor	Inhibition (%)	
	at 10 μ M	
	PI3K α	PI3KC2 β
JP 6-158	70 \pm 5	18 \pm 2
JP 7-42	77 \pm 7	63 \pm 4
JP 7-92	53 \pm 6	5 \pm 2
JP 7-108	63 \pm 8	8 \pm 2
JP 7-118	93 \pm 5	34 \pm 5
JP 7-124	72 \pm 9	25 \pm 2
JP 7-126	80 \pm 10	73 \pm 3
JP 7-160	54 \pm 4	No inhibition
MM 5-150	64 \pm 6	37 \pm 7
MM 5-162	39 \pm 5	18 \pm 6
MM 6-02	71 \pm 12	29 \pm 3

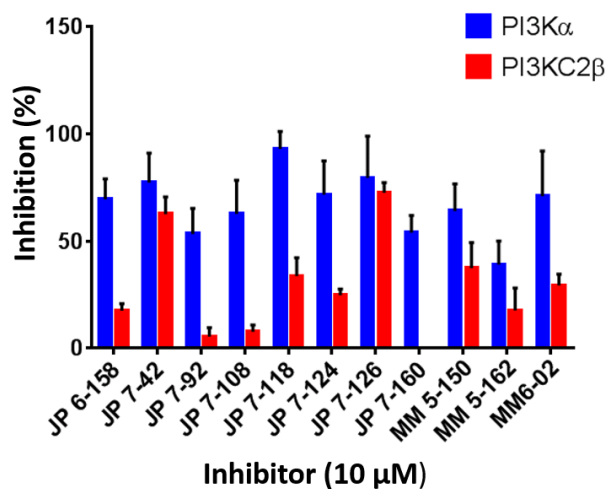


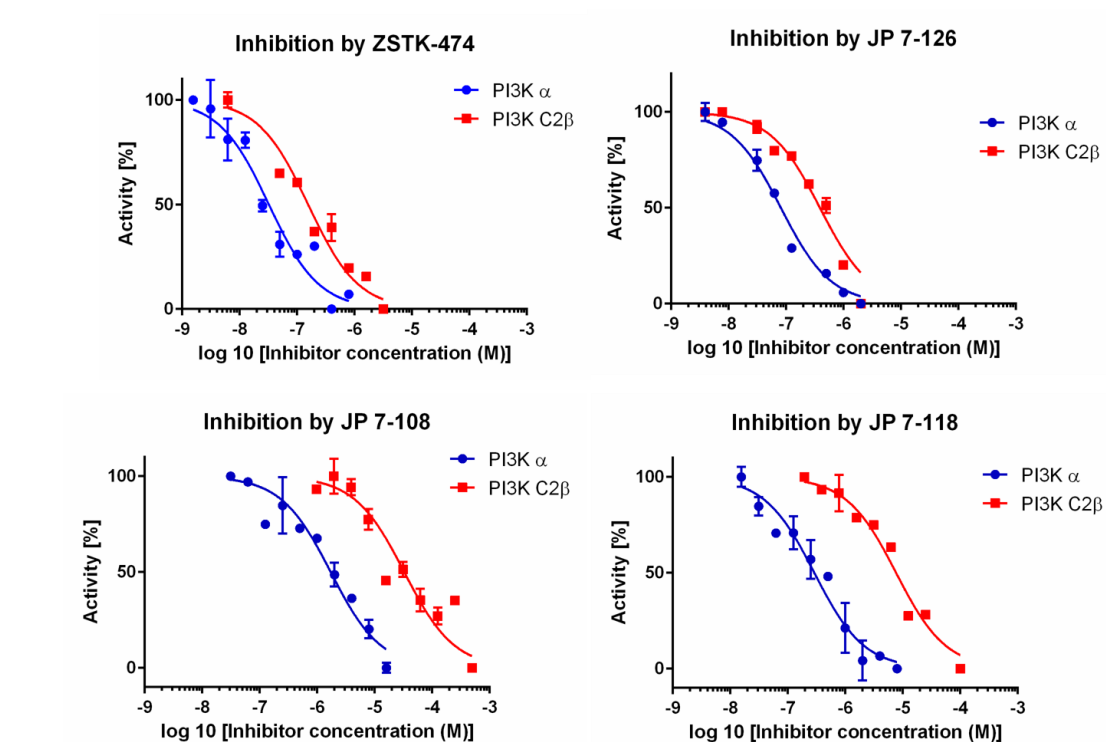
Figure 3-18: Percentages of inhibition at 10 μ M of the eleven compounds for PI3KC2 β (red) and PI3K p110 α (blue) using luminescence assay with ATP and PI as substrate. The graph generated using duplicates of each point in three separate assays and the inhibitory percentages are represented as mean \pm SEM.

Three compounds were chosen for more detailed analysis in dose-response studies to examine the variation in selectivity attributable to the structural changes. The phenolic compound JP 7-126 had the highest inhibition towards PI3KC2 β among the 11 inhibitors; the sulfonamide JP 7-108 showed low inhibition to PI3KC2 β . The methoxypyridine, JP 7-118 was selected as it had high potency at PI3K p110 α (Figure 3-18).

The IC₅₀ values were determined for each of the three inhibitors selected as shown in Figure 3-19. JP 7-126 inhibited both PI3K p110 α (44 nM) and PI3KC2 β (294 nM), however, displayed a 7-fold higher inhibition of PI3K p110 α ; JP 7-108 exhibited a 14-fold specificity for PI3K p110 α (2.3 μ M) over

PI3KC2 β (34 μ M), and JP 7-118 had a 20-fold n IC₅₀ of 0.4 μ M towards PI3K p110 α and 8 μ M towards PI3KC2 β .

As identified in the screen at 10 μ M, all compound had a preference for PI3K p110 α but the levels of selectivity varied, from ZSTK474 which is only 3 fold-selective to JP 7-118 which is 20-fold selective.



	ZSTK-474		JP 7-126		JP 7-118		JP 7-108	
	Mean	SEM	Mean	SEM	Mean	SEM	Mean	SEM
PI3K C2β	0.142 μM	0.390	0.294 μM	0.030	8.047 μM	1.046	33.897 μM	3.011
PI3K α	0.034 μM	0.001	0.044 μM	0.007	0.381 μM	0.128	2.343 μM	0.557

Figure 3-19: Determination of inhibitory potency of the ZSTK-474 and three selected compounds JP7-126, JP 7-118 and JP 7-108 measured using a luminescence vs. ATP consumption assay with PI as a substrate. A range of inhibitor concentrations were tested to identify the IC₅₀ values using a dose-response curve from duplicates of three independent assays (n=3, values represented as mean ± SEM). The inhibitor JP 7-126 showed 7-fold higher inhibition of PI3K p110α (Blue circles) compared to PI3KC2β (Red squares), JP 7-108 and JP 7-118 exhibited 15- and 21-fold higher inhibition of PI3K p110α compared to PI3KC2β.

While not achieving the selectivity for PI3KC2 β , which was the ultimate aim of this project, the modified selectivity due to changing the difluoromethylbenzimidazole substituent of ZSTK474, provides clear evidence that the affinity pocket can be utilized to alter isoform selectivity. Most simply, the difluoromethylbenzimidazole group is well tolerated by both PI3K p110 α and PI3KC2 β while the methoxypyridine of JP7-118 is disfavoured in PI3KC2 β . An attempt to model these compounds in both PI3K p110 α and PI3KC2 β was not successful in identifying any key differences dictating selectivity. It is possible that the selectivity could be obtained via various mechanisms and may not be restricted to enzyme specific amino acids as previously reported by Bergamini *et al.* [268] in the case of class I PI3K p110 γ .

Chapter 4: Conclusions and future outcomes

The discovery of potent compounds that inhibit the class I PI3K isoforms has fuelled the development of isoform-selective inhibitors and resulted in numerous clinical candidates and one approved drug. While there is evidence implying a significant role for the class II PI3KC2 β in cancer, little is known regarding its mechanism and role in signalling pathways. There is a need for the development of PI3KC2 β selective inhibitors to understand the physiology and pathology of the enzyme.

This study focussed on identifying the structural features of PI3KC2 β that may play a role in conferring inhibitor selectivity using homology models while presenting clues to rational design of class II selective inhibitors. Based on the results obtained, we hypothesize that potent PI3KC2 β inhibitors could be accessed by targeting isoform-selective interaction at the affinity pocket and/or non-conserved regions. ZSTK-474, a potent inhibitor of both class I PI3Ks and PI3KC2 β which is currently in clinical trials was chosen as a lead compound for the evaluation of eleven analogues. The eleven compounds, when tested, showed higher selectivity towards class I PI3K p110 α with moderate PI3KC2 β inhibition. Nonetheless, changes in selectivity upon structural modification show that there is heterogeneity in the affinity pocket that could be exploited by further analogue synthesis.

PI-103, NVP-BEZ235, PIK-90 and PIK-93 inhibit PI3KC2 β [249] in nano-molar ranges (26 nM, 44 nM, 64 nM and 144 nM respectively) and

may be suitable leads in the future analogue design to develop more potent inhibitors. Analogues can be synthesized by modifying the substituents occupying the affinity pocket. Modelling studies of PI3KC2 β selective inhibitors PI-701 and PI-702 also revealed the importance of non-conserved residues in imparting selectivity. Further studies could involve site-directed mutagenesis to validate the role of the non-conserved residues in conferring selectivity. The knowledge gained from such experiments can bolster design of potent and selective inhibitors of PI3KC2 β .

Appendices

Appendices and PDB files have been attached to this document in a DVD.

References

1. Klebe, G., *Virtual ligand screening: strategies, perspectives and limitations*. Drug Discovery Today, 2006. **11**(13–14): p. 580-594.
2. Fishman, M.C. and J.A. Porter, *Pharmaceuticals: a new grammar for drug discovery*. Nature, 2005. **437**(7058): p. 491-493.
3. Song, C.M., S.J. Lim, and J.C. Tong, *Recent advances in computer-aided drug design*. Briefings in Bioinformatics, 2009. **10**(5): p. 579-591.
4. Taft, C.A., V.B. Da Silva, and C.H. Tomich De Paula Da Silva, *Current topics in computer-aided drug design*. Journal of Pharmaceutical Sciences, 2008. **97**(3): p. 1089-1098.
5. Veselovsky, A.V. and A.S. Ivanov, *Strategy of computer-aided drug design*. Current drug targets. Infectious disorders, 2003. **3**(1): p. 33-40.
6. Kapetanovic, I., *Computer-aided drug discovery and development (CADD): in silico-chemico-biological approach*. Chemico-biological interactions, 2008. **171**(2): p. 165-176.
7. Sliwoski, G., S. Kothiwale, J. Meiler, and E.W. Lowe, *Computational Methods in Drug Discovery*. Pharmacological Reviews, 2014. **66**(1): p. 334-395.
8. Bleicher, K.H., H.J. Bohm, K. Muller, and A.I. Alanine, *Hit and lead generation: beyond high-throughput screening*. Nat Rev Drug Discov, 2003. **2**(5): p. 369-78.
9. Acharya, C., A. Coop, J.E. Polli, and A.D. MacKerell, *Recent Advances in Ligand-Based Drug Design: Relevance and Utility of the Conformationally Sampled Pharmacophore Approach*. Current computer-aided drug design, 2011. **7**(1): p. 10-22.
10. Lee, C.-H., H.-C. Huang, and H.-F. Juan, *Reviewing ligand-based rational drug design: The search for an ATP synthase inhibitor*. International journal of molecular sciences, 2011. **12**(8): p. 5304-5318.
11. Wang, T., M.-B. Wu, J.-P. Lin, and L.-R. Yang, *Quantitative structure–activity relationship: promising advances in drug discovery platforms*. Expert Opinion on Drug Discovery, 2015: p. 1-18.
12. Zhang, Y., *Progress and challenges in protein structure prediction*. Current opinion in structural biology, 2008. **18**(3): p. 342-348.
13. Robertus, J., *Structures-based drug design ten years on*. Nat Struct Mol Biol, 1994. **1**(6): p. 352-354.
14. Blundell, T.L., H. Jhoti, and C. Abell, *High-throughput crystallography for lead discovery in drug design*. Nat Rev Drug Discov, 2002. **1**(1): p. 45-54.
15. Andricopulo, A.D., L.B. Salum, and D.J. Abraham, *Structure-Based Drug Design Strategies in Medicinal Chemistry*. Current Topics in Medicinal Chemistry, 2009. **9**(9): p. 771-790.
16. John, B. and A. Sali, *Comparative protein structure modeling by iterative alignment, model building and model assessment*. Nucleic Acids Research, 2003. **31**(14): p. 3982-3992.
17. Shoichet, B.K., S.L. McGovern, B.Q. Wei, and J.J. Irwin, *Lead discovery using molecular docking*. Current Opinion in Chemical Biology, 2002. **6**(4): p. 439-446.
18. Šali, A. and T.L. Blundell, *Comparative protein modelling by satisfaction of spatial restraints*. Journal of molecular biology, 1993. **234**(3): p. 779-815.
19. Peitsch, M.C., *ProMod and Swiss-Model: Internet-based tools for automated comparative protein modelling*. Chemical Design Automation News, 1996. **1**(11): p. 13-14.
20. Jacobson, M.P., D.L. Pincus, C.S. Rapp, T.J. Day, B. Honig, D.E. Shaw, and R.A. Friesner, *A hierarchical approach to all-atom protein loop prediction*. Proteins: Structure, Function, and Bioinformatics, 2004. **55**(2): p. 351-367.

21. Yang, A.S. and B. Honig, *Sequence to structure alignment in comparative modeling using PrISM*. Proteins: Structure, Function, and Bioinformatics, 1999. **37**(S3): p. 66-72.
22. Sutcliffe, M., I. Haneef, D. Carney, and T. Blundell, *Knowledge based modelling of homologous proteins, Part I: Three-dimensional frameworks derived from the simultaneous superposition of multiple structures*. Protein Engineering Design and Selection, 1987. **1**(5): p. 377-384.
23. Chothia, C. and A.M. Lesk, *The relation between the divergence of sequence and structure in proteins*. The EMBO journal, 1986. **5**(4): p. 823.
24. Fiser, A., *Template-Based Protein Structure Modeling*. Methods in molecular biology (Clifton, N.J.), 2010. **673**: p. 73-94.
25. Cavasotto, C.N. and S.S. Phatak, *Homology modeling in drug discovery: current trends and applications*. Drug Discovery Today, 2009. **14**(13-14): p. 676-683.
26. Lionta, E., G. Spyrou, D.K. Vassilatis, and Z. Cournia, *Structure-Based Virtual Screening for Drug Discovery: Principles, Applications and Recent Advances*. Current Topics in Medicinal Chemistry, 2014. **14**(16): p. 1923-1938.
27. Ferreira, L.G., R.N. Dos Santos, G. Oliva, and A.D. Andricopulo, *Molecular docking and structure-based drug design strategies*. Molecules (Basel, Switzerland), 2015. **20**(7): p. 13384-421.
28. Meng, X.-Y., H.-X. Zhang, M. Mezei, and M. Cui, *Molecular Docking: A Powerful Approach for Structure-Based Drug Discovery*. Current Computer-Aided Drug Design, 2011. **7**(2): p. 146-157.
29. Leach, A.R., B.K. Shoichet, and C.E. Peishoff, *Prediction of Protein-Ligand Interactions. Docking and Scoring: Successes and Gaps*. Journal of Medicinal Chemistry, 2006. **49**(20): p. 5851-5855.
30. Kitchen, D.B., H. Decornez, J.R. Furr, and J. Bajorath, *Docking and scoring in virtual screening for drug discovery: methods and applications*. Nat Rev Drug Discov, 2004. **3**(11): p. 935-49.
31. Cole, J.C., C.W. Murray, J.W.M. Nissink, R.D. Taylor, and R. Taylor, *Comparing protein-ligand docking programs is difficult*. Proteins: Structure, Function, and Bioinformatics, 2005. **60**(3): p. 325-332.
32. Sousa, S.F., P.A. Fernandes, and M.J. Ramos, *Protein-ligand docking: Current status and future challenges*. Proteins: Structure, Function, and Bioinformatics, 2006. **65**(1): p. 15-26.
33. Warren, G.L., C.W. Andrews, A.-M. Capelli, B. Clarke, J. LaLonde, M.H. Lambert, M. Lindvall, N. Nevins, S.F. Semus, S. Senger, G. Tedesco, I.D. Wall, J.M. Woolven, C.E. Peishoff, and M.S. Head, *A Critical Assessment of Docking Programs and Scoring Functions*. Journal of Medicinal Chemistry, 2006. **49**(20): p. 5912-5931.
34. Perola, E., W.P. Walters, and P.S. Charifson, *A detailed comparison of current docking and scoring methods on systems of pharmaceutical relevance*. Proteins: Structure, Function, and Bioinformatics, 2004. **56**(2): p. 235-249.
35. Friesner, R.A., J.L. Banks, R.B. Murphy, T.A. Halgren, J.J. Klicic, D.T. Mainz, M.P. Repasky, E.H. Knoll, M. Shelley, and J.K. Perry, *Glide: a new approach for rapid, accurate docking and scoring. 1. Method and assessment of docking accuracy*. Journal of medicinal chemistry, 2004. **47**(7): p. 1739-1749.
36. Goodsell, D.S. and A.J. Olson, *Automated docking of substrates to proteins by simulated annealing*. Proteins: Structure, Function, and Bioinformatics, 1990. **8**(3): p. 195-202.
37. Kuntz, I.D., J.M. Blaney, S.J. Oatley, R. Langridge, and T.E. Ferrin, *A geometric approach to macromolecule-ligand interactions*. J Mol Biol, 1982. **161**(2): p. 269-88.

38. Rarey, M., B. Kramer, and T. Lengauer, *Multiple automatic base selection: protein–ligand docking based on incremental construction without manual intervention*. Journal of computer-aided molecular design, 1997. **11**(4): p. 369-384.
39. Jones, G., P. Willett, R.C. Glen, A.R. Leach, and R. Taylor, *Development and validation of a genetic algorithm for flexible docking*. Journal of molecular biology, 1997. **267**(3): p. 727-748.
40. Venkatachalam, C.M., X. Jiang, T. Oldfield, and M. Waldman, *LigandFit: a novel method for the shape-directed rapid docking of ligands to protein active sites*. Journal of Molecular Graphics and Modelling, 2003. **21**(4): p. 289-307.
41. Schulz-Gasch, T. and M. Stahl, *Binding site characteristics in structure-based virtual screening: evaluation of current docking tools*. Journal of molecular modeling, 2003. **9**(1): p. 47-57.
42. Zsoldos, Z., D. Reid, A. Simon, B.S. Sadjad, and A. Peter Johnson, *eHiTS: an innovative approach to the docking and scoring function problems*. Current Protein and Peptide Science, 2006. **7**(5): p. 421-435.
43. Jain, A.N., *Surflex: fully automatic flexible molecular docking using a molecular similarity-based search engine*. Journal of medicinal chemistry, 2003. **46**(4): p. 499-511.
44. Kelley, B.P., S.P. Brown, G.L. Warren, and S.W. Muchmore, *POSIT: Flexible Shape-Guided Docking For Pose Prediction*. Journal of Chemical Information and Modeling, 2015. **55**(8): p. 1771-1780.
45. Pencheva, T., D. Lagorce, I. Pajeva, B.O. Villoutreix, and M.A. Miteva, *AMMOS: Automated Molecular Mechanics Optimization tool for in silico Screening*. BMC Bioinformatics, 2008. **9**: p. 438.
46. Bullock, C., N. Cornia, R. Jacob, A. Remm, T. Peavey, K. Weekes, C. Mallory, J.T. Oxford, O.M. McDougal, and T.L. Andersen, *DockoMatic 2.0: High Throughput Inverse Virtual Screening and Homology Modeling*. Journal of Chemical Information and Modeling, 2013. **53**(8): p. 2161-2170.
47. Agostino, M., R.L. Mancera, P.A. Ramsland, and E. Yuriev, *AutoMap: A tool for analyzing protein–ligand recognition using multiple ligand binding modes*. Journal of Molecular Graphics and Modelling, 2013. **40**: p. 80-90.
48. Meiler, J. and D. Baker, *ROSETTALIGAND: protein-small molecule docking with full side-chain flexibility*. Proteins, 2006. **65**(3): p. 538-48.
49. Shin, W.H. and C. Seok, *GalaxyDock: protein-ligand docking with flexible protein side-chains*. J Chem Inf Model, 2012. **52**(12): p. 3225-32.
50. Yuriev, E., J. Holien, and P.A. Ramsland, *Improvements, trends, and new ideas in molecular docking: 2012–2013 in review*. Journal of Molecular Recognition, 2015. **28**(10): p. 581-604.
51. Cavasotto, C.N. and A.J. Orry, *Ligand docking and structure-based virtual screening in drug discovery*. Curr Top Med Chem, 2007. **7**(10): p. 1006-14.
52. Guido, R.V., G. Oliva, and A.D. Andricopulo, *Virtual screening and its integration with modern drug design technologies*. Curr Med Chem, 2008. **15**(1): p. 37-46.
53. Zweig, M.H. and G. Campbell, *Receiver-operating characteristic (ROC) plots: a fundamental evaluation tool in clinical medicine*. Clinical Chemistry, 1993. **39**(4): p. 561-77.
54. (AIHW), A.I.o.H.a.W., *Australia's Health 2012*, in *The Thirteenth Biennial Health Report of the Australian Institute of Health and Welfare*. 2012, AIHW: Canberra.
55. Futreal, P.A., L. Coin, M. Marshall, T. Down, T. Hubbard, R. Wooster, N. Rahman, and M.R. Stratton, *A census of human cancer genes*. Nat Rev Cancer, 2004. **4**(3): p. 177-183.

56. Jez, J.M., T.G. Flynn, and T.M. Penning, *A new nomenclature for the aldo-keto reductase superfamily*. Biochemical pharmacology, 1997. **54**(6): p. 639-647.
57. Oates, P.J., *Aldose reductase, still a compelling target for diabetic neuropathy*. Current drug targets, 2008. **9**(1): p. 14-36.
58. Seery, L., P. Nestor, and G. FitzGerald, *Molecular evolution of the aldo-keto reductase gene superfamily*. Journal of molecular evolution, 1998. **46**(2): p. 139-146.
59. Jez, J.M. and T.M. Penning, *The aldo-keto reductase (AKR) superfamily: an update*. Chemico-biological interactions, 2001. **130**: p. 499-525.
60. Hyndman, D., D.R. Bauman, V.V. Heredia, and T.M. Penning, *The aldo-keto reductase superfamily homepage*. Chemico-biological interactions, 2003. **143**: p. 621-631.
61. Barski, O.A., S.M. Tipparaju, and A. Bhatnagar, *The aldo-keto reductase superfamily and its role in drug metabolism and detoxification*. Drug metabolism reviews, 2008. **40**(4): p. 553-624.
62. Wilson, D.K., K.M. Bohren, K.H. Gabbay, and F.A. Quiocho, *An unlikely sugar substrate site in the 1.65 Å structure of the human aldose reductase holoenzyme implicated in diabetic complications*. Science, 1992. **257**(5066): p. 81-84.
63. Rondeau, J.M., F. Tete-Favier, A. Podjarny, J.M. Reymann, P. Barth, J.F. Biellmann, and D. Moras, *Novel NADPH-binding domain revealed by the crystal structure of aldose reductase*. Nature, 1992. **355**(6359): p. 469-72.
64. Jez, J.M., M.J. Bennett, B.P. Schlegel, M. Lewis, and T.M. Penning, *Comparative anatomy of the aldo-keto reductase superfamily*. Biochem J, 1997. **326** (Pt 3)(Pt 3): p. 625-36.
65. El-Kabbani, O., D.K. Wilson, M. Petrash, and F.A. Quiocho, *Structural features of the aldose reductase and aldehyde reductase inhibitor-binding sites*. Mol Vis, 1998. **4**: p. 19-25.
66. Hoog, S.S., J.E. Pawlowski, P.M. Alzari, T.M. Penning, and M. Lewis, *Three-dimensional structure of rat liver 3 alpha-hydroxysteroid/dihydrodiol dehydrogenase: a member of the aldo-keto reductase superfamily*. Proceedings of the National Academy of Sciences, 1994. **91**(7): p. 2517-2521.
67. Lovering, A.L., J.P. Ride, C.M. Bunce, J.C. Desmond, S.M. Cummings, and S.A. White, *Crystal structures of prostaglandin D2 11-ketoreductase (AKR1C3) in complex with the nonsteroidal anti-inflammatory drugs flufenamic acid and indomethacin*. Cancer research, 2004. **64**(5): p. 1802-1810.
68. Grimshaw, C.E., M. Shahbaz, and C. Putney, *Mechanistic basis for nonlinear kinetics of aldehyde reduction catalyzed by aldose reductase*. Biochemistry, 1990. **29**(42): p. 9947-9955.
69. Austin, M.B. and J.P. Noel, *The chalcone synthase superfamily of type III polyketide synthases*. Natural product reports, 2003. **20**(1): p. 79-110.
70. Tipparaju, S.M., O.A. Barski, S. Srivastava, and A. Bhatnagar, *Catalytic Mechanism and Substrate Specificity of the β -Subunit of the Voltage-Gated Potassium Channel[†]*. Biochemistry, 2008. **47**(34): p. 8840-8854.
71. Knight, L.P., T. Primiano, J.D. Groopman, T.W. Kensler, and T.R. Sutter, *cDNA cloning, expression and activity of a second human aflatoxin B1-metabolizing member of the aldo-keto reductase superfamily, AKR7A3*. Carcinogenesis, 1999. **20**(7): p. 1215-1223.
72. Suzen, S. and E. Buyukbingol, *Recent studies of aldose reductase enzyme inhibition for diabetic complications*. Current medicinal chemistry, 2003. **10**(15): p. 1329-1352.
73. Tang, W.H., K.A. Martin, and J. Hwa, *Aldose reductase, oxidative stress, and diabetic mellitus*. Frontiers in pharmacology, 2012. **3**.
74. Chung, S. and S. Chung, *Aldose reductase in diabetic microvascular complications*. Current drug targets, 2005. **6**(4): p. 475-486.

75. bander Jagt, D.L., N.S. Kolb, T.J. bander Jagt, J. Chino, F.J. Martinez, L.A. Hunsaker, and R.E. Royer, *Substrate specificity of human aldose reductase: identification of 4-hydroxynonenal as an endogenous substrate*. Biochimica et Biophysica Acta (BBA)-Protein Structure and Molecular Enzymology, 1995. **1249**(2): p. 117-126.
76. Bresson, E., S. Boucher-Kovalik, P. Chapdelaine, E. Madore, N. Harvey, P.Y. Laberge, M. Leboeuf, and M.A. Fortier, *The human aldose reductase AKR1B1 qualifies as the primary prostaglandin F synthase in the endometrium*. The Journal of Clinical Endocrinology & Metabolism, 2011. **96**(1): p. 210-219.
77. Cao, D., S.T. Fan, and S.S. Chung, *Identification and characterization of a novel human aldose reductase-like gene*. Journal of Biological Chemistry, 1998. **273**(19): p. 11429-11435.
78. Saraswat, M., T. Mrudula, P.U. Kumar, A. Suneetha, T.S. Rao, M. Srinivasulu, and G.B. Reddy, *Overexpression of aldose reductase in human cancer tissues*. Annals of Transplantation, 2006. **12**(12): p. CR525-CR529.
79. Pailhoux, E.A., A. Martinez, G.M. Veyssiere, and C.G. Jean, *Androgen-dependent protein from mouse vas deferens. cDNA cloning and protein homology with the aldo-keto reductase superfamily*. Journal of Biological Chemistry, 1990. **265**(32): p. 19932-19936.
80. Lau, E., D. Cao, C. Lin, S. Chung, and S. Chung, *Tissue-specific expression of two aldose reductase-like genes in mice: abundant expression of mouse vas deferens protein and fibroblast growth factor-regulated protein in the adrenal gland*. Biochem. J, 1995. **312**: p. 609-615.
81. Donohue, P.J., G.F. Alberts, B.S. Hampton, and J.A. Winkles, *A delayed-early gene activated by fibroblast growth factor-1 encodes a protein related to aldose reductase*. Journal of Biological Chemistry, 1994. **269**(11): p. 8604-8609.
82. Kabututu, Z., M. Manin, J.-C. Pointud, T. Maruyama, N. Nagata, S. Lambert, A.-M. Lefrançois-Martinez, A. Martinez, and Y. Urade, *Prostaglandin f2 α synthase activities of aldo-keto reductase 1b1, 1b3 and 1b7*. Journal of biochemistry, 2009. **145**(2): p. 161-168.
83. Martinez, A., C. Aigueperse, P. Val, M.-H. Dussault, C. Tournaire, M. Berger, G. Veyssière, C. Jean, and A.-M. Lefrançois Martinez, *Physiological functions and hormonal regulation of mouse vas deferens protein (AKR1B7) in steroidogenic tissues*. Chemico-biological interactions, 2001. **130**: p. 903-917.
84. Zeindl-Eberhart, E., S. Klugbauer, N. Dimitrijevic, P.R. Jungblut, S. Lamer, and H.M. Rabes, *Proteome analysis of rat hepatomas: Carcinogen-dependent tumor-associated protein variants*. Electrophoresis, 2001. **22**(14): p. 3009-3018.
85. Val, P., A. Martinez, I. Sahut-Barnola, C. Jean, G. Veyssière, and A.-M. Lefrançois-Martinez, *A 77-Base Pair LINE-Like Sequence Elicits Androgen-Dependent mvdP/akr1-b7 Expression in Mouse Vas Deferens, But Is Dispensable for Adrenal Expression in Rats 1*. Endocrinology, 2002. **143**(9): p. 3435-3448.
86. Endo, S., T. Matsunaga, H. Mamiya, A. Hara, Y. Kitade, K. Tajima, and O. El-Kabbani, *Characterization of a rat NADPH-dependent aldo-keto reductase (AKR1B13) induced by oxidative stress*. Chemico-biological interactions, 2009. **178**(1): p. 151-157.
87. Kotokorpi, P., C. Gardmo, C.S. Nyström, and A. Mode, *Activation of the glucocorticoid receptor or liver X receptors interferes with growth hormone-induced akr1b7 gene expression in rat hepatocytes*. Endocrinology, 2004. **145**(12): p. 5704-5713.
88. Jia, G., R. Takahashi, Z. Zhang, Y. Tsuji, and H. Sone, *Aldo-keto reductase 1 family B7 is the gene induced in response to oxidative stress in the livers of Long-Evans Cinnamon rats*. International journal of oncology, 2006. **29**(4): p. 829-838.

89. Endo, S., T. Matsunaga, A. Fujita, K. Tajima, O. El-Kabbani, and A. Hara, *Rat aldose reductase-like protein (AKR1B14) efficiently reduces the lipid peroxidation product 4-oxo-2-nonenal*. Biological and Pharmaceutical Bulletin, 2010. **33**(11): p. 1886-1890.
90. Endo, S., T. Matsunaga, A. Fujita, T. Kuragano, M. Soda, K. Sundaram, U. Dhagat, K. Tajima, O. El-Kabbani, and A. Hara, *Activation of aldo-keto reductase family member 1B14 (AKR1B14) by bile acids: Activation mechanism and bile acid-binding site*. Biochimie, 2011. **93**(9): p. 1476-86.
91. Lambert-Langlais, S., J.-C. Pointud, A.-M. Lefrançois-Martinez, F. Volat, M. Manin, F. Coudore, P. Val, I. Sahut-Barnola, B. Ragazzon, and E. Louiset, *Aldo keto reductase 1B7 and prostaglandin F2alpha are regulators of adrenal endocrine functions*. PloS one, 2009. **4**(10): p. e7309-e7309.
92. Dhagat, U., *Structural and functional studies on members of the Aldo-Keto reductase family: Identifying molecular determinants responsible for substrate selectivity and inhibitor potency*. 2011, Monash University. Faculty of Pharmacy and Pharmaceutical Sciences. Medicinal Chemistry.
93. Sundaram, K., U. Dhagat, S. Endo, R. Chung, T. Matsunaga, A. Hara, and O. El-Kabbani, *Structure of rat aldose reductase-like protein AKR1B14 holoenzyme: Probing the role of His269 in coenzyme binding by site-directed mutagenesis*. Bioorganic & medicinal chemistry letters, 2011. **21**(2): p. 801-804.
94. Bauman, D.R., S. Steckelbroeck, and T.M. Penning, *The roles of aldo-keto reductases in steroid hormone action*. Drug News Perspect, 2004. **17**(9): p. 563-578.
95. Hevir, N., K. Vouk, J. Šinkovec, M. Ribič-Pucelj, and T.L. Rižner, *Aldo-keto reductases AKR1C1, AKR1C2 and AKR1C3 may enhance progesterone metabolism in ovarian endometriosis*. Chemico-biological interactions, 2011. **191**(1): p. 217-226.
96. Mindnich, R., G. Möller, and J. Adamski, *The role of 17 beta-hydroxysteroid dehydrogenases*. Molecular and cellular endocrinology, 2004. **218**(1): p. 7-20.
97. Nishizawa, M., T. Nakajima, K. Yasuda, H. Kanzaki, Y. Sasaguri, K. Watanabe, and S. Ito, *Close kinship of human 20 α -hydroxysteroid dehydrogenase gene with three aldo-keto reductase genes*. Genes to Cells, 2000. **5**(2): p. 111-125.
98. Penning, T.M., Y. Jin, V.V. Heredia, and M. Lewis, *Structure-function relationships in 3 α -hydroxysteroid dehydrogenases: a comparison of the rat and human isoforms*. The Journal of steroid biochemistry and molecular biology, 2003. **85**(2): p. 247-255.
99. Dufort, I., P. Soucy, F. Labrie, and V. Luu-The, *Molecular Cloning of Human Type 3 3 α -Hydroxysteroid Dehydrogenase That Differs from 20 α -Hydroxysteroid Dehydrogenase by Seven Amino Acids*. Biochem Biophys Res Commun, 1996. **228**(2): p. 474-479.
100. Lin, H.K., S. Steckelbroeck, K.M. Fung, A.N. Jones, and T.M. Penning, *Characterization of a monoclonal antibody for human aldo-keto reductase AKR1C3 (type 2 3 α -hydroxysteroid dehydrogenase/type 5 17 β -hydroxysteroid dehydrogenase); immunohistochemical detection in breast and prostate*. Steroids, 2004. **69**(13-14): p. 795-801.
101. Matsuura, K., H. Shiraishi, A. Hara, K. Sato, Y. Deyashiki, M. Ninomiya, and S. Sakai, *Identification of a principal mRNA species for human 3 α -hydroxysteroid dehydrogenase isoform (AKR1C3) that exhibits high prostaglandin D2 11-ketoreductase activity*. J Biochem, 1998. **124**(5): p. 940-946.
102. Feldman, B. and D. Feldman, *The development of androgen-independent prostate cancer*. Nat Rev Cancer, 2001. **1**(1): p. 34-45.
103. Zhou, W. and J.M. Slingerland, *Links between oestrogen receptor activation and proteolysis: relevance to hormone-regulated cancer therapy*. Nature Reviews Cancer, 2014. **14**(1): p. 26-38.
104. Jemal, A., R. Siegel, E. Ward, Y. Hao, J. Xu, T. Murray, and M.J. Thun, *Cancer statistics, 2008*. CA Cancer J Clin, 2008. **58**(2): p. 71-96.

105. Dozmorov, M.G., J.T. Azzarello, J.D. Wren, K.M. Fung, Q. Yang, J.S. Davis, R.E. Hurst, D.J. Culkin, T.M. Penning, and H.K. Lin, *Elevated AKR1C3 expression promotes prostate cancer cell survival and prostate cell-mediated endothelial cell tube formation: implications for prostate cancer progression*. BMC Cancer, 2010. **10**(1): p. 672.
106. Diaz, M. and S.G. Patterson, *Management of androgen-independent prostate cancer*. Cancer Control, 2004. **11**(6): p. 364-73.
107. Rathkopf, D. and H.I. Scher, *Androgen receptor antagonists in castration-resistant prostate cancer*. Cancer journal (Sudbury, Mass.), 2013. **19**(1): p. 43.
108. Deyashiki, Y., K. Ohshima, M. Nakanishi, K. Sato, K. Matsuura, and A. Hara, *Molecular cloning and characterization of mouse estradiol 17-dehydrogenase (A-specific), a member of the aldoketoreductase family*. Journal of Biological Chemistry, 1995. **270**(18): p. 10461-10467.
109. Nakamura, Y., P.J. Hornsby, P. Casson, R. Morimoto, F. Satoh, Y. Xing, M.R. Kennedy, H. Sasano, and W.E. Rainey, *Type 5 17beta-hydroxysteroid dehydrogenase (AKR1C3) contributes to testosterone production in the adrenal reticularis*. J Clin Endocrinol Metab, 2009. **94**(6): p. 2192-8.
110. Knudsen, K.E. and T.M. Penning, *Partners in crime: deregulation of AR activity and androgen synthesis in prostate cancer*. Trends Endocrinol Metab, 2010. **21**(5): p. 315-24.
111. Byrns, M.C., S. Steckelbroeck, and T.M. Penning, *An indomethacin analogue, N-(4-chlorobenzoyl)-melatonin, is a selective inhibitor of aldo-keto reductase 1C3 (type 2 3 [alpha]-HSD, type 5 17 [beta]-HSD, and prostaglandin F synthase), a potential target for the treatment of hormone dependent and hormone independent malignancies*. Biochem Pharmacol, 2008. **75**(2): p. 484-493.
112. Penning, T.M. and M.C. Byrns, *Steroid Hormone Transforming Aldo-Keto Reductases and Cancer*. Annals of the New York Academy of Sciences, 2009. **1155**(1): p. 33-42.
113. Adeniji, A.O., M. Chen, and T.M. Penning, *AKR1C3 as a target in castrate resistant prostate cancer*. The Journal of steroid biochemistry and molecular biology, 2013. **137**: p. 136-149.
114. Tian, Y., L. Zhao, H. Zhang, X. Liu, L. Zhao, X. Zhao, Y. Li, and J. Li, *AKR1C3 overexpression may serve as a promising biomarker for prostate cancer progression*. Diagn Pathol, 2014. **9**: p. 42.
115. Gobec, S., P. Brožič, and T.L. Rižner, *Nonsteroidal anti-inflammatory drugs and their analogues as inhibitors of aldo-keto reductase AKR1C3: new lead compounds for the development of anticancer agents*. Bioorg Med Chem Lett, 2005. **15**(23): p. 5170-5175.
116. Jansson, A.K., C. Gunnarsson, M. Cohen, T. Sivik, and O. Stal, *17beta-hydroxysteroid dehydrogenase 14 affects estradiol levels in breast cancer cells and is a prognostic marker in estrogen receptor-positive breast cancer*. Cancer Res, 2006. **66**(23): p. 11471-7.
117. Byrns, M.C. and T.M. Penning, *Type 5 17 [beta]-hydroxysteroid dehydrogenase/prostaglandin F synthase (AKR1C3): Role in breast cancer and inhibition by non-steroidal anti-inflammatory drug analogs*. Chem Biol Interact, 2009. **178**(1-3): p. 221-227.
118. Byrns, M.C. and T.M. Penning, *Type 5 17β-hydroxysteroid dehydrogenase/prostaglandin F synthase (AKR1C3): role in breast cancer and inhibition by non-steroidal anti-inflammatory drug analogs*. Chemico-biological interactions, 2009. **178**(1): p. 221-227.
119. Byrns, M.C., L. Duan, S.H. Lee, I.A. Blair, and T.M. Penning, *Aldo-keto reductase 1C3 expression in MCF-7 cells reveals roles in steroid hormone and prostaglandin*

- metabolism that may explain its over-expression in breast cancer. *J Steroid Biochem Mol Biol*, 2010. **118**(3): p. 177-87.
120. Yin, Y.D., M. Fu, D.G. Brooke, D.M. Heinrich, W.A. Denny, and S.M. Jamieson, *The activity of SN33638, an inhibitor of AKR1C3, on testosterone and 17 β -estradiol production and function in castration-resistant prostate cancer and ER-positive breast cancer*. *Frontiers in oncology*, 2014. **4**.
 121. Komoto, J., T. Yamada, K. Watanabe, and F. Takusagawa, *Crystal structure of human prostaglandin F synthase (AKR1C3)*. *Biochemistry*, 2004. **43**(8): p. 2188-2198.
 122. Piekorz, R.P., S.b. Gingras, A. Hoffmeyer, J.N. Ihle, and Y. Weinstein, *Regulation of progesterone levels during pregnancy and parturition by signal transducer and activator of transcription 5 and 20 α -hydroxysteroid dehydrogenase*. *Molecular Endocrinology*, 2005. **19**(2): p. 431-440.
 123. Suzuki-Yamamoto, T., M. Nishizawa, M. Fukui, E. Okuda-Ashitaka, T. Nakajima, S. Ito, and K. Watanabe, *cDNA cloning, expression and characterization of human prostaglandin F synthase*. *FEBS letters*, 1999. **462**(3): p. 335-340.
 124. Beasley, C., C. Robinson, R. Featherstone, J. Varley, C. Hardy, M. Church, and S. Holgate, *9 α , 11 β -prostaglandin F₂, a novel metabolite of prostaglandin D₂ is a potent contractile agonist of human and guinea pig airways*. *Journal of Clinical Investigation*, 1987. **79**(3): p. 978.
 125. Liston, T.E. and L.J. Roberts, *Transformation of prostaglandin D₂ to 9 α , 11 β -(15S)-trihydroxyprosta-(5Z, 13E)-dien-1-oic acid (9 α , 11 β -prostaglandin F₂): a unique biologically active prostaglandin produced enzymatically in vivo in humans*. *Proceedings of the National Academy of Sciences*, 1985. **82**(18): p. 6030-6034.
 126. Ricciotti, E. and G.A. FitzGerald, *Prostaglandins and inflammation*. *Arteriosclerosis, thrombosis, and vascular biology*, 2011. **31**(5): p. 986-1000.
 127. Obata, T., T. Nagakura, M. Kammuri, T. Masaki, K. Maekawa, and K. Yamashita, *Determination of 9 α , 11 β -prostaglandin F₂ in human urine and plasma by gas chromatography—mass spectrometry*. *Journal of Chromatography B: Biomedical Sciences and Applications*, 1994. **655**(2): p. 173-178.
 128. Matsuoka, T., M. Hirata, H. Tanaka, Y. Takahashi, T. Murata, K. Kabashima, Y. Sugimoto, T. Kobayashi, F. Ushikubi, and Y. Aze, *Prostaglandin D₂ as a mediator of allergic asthma*. *Science*, 2000. **287**(5460): p. 2013-2017.
 129. Qiu, W., M. Zhou, M. Mazumdar, A. Azzi, D. Ghanmi, F. Labrie, and S.-X. Lin, *Structure-based Inhibitor Design for an Enzyme That Binds Different Steroids*. *Journal of Biological Chemistry*, 2007. **282**(11): p. 8368-8379.
 130. Byrns, M.C., Y. Jin, and T.M. Penning, *Inhibitors of type 5 17 β -hydroxysteroid dehydrogenase (AKR1C3): overview and structural insights*. *J Steroid Biochem Mol Biol*, 2011. **125**(1-2): p. 95-104.
 131. Adeniji, A.O., B.M. Twenter, M.C. Byrns, Y. Jin, M. Chen, J.D. Winkler, and T.M. Penning, *Development of Potent and Selective Inhibitors of Aldo–Keto Reductase 1C3 (Type 5 17 β -Hydroxysteroid Dehydrogenase) Based on N-Phenyl-Aminobenzoates and Their Structure–Activity Relationships*. *Journal of Medicinal Chemistry*, 2012. **55**(5): p. 2311-2323.
 132. Jamieson, S.M.F., D.G. Brooke, D. Heinrich, G.J. Atwell, S. Silva, E.J. Hamilton, A.P. Turnbull, L.J.M. Rigoreau, E. Trivier, C. Soudy, S.S. Samlal, P.J. Owen, E. Schroeder, T. Raynham, J.U. Flanagan, and W.A. Denny, *3-(3,4-Dihydroisoquinolin-2(1H)-ylsulfonyl)benzoic Acids: Highly Potent and Selective Inhibitors of the Type 5 17 β -Hydroxysteroid Dehydrogenase AKR1C3*. *Journal of Medicinal Chemistry*, 2012. **55**(17): p. 7746-7758.
 133. Endo, S., T. Matsunaga, C. Ohta, M. Soda, A. Kanamori, Y. Kitade, S. Ohno, K. Tajima, O. El-Kabbani, and A. Hara, *Roles of rat and human aldo–keto reductases in*

- metabolism of farnesol and geranylgeraniol*. Chemico-biological interactions, 2011. **191**(1): p. 261-268.
134. Khanim, F.L., R.E. Hayden, J. Birtwistle, A. Lodi, S. Tiziani, N.J. Davies, J.P. Ride, M.R. Viant, U.L. Gunther, and J.C. Mountford, *Combined bezafibrate and medroxyprogesterone acetate: potential novel therapy for acute myeloid leukaemia*. PLoS One, 2009. **4**(12): p. e8147.
 135. Poirier, D., *Inhibitors of 17 β -hydroxysteroid dehydrogenases*. Current medicinal chemistry, 2003. **10**(6): p. 453-477.
 136. Škarydová, L., L. Živná, G. Xiong, E. Maser, and V. Wsól, *AKR1C3 as a potential target for the inhibitory effect of dietary flavonoids*. Chemico-biological interactions, 2009. **178**(1): p. 138-144.
 137. Brožič, P., B. Golob, N. Gomboc, T.L. Rižner, and S. Gobec, *Cinnamic acids as new inhibitors of 17 β -hydroxysteroid dehydrogenase type 5 (AKR1C3)*. Molecular and cellular endocrinology, 2006. **248**(1): p. 233-235.
 138. Kimoto, T., S. Arai, M. Kohguchi, M. Aga, Y. Nomura, M.J. Micallef, M. Kurimoto, and K. Mito, *Apoptosis and suppression of tumor growth by artemisinin C extracted from Brazilian propolis*. Cancer detection and prevention, 1998. **22**(6): p. 506-515.
 139. Mishima, S., Y. Ono, Y. Araki, Y. Akao, and Y. Nozawa, *Two related cinnamic acid derivatives from Brazilian honey bee propolis, baccharin and drupanin, induce growth inhibition in allografted sarcoma S-180 in mice*. Biological and Pharmaceutical Bulletin, 2005. **28**(6): p. 1025-1030.
 140. Endo, S., T. Matsunaga, A. Kanamori, Y. Otsuji, H. Nagai, K. Sundaram, O. El-Kabbani, N. Toyooka, S. Ohta, and A. Hara, *Selective inhibition of human type-5 17 β -hydroxysteroid dehydrogenase (AKR1C3) by baccharin, a component of Brazilian propolis*. J Nat Prod, 2012. **75**(4): p. 716-21.
 141. Koda, N., Y. Tsutsui, H. Niwa, S. Ito, D.F. Woodward, and K. Watanabe, *Synthesis of prostaglandin F ethanolamide by prostaglandin F synthase and identification of Bimatoprost as a potent inhibitor of the enzyme: new enzyme assay method using LC/ESI/MS*. Archives of biochemistry and biophysics, 2004. **424**(2): p. 128-136.
 142. Usami, N., T. Yamamoto, S. Shintani, Y. Higaki, S. Ishikura, Y. Patagiri, and A. Hara, *Substrate Specificity of Human 3 (20). ALPHA.-Hydroxysteroid Dehydrogenase for Neurosteroids and Its Inhibition by Benzodiazepines*. Biological and Pharmaceutical Bulletin, 2002. **25**(4): p. 441-445.
 143. Byrns, M.C., Y. Jin, and T.M. Penning, *Inhibitors of type 5 17 β -hydroxysteroid dehydrogenase (AKR1C3): overview and structural insights*. The Journal of steroid biochemistry and molecular biology, 2011. **125**(1): p. 95-104.
 144. Otwinowski, Z. and W. Minor, *Denzo and Scalepack*, in *International Tables for Crystallography Volume F: Crystallography of biological macromolecules*. 2001, Springer. p. 226-235.
 145. Matthews, B.W., *Solvent content of protein crystals*. Journal of molecular biology, 1968. **33**(2): p. 491-497.
 146. Winn, M.D., C.C. Ballard, K.D. Cowtan, E.J. Dodson, P. Emsley, P.R. Evans, R.M. Keegan, E.B. Krissinel, A.G. Leslie, and A. McCoy, *Overview of the CCP4 suite and current developments*. Acta Crystallographica Section D: Biological Crystallography, 2011. **67**(4): p. 235-242.
 147. Murshudov, G.N., P. Skubák, A.A. Lebedev, N.S. Pannu, R.A. Steiner, R.A. Nicholls, M.D. Winn, F. Long, and A.A. Vagin, *REFMAC5 for the refinement of macromolecular crystal structures*. Acta Crystallographica Section D: Biological Crystallography, 2011. **67**(4): p. 355-367.
 148. Laskowski, R.A., D.S. Moss, and J.M. Thornton, *Main-chain bond lengths and bond angles in protein structures*. Journal of molecular biology, 1993. **231**(4): p. 1049-1067.

149. Sievers, F., A. Wilm, D. Dineen, T.J. Gibson, K. Karplus, W. Li, R. Lopez, H. McWilliam, M. Remmert, and J. Söding, *Fast, scalable generation of high-quality protein multiple sequence alignments using Clustal Omega*. Molecular systems biology, 2011. **7**(1): p. 539.
150. El-Kabbani, O., U. Dhagat, M. Soda, S. Endo, T. Matsunaga, and A. Hara, *Probing the inhibitor selectivity pocket of human 20 α -hydroxysteroid dehydrogenase (AKR1C1) with X-ray crystallography and site-directed mutagenesis*. Bioorganic & medicinal chemistry letters, 2011. **21**(8): p. 2564-2567.
151. Emsley, P. and K. Cowtan, *Coot: model-building tools for molecular graphics*. Acta Crystallographica Section D: Biological Crystallography, 2004. **60**(12): p. 2126-2132.
152. El-Kabbani, O., F. Ruiz, C. Darmanin, and R.-T. Chung, *Aldose reductase structures: implications for mechanism and inhibition*. Cellular and Molecular Life Sciences CMLS, 2004. **61**(7-8): p. 750-762.
153. Gobec, S., P. Brožič, and T.L. Rižner, *Nonsteroidal anti-inflammatory drugs and their analogues as inhibitors of aldo-keto reductase AKR1C3: new lead compounds for the development of anticancer agents*. Bioorganic & medicinal chemistry letters, 2005. **15**(23): p. 5170-5175.
154. Flanagan, J.U., Y. Yosaatmadja, R.M. Teague, M. Chai, A.P. Turnbull, and C.J. Squire, *Crystal structures of three classes of non-steroidal anti-inflammatory drugs in complex with aldo-keto reductase 1C3*. PloS one, 2012. **7**(8): p. e43965-e43965.
155. Endo, S., T. Matsunaga, A. Kanamori, Y. Otsuji, H. Nagai, K. Sundaram, O. El-Kabbani, N. Toyooka, S. Ohta, and A. Hara, *Selective inhibition of human type-5 17 β -hydroxysteroid dehydrogenase (AKR1C3) by baccharin, a component of Brazilian propolis*. Journal of natural products, 2012. **75**(4): p. 716-721.
156. Zang, T., K. Verma, M. Chen, Y. Jin, P.C. Trippier, and T.M. Penning, *Screening baccharin analogs as selective inhibitors against type 5 17 β -hydroxysteroid dehydrogenase (AKR1C3)*. Chem Biol Interact, 2015. **234**: p. 339-48.
157. Endo, S., D. Hu, T. Matsunaga, Y. Otsuji, O. El-Kabbani, M. Kandeel, A. Ikari, A. Hara, Y. Kitade, and N. Toyooka, *Synthesis of non-prenyl analogues of baccharin as selective and potent inhibitors for aldo-keto reductase 1C3*. Bioorg Med Chem, 2014. **22**(19): p. 5220-33.
158. Triballeau, N., F. Acher, I. Brabet, J.-P. Pin, and H.-O. Bertrand, *Virtual screening workflow development guided by the "receiver operating characteristic" curve approach. Application to high-throughput docking on metabotropic glutamate receptor subtype 4*. Journal of medicinal chemistry, 2005. **48**(7): p. 2534-2547.
159. Brožič, P., S. Turk, A.O. Adeniji, J. Konc, D.a. Janežič, T.M. Penning, T. Lanišnik Rižner, and S. Gobec, *Selective inhibitors of aldo-keto reductases AKR1C1 and AKR1C3 discovered by virtual screening of a fragment library*. Journal of medicinal chemistry, 2012. **55**(17): p. 7417-7424.
160. Vanhaesebroeck, B., S.J. Leever, G. Panayotou, and M.D. Waterfield, *Phosphoinositide 3-kinases: a conserved family of signal transducers*. Trends in biochemical sciences, 1997. **22**(7): p. 267-272.
161. Rameh, L.E. and L.C. Cantley, *The role of phosphoinositide 3-kinase lipid products in cell function*. Journal of Biological Chemistry, 1999. **274**(13): p. 8347-8350.
162. Cantley, L.C., *The phosphoinositide 3-kinase pathway*. Science Signalling, 2002. **296**(5573): p. 1655.
163. Yuan, T. and L. Cantley, *PI3K pathway alterations in cancer: variations on a theme*. Oncogene, 2008. **27**(41): p. 5497-5510.
164. Katso, R., K. Okkenhaug, K. Ahmadi, S. White, J. Timms, and M.D. Waterfield, *Cellular function of phosphoinositide 3-kinases: implications for development, immunity,*

- homeostasis, and cancer*. Annual review of cell and developmental biology, 2001. **17**(1): p. 615-675.
165. Samuels, Y., Z. Wang, A. Bardelli, N. Silliman, J. Ptak, S. Szabo, H. Yan, A. Gazdar, S.M. Powell, and G.J. Riggins, *High frequency of mutations of the PIK3CA gene in human cancers*. Science, 2004. **304**(5670): p. 554-554.
 166. Stephens, L., R. Williams, and P. Hawkins, *Phosphoinositide 3-kinases as drug targets in cancer*. Current Opinion in Pharmacology, 2005. **5**(4): p. 357-365.
 167. Osaki, M., M. Oshimura, and H. Ito, *PI3K-Akt pathway: its functions and alterations in human cancer*. Apoptosis, 2004. **9**(6): p. 667-676.
 168. Stein, R.C. and M.D. Waterfield, *PI3-kinase inhibition: a target for drug development?* Molecular medicine today, 2000. **6**(9): p. 347-358.
 169. Whitman, M., C.P. Downes, M. Keeler, T. Keller, and L. Cantley, *Type I phosphatidylinositol kinase makes a novel inositol phospholipid, phosphatidylinositol-3-phosphate*. Nature, 1988. **332**(6165): p. 644-646.
 170. Foster, F.M., C.J. Traer, S.M. Abraham, and M.J. Fry, *The phosphoinositide (PI) 3-kinase family*. Journal of cell science, 2003. **116**(15): p. 3037-3040.
 171. Vanhaesebroeck, B., S.J. Leever, K. Ahmadi, J. Timms, R. Katso, P.C. Driscoll, R. Woscholski, P.J. Parker, and M.D. Waterfield, *Synthesis and function of 3-phosphorylated inositol lipids*. Annual review of biochemistry, 2001. **70**(1): p. 535-602.
 172. Zvelebil, M., L. MacDougall, S. Leever, S. Volinia, B. Vanhaesebroeck, I. Gout, G. Panayotou, J. Domin, R. Stein, and F. Pages, *Structural and Functional Diversity of Phosphoinositide 3-Kinases [and Discussion]*. Philosophical Transactions: Biological Sciences, 1996: p. 217-223.
 173. Hiles, I.D., M. Otsu, S. Volinia, M.J. Fry, I. Gout, R. Dhand, G. Panayotou, F. Ruiz-Larrea, A. Thompson, and N.F. Totty, *Phosphatidylinositol 3-kinase: structure and expression of the 110 kd catalytic subunit*. Cell, 1992. **70**(3): p. 419-429.
 174. MORGAN, S.J., A.D. SMITH, and P.J. PARKER, *Purification and characterization of bovine brain type I phosphatidylinositol kinase*. European journal of biochemistry, 1990. **191**(3): p. 761-767.
 175. Dhand, R., I. Hiles, G. Panayotou, S. Roche, M. Fry, I. Gout, N. Totty, O. Truong, P. Vicendo, and K. Yonezawa, *PI 3-kinase is a dual specificity enzyme: autoregulation by an intrinsic protein-serine kinase activity*. The EMBO journal, 1994. **13**(3): p. 522.
 176. Chantry, D., A. Vojtek, A. Kashishian, D.A. Holtzman, C. Wood, P.W. Gray, J.A. Cooper, and M.F. Hoekstra, *p110 δ , a novel phosphatidylinositol 3-kinase catalytic subunit that associates with p85 and is expressed predominantly in leukocytes*. Journal of Biological Chemistry, 1997. **272**(31): p. 19236-19241.
 177. Vanhaesebroeck, B., J. Guillermet-Guibert, M. Graupera, and B. Bilanges, *The emerging mechanisms of isoform-specific PI3K signalling*. Nature reviews Molecular cell biology, 2010. **11**(5): p. 329-341.
 178. Fruman, D.A., R.E. Meyers, and L.C. Cantley, *Phosphoinositide kinases*. Annual review of biochemistry, 1998. **67**(1): p. 481-507.
 179. Vanhaesebroeck, B., K. Ali, A. Bilancio, B. Geering, and L.C. Foukas, *Signalling by PI3K isoforms: insights from gene-targeted mice*. Trends in Biochemical Sciences, 2005. **30**(4): p. 194-204.
 180. Zhao, L. and P.K. Vogt, *Helical domain and kinase domain mutations in p110 α of phosphatidylinositol 3-kinase induce gain of function by different mechanisms*. Proceedings of the National Academy of Sciences, 2008. **105**(7): p. 2652-2657.
 181. Asano, T., M. Fujishiro, A. Kushiyama, Y. Nakatsu, M. Yoneda, H. Kamata, and H. Sakoda, *Role of phosphatidylinositol 3-kinase activation on insulin action and its alteration in diabetic conditions*. Biological and Pharmaceutical Bulletin, 2007. **30**(9): p. 1610-1616.

182. Foukas, L.C., M. Claret, W. Pearce, K. Okkenhaug, S. Meek, E. Peskett, S. Sancho, A.J. Smith, D.J. Withers, and B. Vanhaesebroeck, *Critical role for the p110 α phosphoinositide-3-OH kinase in growth and metabolic regulation*. *Nature*, 2006. **441**(7091): p. 366-370.
183. Benistant, C., H. Chapuis, and S. Roche, *A specific function for phosphatidylinositol 3-kinase α (p85 α -p110 α) in cell survival and for phosphatidylinositol 3-kinase β (p85 α -p110 β) in de novo DNA synthesis of human colon carcinoma cells*. *Oncogene*, 2000. **19**: p. 5083-5090.
184. Fry, M.J., *Phosphoinositide 3-kinase signalling in breast cancer: how big a role might it play?* *Breast Cancer Research*, 2001. **3**(5): p. 304-312.
185. Kulkarni, S., C. Sitaru, Z. Jakus, K.E. Anderson, G. Damoulakis, K. Davidson, M. Hirose, J. Juss, D. Oxley, and T.A. Chessa, *PI3K β plays a critical role in neutrophil activation by immune complexes*. *Science signaling*, 2011. **4**(168): p. ra23-ra23.
186. Leverrier, Y., K. Okkenhaug, C. Sawyer, A. Bilancio, B. Vanhaesebroeck, and A.J. Ridley, *Class I Phosphoinositide 3-Kinase p110 β Is Required for Apoptotic Cell and Fc γ Receptor-mediated Phagocytosis by Macrophages*. *Journal of Biological Chemistry*, 2003. **278**(40): p. 38437-38442.
187. Ramadani, F., D.J. Bolland, F. Garcon, J.L. Emery, B. Vanhaesebroeck, A.E. Corcoran, and K. Okkenhaug, *The PI3K isoforms p110 α and p110 δ are essential for pre-B cell receptor signaling and B cell development*. *Science signaling*, 2010. **3**(134): p. ra60.
188. Patton, D., J. Emery, W. Rowan, and K. Okkenhaug. *PI3K p110 delta controls the differentiation and function of regulatory T cells*. in *Immunology*. 2008. Wiley-Blackwell Publishing, Inc.
189. Park, S.J., K.H. Min, and Y.C. Lee, *Phosphoinositide 3-kinase δ inhibitor as a novel therapeutic agent in asthma*. *Respirology*, 2008. **13**(6): p. 764-771.
190. Ali, K., A. Bilancio, M. Thomas, W. Pearce, A.M. Gilfillan, C. Tkaczyk, N. Kuehn, A. Gray, J. Giddings, and E. Peskett, *Essential role for the p110 δ phosphoinositide 3-kinase in the allergic response*. *Nature*, 2004. **431**(7011): p. 1007-1011.
191. Krugmann, S., P.T. Hawkins, N. Pryer, and S. Braselmann, *Characterizing the interactions between the two subunits of the p101/p110 γ phosphoinositide 3-kinase and their role in the activation of this enzyme by G $\beta\gamma$ subunits*. *Journal of Biological Chemistry*, 1999. **274**(24): p. 17152-17158.
192. Suire, S., J. Coadwell, G.J. Ferguson, K. Davidson, P. Hawkins, and L. Stephens, *p84, a new G $\beta\gamma$ -activated regulatory subunit of the type IB phosphoinositide 3-kinase p110 γ* . *Current Biology*, 2005. **15**(6): p. 566-570.
193. Stephens, L., A. Eguinoa, H. Erdjument-Bromage, M. Lui, F. Cooke, J. Coadwell, A. Smrcka, M. Thelen, K. Cadwallader, and P. Tempst, *The G $\beta\gamma$ sensitivity of a PI3K is dependent upon a tightly associated adaptor, p101*. *Cell*, 1997. **89**(1): p. 105-114.
194. Sasaki, T., J. Irie-Sasaki, R.G. Jones, A.J. Oliveira-dos-Santos, W.L. Stanford, B. Bolon, A. Wakeham, A. Itie, D. Bouchard, and I. Kozieradzki, *Function of PI3K γ in thymocyte development, T cell activation and neutrophil migration*. *CLINICAL IMMUNOLOGY-TOKYO*, 2001. **35**(6): p. 769-774.
195. Hirsch, E., V.L. Katanaev, C. Garlanda, O. Azzolino, L. Pirola, L. Silengo, S. Sozzani, A. Mantovani, F. Altruda, and M.P. Wymann, *Central role for G protein-coupled phosphoinositide 3-kinase γ in inflammation*. *Science*, 2000. **287**(5455): p. 1049-1053.
196. Wymann, M.P., M. Zvelebil, and M. Laffargue, *Phosphoinositide 3-kinase signalling— which way to target?* *Trends in pharmacological sciences*, 2003. **24**(7): p. 366-376.
197. Ghigo, A., F. Damilano, L. Braccini, and E. Hirsch, *PI3K inhibition in inflammation: Toward tailored therapies for specific diseases*. *Bioessays*, 2010. **32**(3): p. 185-196.

198. Crackower, M.A., G.Y. Oudit, I. Kozieradzki, R. Sarao, H. Sun, T. Sasaki, E. Hirsch, A. Suzuki, T. Shioi, and J. Irie-Sasaki, *Regulation of myocardial contractility and cell size by distinct PI3K-PTEN signaling pathways*. Cell, 2002. **110**(6): p. 737-749.
199. Oudit, G.Y., H. Sun, B.-G. Kerfant, M.A. Crackower, J.M. Penninger, and P.H. Backx, *The role of phosphoinositide-3 kinase and PTEN in cardiovascular physiology and disease*. Journal of molecular and cellular cardiology, 2004. **37**(2): p. 449-471.
200. Fougerat, A., S. Gayral, P. Gourdy, A. Schambourg, T. Rückle, M.K. Schwarz, C. Rommel, E. Hirsch, J.-F. Arnal, and J.-P. Salles, *Genetic and pharmacological targeting of phosphoinositide 3-kinase- γ reduces atherosclerosis and favors plaque stability by modulating inflammatory processes*. Circulation, 2008. **117**(10): p. 1310-1317.
201. Domin, J., F. Pages, S. Volinia, S.E. Rittenhouse, M.J. Zvelebil, R.C. Stein, and M.D. Waterfield, *Cloning of a human phosphoinositide 3-kinase with a C2 domain that displays reduced sensitivity to the inhibitor wortmannin*. Biochemical Journal, 1997. **326**(Pt 1): p. 139.
202. Brown, R.A., J. Domin, A. Arcaro, M.D. Waterfield, and P.R. Shepherd, *Insulin activates the α isoform of class II phosphoinositide 3-kinase*. Journal of Biological Chemistry, 1999. **274**(21): p. 14529-14532.
203. Misawa, H., M. Ohtsubo, N.G. Copeland, D.J. Gilbert, N.A. Jenkins, and A. Yoshimura, *Cloning and characterization of a novel class II phosphoinositide 3-kinase containing C2 domain*. Biochemical and biophysical research communications, 1998. **244**(2): p. 531-539.
204. Ono, F., T. Nakagawa, S. Saito, Y. Owada, H. Sakagami, K. Goto, M. Suzuki, S. Matsuno, and H. Kondo, *A novel class II phosphoinositide 3-kinase predominantly expressed in the liver and its enhanced expression during liver regeneration*. Journal of Biological Chemistry, 1998. **273**(13): p. 7731-7736.
205. Rozycka, M., Y.-J. Lu, R.A. Brown, M.R. Lau, J.M. Shipley, and M.J. Fry, *cDNA cloning of a third human C2-domain-containing class II phosphoinositide 3-kinase, PI3K-C2 γ , and chromosomal assignment of this gene (PIK3C2G) to 12p12*. Genomics, 1998. **54**(3): p. 569-574.
206. MacDougall, L.K., J. Domin, and M.D. Waterfield, *A family of phosphoinositide 3-kinases in Drosophila identifies a new mediator of signal transduction*. Current Biology, 1995. **5**(12): p. 1404-1415.
207. Djordjevic, S. and P.C. Driscoll, *Structural insight into substrate specificity and regulatory mechanisms of phosphoinositide 3-kinases*. Trends in biochemical sciences, 2002. **27**(8): p. 426-432.
208. Chaussade, C., L. Pirola, S. Bonnafous, F. Blondeau, S. Brenz-Verca, H. Tronchère, F. Portis, S. Rusconi, B. Payrastre, J. Laporte, and E. Van Obberghen, *Expression of Myotubularin by an Adenoviral Vector Demonstrates Its Function as a Phosphatidylinositol 3-Phosphate [PtdIns(3)P] Phosphatase in Muscle Cell Lines: Involvement of PtdIns(3)P in Insulin-Stimulated Glucose Transport*. Molecular Endocrinology, 2003. **17**(12): p. 2448-2460.
209. Maffucci, T., A. Brancaccio, E. Piccolo, R.C. Stein, and M. Falasca, *Insulin induces phosphatidylinositol-3-phosphate formation through TC10 activation*. EMBO Journal, 2003. **22**(16): p. 4178-4189.
210. Falasca, M., W.E. Hughes, V. Dominguez, G. Sala, F. Fostira, M.Q. Fang, R. Cazzolli, P.R. Shepherd, D.E. James, and T. Maffucci, *The role of phosphoinositide 3-kinase C2 α in insulin signaling*. Journal of Biological Chemistry, 2007. **282**(38): p. 28226-28236.
211. Yoshioka, K., K. Yoshida, H. Cui, T. Wakayama, N. Takuwa, Y. Okamoto, W. Du, X. Qi, K. Asanuma, and K. Sugihara, *Endothelial PI3K-C2 [alpha], a class II PI3K, has an essential role in angiogenesis and vascular barrier function*. Nature Medicine, 2012.

212. Wen, P.J., S.L. Osborne, I.C. Morrow, R.G. Parton, J. Domin, and F.A. Meunier, *Ca²⁺-regulated pool of phosphatidylinositol-3-phosphate produced by phosphatidylinositol 3-kinase C2 α on neurosecretory vesicles*. Molecular biology of the cell, 2008. **19**(12): p. 5593-5603.
213. Gaidarov, I., Y. Zhao, and J.H. Keen, *Individual phosphoinositide 3-kinase C2 α domain activities independently regulate clathrin function*. Journal of Biological Chemistry, 2005. **280**(49): p. 40766-40772.
214. Gaidarov, I., M.E. Smith, J. Domin, and J.H. Keen, *The class II phosphoinositide 3-kinase C2 α is activated by clathrin and regulates clathrin-mediated membrane trafficking*. Molecular cell, 2001. **7**(2): p. 443-449.
215. Yoshioka, K., N. Sugimoto, N. Takuwa, and Y. Takuwa, *Essential role for class II phosphoinositide 3-kinase α -isoform in Ca²⁺-induced, Rho-and Rho kinase-dependent regulation of myosin phosphatase and contraction in isolated vascular smooth muscle cells*. Molecular pharmacology, 2007. **71**(3): p. 912-920.
216. Brown, R.A., L.K. Ho, S.J. Weber-Hall, J.M. Shipley, and M.J. Fry, *Identification and cDNA cloning of a novel mammalian C2 domain-containing phosphoinositide 3-kinase, HsC2-PI3K*. Biochemical and biophysical research communications, 1997. **233**(2): p. 537-544.
217. Maffucci, T., F.T. Cooke, F.M. Foster, C.J. Traer, M.J. Fry, and M. Falasca, *Class II phosphoinositide 3-kinase defines a novel signaling pathway in cell migration*. J Cell Biol, 2005. **169**(5): p. 789-99.
218. Srivastava, S., L. Di, O. Zhdanova, Z. Li, S. Vardhana, Q. Wan, Y. Yan, R. Varma, J. Backer, and H. Wulff, *The class II phosphatidylinositol 3 kinase C2 β is required for the activation of the K⁺ channel KCa3. 1 and CD4 T-cells*. Molecular biology of the cell, 2009. **20**(17): p. 3783-3791.
219. Arcaro, A., U.K. Khanzada, B. Vanhaesebroeck, T.D. Tetley, M.D. Waterfield, and M.J. Seckl, *Two distinct phosphoinositide 3-kinases mediate polypeptide growth factor-stimulated PKB activation*. The EMBO journal, 2002. **21**(19): p. 5097-5108.
220. Boller, D., K.T. Doepfner, A. De Laurentiis, A.S. Guerreiro, M. Marinov, T. Shalaby, P. Depledge, A. Robson, N. Saghir, M. Hayakawa, H. Kaizawa, T. Koizumi, T. Ohishi, S. Fattet, O. Delattre, A. Schweri-Olac, K. Holand, M.A. Grotzer, K. Frei, O. Spertini, M.D. Waterfield, and A. Arcaro, *Targeting PI3KC2 β impairs proliferation and survival in acute leukemia, brain tumours and neuroendocrine tumours*. Anticancer Res, 2012. **32**(8): p. 3015-27.
221. Herman, P.K. and S.D. Emr, *Characterization of VPS34, a gene required for vacuolar protein sorting and vacuole segregation in Saccharomyces cerevisiae*. Molecular and Cellular Biology, 1990. **10**(12): p. 6742-6754.
222. Volinia, S., R. Dhand, B. Vanhaesebroeck, L. MacDougall, R. Stein, M. Zvelebil, J. Domin, C. Panaretou, and M. Waterfield, *A human phosphatidylinositol 3-kinase complex related to the yeast Vps34p-Vps15p protein sorting system*. The EMBO journal, 1995. **14**(14): p. 3339.
223. Kihara, A., T. Noda, N. Ishihara, and Y. Ohsumi, *Two Distinct Vps34 Phosphatidylinositol 3-Kinase Complexes Function in Autophagy and Carboxypeptidase Y Sorting in Saccharomyces cerevisiae*. The Journal of cell biology, 2001. **152**(3): p. 519-530.
224. Vieira, O.V., R.J. Botelho, L. Rameh, S.M. Brachmann, T. Matsuo, H.W. Davidson, A. Schreiber, J.M. Backer, L.C. Cantley, and S. Grinstein, *Distinct roles of class I and class III phosphatidylinositol 3-kinases in phagosome formation and maturation*. The Journal of cell biology, 2001. **155**(1): p. 19-26.
225. Vanhaesebroeck, B. and M. Waterfield, *Signaling by distinct classes of phosphoinositide 3-kinases*. Experimental cell research, 1999. **253**(1): p. 239-254.

226. Lempiäinen, H. and T.D. Halazonetis, *Emerging common themes in regulation of PIKKs and PI3Ks*. The EMBO journal, 2009. **28**(20): p. 3067-3073.
227. Wong, K.-K., J.A. Engelman, and L.C. Cantley, *Targeting the PI3K signaling pathway in cancer*. Current opinion in genetics & development, 2010. **20**(1): p. 87-90.
228. Engelman, J.A., *Targeting PI3K signalling in cancer: opportunities, challenges and limitations*. Nature Reviews Cancer, 2009. **9**(8): p. 550-562.
229. Vara, J.Á.F., E. Casado, J. de Castro, P. Cejas, C. Belda-Iniesta, and M. González-Barón, *PI3K/Akt signalling pathway and cancer*. Cancer treatment reviews, 2004. **30**(2): p. 193-204.
230. Liu, P., H. Cheng, T.M. Roberts, and J.J. Zhao, *Targeting the phosphoinositide 3-kinase pathway in cancer*. Nature reviews Drug discovery, 2009. **8**(8): p. 627-644.
231. Thorpe, L.M., H. Yuzugullu, and J.J. Zhao, *PI3K in cancer: divergent roles of isoforms, modes of activation and therapeutic targeting*. Nature Reviews Cancer, 2015. **15**(1): p. 7-24.
232. Lui, V.W., M.L. Hedberg, H. Li, B.S. Vangara, K. Pendleton, Y. Zeng, Y. Lu, Q. Zhang, Y. Du, and B.R. Gilbert, *Frequent mutation of the PI3K pathway in head and neck cancer defines predictive biomarkers*. Cancer discovery, 2013. **3**(7): p. 761-769.
233. Samuels, Y. and K. Ericson, *Oncogenic PI3K and its role in cancer*. Current opinion in oncology, 2006. **18**(1): p. 77-82.
234. Traer, C.J., F.M. Foster, S.M. Abraham, and M.J. Fry, *Are class II phosphoinositide 3-kinases potential targets for anticancer therapies?* Bulletin du cancer, 2006. **93**(5): p. 10053-10058.
235. Armstrong, S.A., J.E. Staunton, L.B. Silverman, R. Pieters, M.L. den Boer, M.D. Minden, S.E. Sallan, E.S. Lander, T.R. Golub, and S.J. Korsmeyer, *MLL translocations specify a distinct gene expression profile that distinguishes a unique leukemia*. Nature genetics, 2002. **30**(1): p. 41-47.
236. Qian, Z., A.A. Fernald, L.A. Godley, R.A. Larson, and M.M. Le Beau, *Expression profiling of CD34+ hematopoietic stem/progenitor cells reveals distinct subtypes of therapy-related acute myeloid leukemia*. Proceedings of the National Academy of Sciences, 2002. **99**(23): p. 14925-14930.
237. Wiesinger, D., H. Gubler, W. Haefliger, and D. Hauser, *Antiinflammatory activity of the new mould metabolite 11-desacetoxy-wortmannin and of some of its derivatives*. Cellular and Molecular Life Sciences, 1974. **30**(2): p. 135-136.
238. Arcaro, A., S. Volinia, M.J. Zvelebil, R. Stein, S.J. Watton, M.J. Layton, I. Gout, K. Ahmadi, J. Downward, and M.D. Waterfield, *Human phosphoinositide 3-kinase C2 β , the role of calcium and the C2 domain in enzyme activity*. Journal of Biological Chemistry, 1998. **273**(49): p. 33082-33090.
239. Matter, W.F., R.F. Brown, and C.J. Vlahos, *The inhibition of phosphatidylinositol 3-kinase by quercetin and analogs*. Biochemical and Biophysical Research Communications, 1992. **186**(2): p. 624-631.
240. Agullo, G., L. Gamet-Payrastre, S. Manenti, C. Viala, C. Rémésy, H. Chap, and B. Payrastre, *Relationship between flavonoid structure and inhibition of phosphatidylinositol 3-kinase: A comparison with tyrosine kinase and protein kinase C inhibition*. Biochemical Pharmacology, 1997. **53**(11): p. 1649-1657.
241. Vlahos, C.J., W.F. Matter, K.Y. Hui, and R.F. Brown, *A specific inhibitor of phosphatidylinositol 3-kinase, 2-(4-morpholinyl)-8-phenyl-4H-1-benzopyran-4-one (LY294002)*. Journal of Biological Chemistry, 1994. **269**(7): p. 5241-5248.
242. Brunn, G.J., J. Williams, C. Sabers, G. Wiederrecht, J. Lawrence Jr, and R.T. Abraham, *Direct inhibition of the signaling functions of the mammalian target of rapamycin by the phosphoinositide 3-kinase inhibitors, wortmannin and LY294002*. The EMBO journal, 1996. **15**(19): p. 5256.

243. Knight, Z.A., G.G. Chiang, P.J. Alaimo, D.M. Kenski, C.B. Ho, K. Coan, R.T. Abraham, and K.M. Shokat, *Isoform-specific phosphoinositide 3-kinase inhibitors from an arylmorpholine scaffold*. *Bioorganic & Medicinal Chemistry*, 2004. **12**(17): p. 4749-4759.
244. Kong, D.X., S.G. Dan, K. Yamazaki, and T. Yamori, *Inhibition profiles of phosphatidylinositol 3-kinase inhibitors against PI3K superfamily and human cancer cell line panel JFCR39*. *European Journal of Cancer*, 2010. **46**(6): p. 1111-1121.
245. Wymann, M., *PI3Ks—Drug Targets in Inflammation and Cancer*, in *Phosphoinositides I: Enzymes of Synthesis and Degradation*. 2012, Springer Science & Business Media.
246. Knight, Z.A., B. Gonzalez, M.E. Feldman, E.R. Zunder, D.D. Goldenberg, O. Williams, R. Loewith, D. Stokoe, A. Balla, B. Toth, T. Balla, W.A. Weiss, R.L. Williams, and K.M. Shokat, *A pharmacological map of the PI3-K family defines a role for p110alpha in insulin signaling*. *Cell*, 2006. **125**(4): p. 733-47.
247. Folkes, A.J., K. Ahmadi, W.K. Alderton, S. Alix, S.J. Baker, G. Box, I.S. Chuckowree, P.A. Clarke, P. Depledge, and S.A. Eccles, *The identification of 2-(1 H-Indazol-4-yl)-6-(4-methanesulfonyl-piperazin-1-ylmethyl)-4-morpholin-4-yl-thieno [3, 2-d] pyrimidine (GDC-0941) as a potent, selective, orally bioavailable inhibitor of class I PI3 kinase for the treatment of cancer†*. *Journal of medicinal chemistry*, 2008. **51**(18): p. 5522-5532.
248. Maira, S.-M., F. Stauffer, J. Brueggen, P. Furet, C. Schnell, C. Fritsch, S. Brachmann, P. Chène, A. De Pover, and K. Schoemaker, *Identification and characterization of NVP-BEZ235, a new orally available dual phosphatidylinositol 3-kinase/mammalian target of rapamycin inhibitor with potent in vivo antitumor activity*. *Molecular cancer therapeutics*, 2008. **7**(7): p. 1851-1863.
249. Mountford, S.J., Z. Zheng, K. Sundaram, I.G. Jennings, J.R. Hamilton, and P.E. Thompson, *Class II but Not Second Class—Prospects for the Development of Class II PI3K Inhibitors*. *ACS Medicinal Chemistry Letters*, 2015. **6**(1): p. 3-6.
250. Boller, D., K.T. Doepfner, A. De Laurentiis, A.S. Guerreiro, M. Marinov, T. Shalaby, P. Depledge, A. Robson, N. Saghir, and M. Hayakawa, *Targeting PI3KC2B impairs proliferation and survival in acute leukemia, brain tumours and neuroendocrine tumours*. *Anticancer research*, 2012. **32**(8): p. 3015-3027.
251. Freitag, A., P. Prajwal, A. Shymanets, C. Harteneck, B. Nürnberg, C. Schächtele, M. Kubbutat, F. Totzke, and S.A. Laufer, *Development of First Lead Structures for Phosphoinositide 3-Kinase-C2γ Inhibitors*. *Journal of medicinal chemistry*, 2014. **58**(1): p. 212-221.
252. Galperin, M.Y., D.J. Rigden, and X.M. Fernández-Suárez, *The 2015 Nucleic Acids Research Database Issue and Molecular Biology Database Collection*. *Nucleic acids research*, 2015. **43**(D1): p. D1-D5.
253. Halgren, T.A., R.B. Murphy, R.A. Friesner, H.S. Beard, L.L. Frye, W.T. Pollard, and J.L. Banks, *Glide: a new approach for rapid, accurate docking and scoring. 2. Enrichment factors in database screening*. *Journal of medicinal chemistry*, 2004. **47**(7): p. 1750-1759.
254. Sander, C. and R. Schneider, *Database of homology-derived protein structures and the structural meaning of sequence alignment*. *Proteins*, 1991. **9**(1): p. 56-68.
255. Chen, P., Y.L. Deng, S. Bergqvist, M.D. Falk, W. Liu, S. Timofeevski, and A. Brooun, *Engineering of an isolated p110alpha subunit of PI3Kalpha permits crystallization and provides a platform for structure-based drug design*. *Protein Sci*, 2014. **23**(10): p. 1332-40.
256. Hon, W.-C., A. Berndt, and R.L. Williams, *Regulation of lipid binding underlies the activation mechanism of class IA PI3-kinases*. *Oncogene*, 2012. **31**(32): p. 3655-3666.
257. Walker, E.H., M.E. Pacold, O. Perisic, L. Stephens, P.T. Hawkins, M.P. Wymann, and R.L. Williams, *Structural determinants of phosphoinositide 3-kinase inhibition by*

- wortmannin, LY294002, quercetin, myricetin, and staurosporine. *Molecular cell*, 2000. **6**(4): p. 909-919.
258. Camps, M., T. Ruckle, H. Ji, V. Ardisson, F. Rintelen, J. Shaw, C. Ferrandi, C. Chabert, C. Gillieron, B. Francon, T. Martin, D. Gretener, D. Perrin, D. Leroy, P.A. Vitte, E. Hirsch, M.P. Wymann, R. Cirillo, M.K. Schwarz, and C. Rommel, *Blockade of PI3Kgamma suppresses joint inflammation and damage in mouse models of rheumatoid arthritis*. *Nat Med*, 2005. **11**(9): p. 936-43.
 259. Frazzetto, M., C. Suphioglu, J. Zhu, O. Schmidt-Kittler, I. Jennings, S. Cranmer, S. Jackson, K. Kinzler, B. Vogelstein, and P. Thompson, *Dissecting isoform selectivity of PI3K inhibitors: the role of non-conserved residues in the catalytic pocket*. *Biochem. J*, 2008. **414**: p. 383-390.
 260. Zheng, Z., S.I. Amran, P.E. Thompson, and I.G. Jennings, *Isoform-Selective Inhibition of Phosphoinositide 3-Kinase: Identification of a New Region of Nonconserved Amino Acids Critical for p110 α Inhibition*. *Molecular Pharmacology*, 2011. **80**(4): p. 657-664.
 261. Zhao, Y., X. Zhang, Y. Chen, S. Lu, Y. Peng, X. Wang, C. Guo, A. Zhou, J. Zhang, Y. Luo, Q. Shen, J. Ding, L. Meng, and J. Zhang, *Crystal Structures of PI3K α Complexed with PI103 and Its Derivatives: New Directions for Inhibitors Design*. *ACS Medicinal Chemistry Letters*, 2014. **5**(2): p. 138-142.
 262. Berndt, A., S. Miller, O. Williams, D.D. Le, B.T. Houseman, J.I. Pacold, F. Gorrec, W.-C. Hon, Y. Liu, C. Rommel, P. Gaillard, T. Ruckle, M.K. Schwarz, K.M. Shokat, J.P. Shaw, and R.L. Williams, *The p110 δ crystal structure uncovers mechanisms for selectivity and potency of novel PI3K inhibitors*. *Nature chemical biology*, 2010. **6**(2): p. 117-124.
 263. Yaguchi, S.-i., Y. Fukui, I. Koshimizu, H. Yoshimi, T. Matsuno, H. Gouda, S. Hirono, K. Yamazaki, and T. Yamori, *Antitumor activity of ZSTK474, a new phosphatidylinositol 3-kinase inhibitor*. *Journal of the National Cancer Institute*, 2006. **98**(8): p. 545-556.
 264. Brondyk, W.H., *Selecting an appropriate method for expressing a recombinant protein*. *Methods in enzymology*, 2009. **463**: p. 131-147.
 265. Engelman, J.A., J. Luo, and L.C. Cantley, *The evolution of phosphatidylinositol 3-kinases as regulators of growth and metabolism*. *Nature Reviews Genetics*, 2006. **7**(8): p. 606-619.
 266. Bader, A.G., S. Kang, L. Zhao, and P.K. Vogt, *Oncogenic PI3K deregulates transcription and translation*. *Nature Reviews Cancer*, 2005. **5**(12): p. 921-929.
 267. Kong, D. and T. Yamori, *ZSTK474 is an ATP -competitive inhibitor of class I phosphatidylinositol 3 kinase isoforms*. *Cancer science*, 2007. **98**(10): p. 1638-1642.
 268. Bergamini, G., K. Bell, S. Shimamura, T. Werner, A. Cansfield, K. Müller, J. Perrin, C. Rau, K. Ellard, C. Hopf, C. Doce, D. Leggate, R. Mangano, T. Mathieson, A. O'Mahony, I. Plavec, F. Rharbaoui, F. Reinhard, M.M. Savitski, N. Ramsden, E. Hirsch, G. Drewes, O. Rausch, M. Bantscheff, and G. Neubauer, *A selective inhibitor reveals PI3K γ dependence of TH17 cell differentiation*. *Nat Chem Biol*, 2012. **8**(6): p. 576-582.